TWO-DIMENSIONAL LAKE AND RESERVOIR MODELING: NATURAL AND PLUME-INDUCED MIXING MECHANISMS

Daniel F. McGinnis

Dissertation submitted to the Faculty of the
Virginia Polytechnic Institute and State University
in partial fulfillment of the requirements for the degree of

Doctor of Philosophy
in
Civil Engineering

Dr. John C. Little, Chair and Advisor
Dr. Panayiotis Diplas
Dr. Daniel Gallagher
Dr. Andreas Lorke
Dr. Nancy Love
Dr. Alfred Wüest

2 October, 2003
Blacksburg, Virginia

Keywords: bubble-plume, hypolimnetic oxygenation, modeling, sedimentation, transport

Copyright 2003, Daniel Frank McGinnis

TWO-DIMENSIONAL LAKE AND RESERVOIR MODELING: NATURAL AND PLUME-INDUCED MIXING MECHANISMS

Daniel F. McGinnis

(Abstract)

Lakes and reservoirs exhibit a number of mixing and transport mechanisms. Understanding the transport is crucial to understanding and predicting constituent and density structures. Transport in waterbodies can be natural, such as seiche-induced boundary mixing or advectively-driven inflows. Hypolimnetic oxygenation using bubble-plumes also leads to enhanced mixing. Whether natural or plume-induced, increased mixing will alter the waterbody properties. Conversely, the density structure affects the behavior of plumes as well as inflowing and outflowing water. For example, stratification resulting from impounding a river can result in nutrient and suspended solids retention. Similarly, operation of plumes can induce mixing in the hypolimnion, resulting in warming, increased nutrient transport, and resuspension of settled particles.

Modeling is extremely useful in determining the effects of dams on water quality constituents, enhanced transport, and the performance of mitigation techniques, such as hypolimnetic oxygenation. In this work, a variety of modeling techniques are used to evaluate natural and man-made mixing mechanisms. These include simple temperature and mass budgets, a two-dimensional lake model, and a two-phase plume model.

A bubble-plume and plume-enhanced mixing was studied in Lake Hallwil. It was found that the plume-lake interaction was much more complex then previously expected, and knowledge of the seiche- and plume-enhanced near-field was necessary to accurately model the plume performance. A two-dimensional lake model was then coupled with a linear-plume model to accurately predict not only the plume performance, but also the plume-enhanced mixing in Spring Hollow Reservoir. The same two-dimensional lake model, used in conjunction with data analysis, demonstrated that the Iron Gate I

Reservoir was not a significant sink for suspended solids, with only the large, adjacent side bay (Orsova Bay) thought to be the permanent sink. Furthermore, significant stratification did not develop, preventing substantial primary productivity. While the impoundment did change the water quality characteristics, the extent is much less than previously expected. The modeling methods presented here and the coupled plume-reservoir model should be useful tools for the design, modeling and greater understanding of bubble-plumes and other transport-related phenomena in lakes and reservoirs.

ACKNOWLEDGEMENTS

On a 12-year road of education, there are many people to thank along the way. It is impossible for me to acknowledge everyone who helped me within the confines of a single page; however, I will attempt to give credit to those people whom, knowingly or not, provided support, encouragement, and occasionally, a shoulder to cry on. First and foremost, I would like to thank my parents, Rev. Stephen J. McGinnis and D. Deanna McGinnis for leading me to believe that I can be anything I want to be. Their encouragement and support provided the basic, but solid, foundation that made it possible for me to complete my degree. I would also like to thank Henry and Silvia Lopez, and the Welch family for teaching me the value of hard work and responsibility, and for being there for me. Special thanks also to Gabrielle Kenison; without her, I may have never discovered engineering.

I would like to express my deep gratitude to my advisor, mentor and good friend Dr. John C. Little for providing me with this, and many other unique opportunities and never giving up on me, and Dr. Johny Wüest for many interesting conversations and for being a great teacher. My deepest thanks to my friend and officemate Dr. Andreas Lorke for many stimulating conversations, always having time for me, and for being a great field partner. I would also like to express my gratitude to my co-fieldworkers and friends Manuela Saballus, Vickie Singleton, and Cristian Teodoru, and the many others that helped me with fieldwork and data analysis, including Michi Schurter and Erwin Schäffer.

Special thanks to Dr. Alfred Johny Wüest and Dr. John Little for providing me with a unique opportunity to study at EAWAG's Limnological Center in Kastanienbaum, Switzerland. They provided me with a wonderful experience. Thanks to my great friends in Kastanienbaum and in the U.S. for their help and support. Many thanks also to Betty Wingate and Sherry Burke for their exemplary support with logistics. And last but not least, I would like to express my gratitude to my committee, Dr. John Little, Dr. Panayiotis Diplas, Dr. Daniel Gallagher, Dr. Andreas Lorke, Dr. Nancy Love, and Dr. Alfred Wüest.

Table of Contents

List of Figures

List of Tables

CHAPTER 1: INTRODUCTION

1. Overview

Lakes and reservoirs provide many valuable resources, including drinking water, fisheries, flood control, water supply and irrigation, enhanced navigation, recreation and tourism (Stephenson, 2000; Truffer et al., 2001). However, there is an overall trend towards lake and reservoir degradation (eutrophication). Once thought of as a clean energy source, hydropower reservoirs are coming under increasing scrutiny for their negative environmental impacts, particularly downstream water quality. Additionally, eutrophication leads to water quality problems that impact cold-water fisheries and drinking water sources. Therefore, the application of various technologies, particularly lake and reservoir modeling, can be valuable tools for understanding and improving conditions in lakes and reservoirs.

In this thesis, modeling techniques are investigated as a means of understanding transport and mixing phenomena and their affects on the temperature and water quality in lakes and reservoirs. Three specific cases are investigated. First, a lake and reservoir mitigation technique, hypolimnetic oxygenation using a bubble plume diffuser, is studied. Bubble-plume diffusers were added to a natural lake to improve dissolved oxygen levels as a lake management strategy and to maintain a cold-water fishery. Various data collection and analysis techniques are applied to study the near- and far-field plume effects. In addition, an existing circular-plume model is evaluated. Next, modeling of hypolimnetic oxygenation using a linear bubble-plume as a pre-treatment step in a drinking water reservoir is undertaken. The same plume model is modified to conform to linear as opposed to circular geometry. The linear plume model is then coupled with a two-dimensional reservoir model to investigate the impact of the bubble-plume diffuser on mixing and oxygen transport in the hypolimnion. The reservoir model is used to predict the ambient boundary conditions, upon which the bubble-plume performance depends. Finally, the same two-dimensional reservoir model is used, in conjunction with data analysis and simple analytical techniques, to determine the environmental impact of a reservoir with regards to nutrient retention and sediment transport.

The result is a coupled bubble-plume/reservoir model that has been validated under a variety of conditions, including a riverine hydropower reservoir, a relatively quiescent side-stream reservoir, and a natural lake. This will provide a useful tool for engineers and scientists to evaluate mitigation techniques and for understanding natural and man-made mixing mechanisms.

2. Organization

This thesis is organized into four chapters. Chapter 1 includes the Overview, Organization, Engineering Significance, Introduction, Motivation and Conclusions sections. Chapters 2-4 are independent, stand-alone manuscripts. The manuscripts are in approximate publication formats, and minor editing changes will be made before final submission.

Chapter 2 provides an introduction and detailed description of the circular bubble-plume model as well as natural and man-made mixing mechanisms in a lake. A circular bubble-plume was installed as a mitigation technique to maintain a cold-water fishery. In this study, a full-scale evaluation of the bubble-plume itself and the plume/lake interaction is undertaken. The primary focus is the full-scale testing and validation of an existing circular bubble-plume model. This led to a much more thorough understanding of the complex plume-lake interaction, and the importance of this interaction on the plume behavior. The study led to a new understanding of the behavior of plumes in lakes, and the importance of the plume-altered near-field boundary conditions. Furthermore, important implications to the far-field transport are revealed, including plume short-circuiting, seiche-enhanced constituent transport, and an enhanced far-field apparent vertical turbulent diffusivity.

Chapter 3 investigates a linear bubble-plume installed for pre-treatment in a drinking water reservoir. The circular plume model from Chapter 2 is modified to conform to the linear-plume geometry. This plume induces substantial mixing in the hypolimnion, resulting in continuously changing boundary conditions. Therefore, the plume-model was coupled with a two-dimensional reservoir model to predict the evolving boundary

conditions necessary to accurately predict the plume performance, as well as the effect of the plume-induced mixing on the temperature and dissolved oxygen (DO) evolution in the reservoir.

Chapter 4 evaluates the environmental impact of a reservoir. Using similar modeling techniques as in the previous chapters, the reservoir is studied to determine how it has altered downstream water quality. The reservoir has long been suspected to cause significant nutrient and suspended solids retentions, which has altered the downstream biology and led to shoreline erosion. Using a range of modeling techniques, it was determined that the impact of the reservoir with respect to solids and nutrient retention, as well as increased thermal stratification supporting primary productivity, was much lower then previously estimated.

3. Engineering Significance

The results presented in this work represent the end product of a wide range of environment issues relating to lakes and reservoirs that were raised by the scientific community, drinking water utilities, and industry. This led to the use of both scientific and engineering approaches to analyze and model aspects of these waterbodies, leading to a deeper understanding of these systems, their impacts, and proposed or existing mitigation techniques. The end results, which are presented here, are therefore the product of many trial-and-error modeling applications, and their subsequent evolution as understanding improved.

This field of environmental engineering, with regards to lakes and reservoirs, typically involves management and restoration. In the past, restoration has also been included. However, restoration refers to returning a waterbody to an arbitrarily defined baseline condition and does not take into account the current water body usage. Furthermore, the restoration of a man-made lake or reservoir is an oxymoron unless the restoration procedure is dam removal. Therefore, it is suggested that a more appropriate description for this field of environmental engineering is lake and reservoir assessment, management and mitigation.

Assessment of a waterbody is the study of a lake or reservoir to determine its potential benefits and environmental impacts, especially with respect to the waterbody's uses. Assessment can include evaluating the waterbody for a potential drinking water source, cold-water fishery, navigational enhancement, recreation or power production. Negative aspects are also explored, such as the effect of damming on water quality, fish habitats and downstream water quality and flow conditions. A specific example is the retention of sediments by dams that can cause downstream erosion, which can lead to costly repairs of structures and alter natural habitats. Additionally, the identification of the source of nutrients in natural lakes that promote eutrophication is also important with respect to coldwater fisheries and drinking water sources. Some degree of eutrophication may be desirable for waterbodies used as fisheries, but as a rule, increased eutrophication in drinking water sources leads to increased treatment costs and potential health concerns.

Lake and reservoir management involves evaluating and implementing appropriate steps to maintain or return the waterbody to the best possible state for the desired use. This encompasses a rather broad range of practices, including best management practices within the watershed, hypolimnetic oxygenation to reduce effects of eutrophication, or periodic flushing of reservoirs to minimize sediment retention. In the case of drinking water sources, multiple-level intakes are highly desirable to provide flexibility in selection of raw water depths. Hypolimnetic oxygenation can be thought of as a management strategy and also as a pretreatment step in the water treatment process. Furthermore, hypolimnetic oxygenation has been used to support and maintain coldwater fisheries.

Lake and reservoir mitigation is the attempt to minimize a negative impact on or by a waterbody, without necessarily considering the waterbody usage. For example, reducing the naturally occurring high carbon dioxide concentration in Lake Nyos in Cameroon in Africa that resulted in a catastrophic eruption in 1986 and claimed the lives of 1700 people. Another example is hypolimnetic oxygenation of Comanche Reservoir in California after anoxic, hydrogen sulfide rich waters were released that resulted in a fish kill in a downstream hatchery. Similarly, hypolimnetic oxygenation is applied in

hydropower reservoirs with the sole purpose of oxygenating the anoxic release waters, which negatively affect the downstream water quality and biology. With growing concern of the impacts of dams and even lakes on downstream water quality, flow rates and temperatures, mitigation is a rapidly growing field. Mitigation also includes the removal and control of pollution events in waterbodies, such as oil spills, or the introduction of other contaminants.

It is the environmental engineer's role to appropriately evaluate and apply management and mitigation techniques by using available technologies, past experience and research, and sound engineering judgment. This involves balancing the waterbody usage with the remediation goals, potential environmental impacts and benefits, and public interest. Fortunately, there are a variety of lake and reservoir models to aid in this process. Caution must be used with models, as they are relatively simple mathematical representations of very complex systems. However, even if models do not accurately reproduce the conditions in a waterbody, they may still provide valuable insights into the dominant forcing mechanisms. Mathematical modeling, when combined with experience, is also a valuable tool for evaluating the feasibility and performance of a management or mitigation strategy. Additionally, using non-steady state boundary conditions, modeling can be used to understand the impacts of reservoirs before they are even built, and therefore allow potential mitigation techniques to be included in the design and construction.

The contribution of this work is, therefore, to provide a guideline for analysis and modeling techniques that can be used for lake and reservoir assessment, management and mitigation. With field data collection, analysis and modeling, natural and man-made mixing mechanisms are better understood, as is their impacts on transport and water quality. While not all-encompassing, the range and applicability of the analysis and modeling tools, as well as the improved knowledge gained in this study of lakes and reservoirs, should provide the engineer with the necessary means to undertake work involving any or all of these issues. This includes environmental assessment and evaluation of management and mitigation techniques. Additionally, modeling tools are

provided for the further performance and economic optimization of proposed or existing assessment, management and mitigation measures, as well as many resources to extend this research.

4. Introduction

Thermal stratification of lakes and reservoirs can lead to oxygen depletion in the hypolimnion. Excess nutrient and organic loading increases primary productivity, which, through decomposition of organic matter, leads to an elevated water column and sediment oxygen demand (Beutel and Horne, 1999). Many stratified lakes and reservoirs do not contain an adequate reserve of hypolimnetic DO during the stratified season to meet this demand and become anoxic before the fall turnover (Beutel and Horne, 1999). As a result, anoxic products form, such as methane, carbon dioxide, hydrogen sulfide, ammonia, and the release of iron, manganese or phosphorus, which may further fuel the growth of algae and promote eutrophication under certain circumstances (Cooke et al. 1993, Galy-Lacaux et al. 1999). These compounds pose environmental and drinking water treatment problems, which vary depending on the water body usage. For drinking water sources, oxygen depleted water may lead to taste and odor problems, increased treatment costs, and increase disinfection byproduct formation (Cooke et al., 1993). If anoxia occurs in a hydropower reservoir, the water that is released can have negative consequences for downstream water quality (Little and McGinnis 2001). Furthermore, hypoxia itself has been shown to be an endocrine disruptor in fish, which can inhibit reproduction (Wu et al. 2003).

4.1 Reservoirs

The production of electricity by hydropower reservoirs has many benefits including very little greenhouse gas emissions, no air pollution, and no waste associated with nuclear facilities (Stephenson 2000, Truffer et al. 2001). Overall, hydropower is very energy efficient and provides power instantly on peak demand (Stephenson 2000). Typically, hydropower projects provide energy at a substantially lower cost than conventional thermal projects, which are often the next lowest cost option (Stephenson 2000). Reservoirs can have many additional benefits as well, including flood control, water

supply, enhanced navigation, recreation and tourism (Stephenson, 2000; Truffer et al., 2001). Globally, they are considered a preferable energy alternative, particularly with respect to greenhouse emissions; however reservoirs do have potentially large negative consequences that must be considered (Truffer et al., 2001).

Local and regional impacts are a growing concern for hydropower reservoirs. These include the extinction or alteration of fish populations, loss of aquatic habitats, ground water level fluctuations, and deterioration of landscapes (Truffer et al., 2001). Higher hydraulic retention times lead to a decrease in turbulence, increase in productivity, and removal of nutrients for downstream ecosystems. Shore erosion due to fluctuating elevations may lead to an increase in turbidity (Friedl and Wüest 2002). The World Commission of Dams recently summarized the major environmental impacts of reservoirs, and the impacts are mostly negative (Friedl and Wüest 2002).

Fish kills are of concern due to loss of habitat resulting from anoxic hypolimnions in reservoirs. In some cases, endangered fish have been killed by withdrawal through the turbines (USACE 1998a). Hydrogen sulfide rich dam releases, resulting from hypolimnetic anoxia in Comanche Reservoir (California), resulted in a massive fishkill in a downstream hatchery (Jung et al. 1998, Beutel and Horne 1999). Alteration of the release water temperature can also be caused by thermally stratified hydropower reservoirs (Friedl and Wüest 2002). This can cause the downstream temperature to be too warm or too cold, which can have negative consequences for fish and biology (Sherman 2000).

In the U.S., the Federal Energy Regulatory Commission (FERC) is the federal agency that oversees the licensing of hydropower projects and is the mechanism by which hydropower reservoirs are required to meet water quality standards (HRC 2003). The license is generally issued for 30-50 years and will be required for over 400 dams in 130 rivers in the next 10 years (HRC 2003). Between 2000 and 2010, approximately 20 percent of applicable hydropower projects will apply for new licenses (Stephenson 2000). Since licenses were issued up to 30-50 years ago, a project may not be in compliance

with recent environmental, land use or other applicable laws (HRC 2003). Additionally, a project may be using outdated, inefficient equipment. FERC relicensing is the only opportunity to compel a facility to meet modern environmental protection laws and to update equipment (HRC, 2003; Stephenson, 2000). Under Section 401 of the Clean Water Act (CWA), FERC may not license a project without first obtaining state water quality certification (or a waiver) (FERC 2001, FWPCA 2002). In Jefferson County v. Washington Department of Ecology, the Supreme Court held that States could regulate water quality (physical and chemical) as well as the volumetric release (minimum flow conditions) and impacts on fishing and boating (Stephenson 2000).

Globally, as there are currently 800,000 artificial lakes and reservoirs covering 500,000 km^2 (approximately 3‰) of land surface worldwide, green power as a licensing and management option has become an increasing focus (Friedl and Wüest 2002). Some countries offer incentive-based environmental protection measures by allowing projects to market hydroelectricity as green electricity (Truffer et al., 2001). This, however, has also come under much scrutiny as the severe impacts on communities, landscapes and ecosystems have become clearer to the public, triggering an increasingly negative public image of hydropower. Hydroelectricity is considered environmentally more desirable than conventional power, so maintaining a positive public image of the green project becomes very important. As compensation for improved environmental measures, the producer may ask higher prices for green-produced power. Green markets have developed in Switzerland, Germany, Holland and England. The US also has an ecolabel Green-e, but it is only applicable to low impact, run-of-river plants (formally <30MW). The Green-e concept was started in 1997, and the single-criterion approach will soon be revised to include a comprehensive set of standards for green hydropower (Truffer et al. 2001).

The lack of uniform criteria and negative examples of the ecolabel application to hydropower have generated some uncertainty among consumers (Truffer et al., 2001). Therefore, a balanced approach is necessary, considering both environmental costs and benefits. As with the FERC procedure, complications arise in that every single plant has

a unique set of local characteristics. A thorough assessment is necessary based on environmental impact analysis including the hydrological regime, connectivity of aquatic systems, morphology and sediment regime, landscape (aesthetic appeal of waterfalls and rapids is considered), and biodiversity (Truffer et al., 2001). A management concept proposed by Truffer et al. (2001) includes specific attention to the 1) minimum flow regime, 2) mode of hydropeaking, 3) reservoir management (including water quality), 4) sediment flushing, and 5) specific operation and technology of the facility. The advantage of this approach is that the process is more scientific and becomes less dependent on national legislation (from Truffer et al., 2001).

Various mitigation technologies may be considered part of the license or renewal and may be required by state agencies as a condition of certification for FERC relicensing. American Rivers and Trout Unlimited are increasingly vocal in requiring dam removal to be considered as a mitigation technique for each relicensing case (Stephenson 2000). Artificial mixing, trunnions (pipes controlling withdrawal depth), surface pumps, draft tube mixers, submerged curtains, and stilling basins may be considered as technology to remedy cold or warm water pollution (Sherman 2000). Hypolimnetic oxygenation was employed in Comanche Reservoir (California) after the build-up and subsequent release of high levels of hydrogen sulfide resulted in a massive fishkill in a downstream hatchery (Jung et al. 1998, Beutel and Horne 1999). Hypolimnetic oxygenation has also been proposed by the U.S. Army Corps of Engineers (USACE) to replace dam-related fish-habitat loss (USACE, 1998), creating an environment upstream of a dam that is conducive to cold-water species. Large quantities of oxygen must frequently be added to hydropower release water prior to or during discharge. Several multi-million dollar bubble-plume diffuser installations in the U.S. are currently being considered to improve release DO (Mobley 2001). For example, Tennessee Valley Authority (TVA) spends about $2M annually on liquid oxygen for several reservoirs (Hauser 2000). As previously stated, between the years 2000 and 2010, roughly 20 percent of hydropower plants in the U.S. will apply for new FERC licenses (Stephenson 2000), raising the likelihood of significant continuing demand for new oxygenation systems.

4.2 Lakes

Many of the same issues described for reservoirs also pertain to lakes. However, because of the typically longer residence times in lakes, it is more important to understand natural and manmade mixing mechanisms in lakes. Enhanced mixing may result from sewage inflows, such as in Alpnachersee (Switzerland) (McGinnis and Wüest 2001), or natural, geothermal sources as in Lake Banyoles (Spain) (Colomer et al. 2000, Serra et al. 2000). In Lake Nyos (Cameroon), the build up of hypolimnetic carbon dioxide (CO_2) concentrations from geological sources led to a catastrophic release, producing a lethal cloud of CO_2 gas responsible for the deaths of approximately 1,700 people (Zhang 1996). Recently, self-sustaining CO_2-driven confined bubble-plumes were installed in Lake Nyos to reduce the CO_2 to safe levels (Clarke 2001). The dissolution of methane hydrates and degradation of organic matter in lakes also results in the release methane contributing to greenhouse gases (Suess et al. 1999). The concern is that global warming will further destabilize methane hydrates, with methane plumes already observed in Lake Baikal. Eutrophication in lakes also limits the use as a cold-water fishery and presents drinking water treatment problems previously described.

4.3 Hypolimnetic Oxygenation

Hypolimnetic oxygenation is also often used to replenish dissolved oxygen in both lakes and reservoir; however, the added energy will to some degree induce large-scale hypolimnetic mixing. Due to the typically longer water residence time in lakes than in reservoirs, this is a greater concern. Hypolimnetic warming due to artificial oxygenation may increase sediment oxygen demand (SOD) (Little and McGinnis 2001). Assuming that the external oxygen transfer rate is limiting, reasons for enhanced SOD include a reduced diffusive boundary layer (DBL) thickness resulting from increased shear velocity at the sediment-water interface (Müller et al. 2001), an enhanced turbulent boundary layer (TBL), an increased oxygen gradient between bulk water and sediments, and increased sediment temperature, and hence microbial activity and kinetics. In large-scale laboratory experiments, Mackenthun and Stefan (Mackenthun and Stefan 1998) showed that increasing near-sediment water velocities from 1 to 3 cm s^{-1} increased SOD by a factor of 2 to 3. Because SOD dominates the overall oxygen demand in most lakes, the

effect of enhanced mixing must be included to avoid serious under-design of oxygenation systems (Mackenthun and Stefan 1998). The reduced mass-transfer resistance due to a decreased DBL may increase other sediment/water biogeochemical flux rates (phosphorus, iron, and manganese, for example). Finally, partial erosion of the thermocline and subsequent warming of the hypolimnion may result in premature destratification of the reservoir (Beutel and Horne 1999), increasing the potential for a late fall algal bloom. Additionally, the generation of a TBL due to seiche-enhanced mixing will also increase these flux rates and SOD.

5. Motivation

In this thesis, an in-depth study was performed on the impact and performance of a bubble-plume diffuser in a lake, and the data collected were used to verify an existing bubble-plume model. A linear version of the bubble-plume model for artificial oxygenation is then coupled with a two-dimensional lake model to explore the impacts of the diffuser system. The coupled model can to be used as a tool for the future design and optimization of bubble-plume diffusers in lakes. The same two-dimensional reservoir model is then used, along with analysis of field data, to better understand sediment and nutrient retention in a hydropower reservoir. The motivation for each study is described in more detail below.

5.1 Chapter 2: Lake Management: Lake Hallwil

Chapter 2 is titled “The interaction between bubble plumes and the near-field in lakes and reservoirs: influences on plume transport and modeling”. In this study, six circular bubble-plume diffusers were installed in a natural lake as a management strategy. The long-term goal was to reduce the negative impacts of eutrophication by returning dissolved oxygen to the hypolimnion and to reduce anoxic products, particularly dissolved nutrient fluxes from the sediments, that lead to increased primary productivity. The short-term goal, however, is to maintain Lake Hallwil as a cold-water fishery for commercial fishermen.

The main focus of the study was to verify an existing plume model in a full-scale lake setting. The validity of the model is crucial for it's use in the design of bubble-plumes, as penetration into the euphotic zone and thermocline can lead to increased productivity due to the introduction of nutrients from the bottom water and increased warming of the hypolimnion. Warming of the hypolimnion is undesirable for reasons previously mentioned. The authors of the bubble-plume model used the diffuser geometry as a calibration parameter. However, it was thought that this is not appropriate, and the actual value for the diffuser diameter should be used. A full-lake study was also performed to better understand the plume-lake interaction. This included studying the seiching and the seiche effects on plume characteristics and transport to the far-field. Additionally, the plume-enhanced far-field vertical turbulent diffusivity was also investigated.

5.2 Chapter 3: Lake Mitigation: Spring Hollow Reservoir

Chapter 3 is titled "Hypolimnetic oxygenation: coupling bubble-plume and reservoir models". This involved coupling a linear version of the bubble-plume model with CE-QUAL-W2, a two-dimensional lake and reservoir model. Spring Hollow Reservoir is a side-stream drinking water reservoir that uses a linear-bubble plume diffuser as a pre-drinking water treatment process to prevent anoxic products, particularly hydrogen sulfide, iron and manganese, which lead to odor and color issues. The motivation of this works stems from previous coupling attempts of the plume/reservoir model for another drinking water reservoir and various hydropower projects. The issue in the drinking water reservoir study was whether enhanced plume mixing would successfully transport dissolved oxygen upstream in the reservoir rapidly enough to reach the point of withdrawal before the oxygen became depleted (Little et al. 1999). Subsequent attempts include the optimization of the placement of a bubble-plume diffuser upstream of a dam. The goal was to create an artificial coldwater fish habitat while maximizing the oxygen in the release water by placing the diffuser in a zone where advective downstream transport of the plume water would reach the discharge at the dam (USACE 1998b). Finally, in the case of Spring Hollow Reservoir, a linear-plume model was developed based on the circular plume model. This model was then coupled with CE-QUAL-W2 and applied to the reservoir. The goal was to determine if the coupling could activate the proper mixing

mechanisms in the lake model and reproduced the relatively significant warming and oxygen increase that was observed in Spring Hollow Reservoir during diffuser operation. The coupled model was also used to validate the uncalibrated linear-plume model.

5.3 Chapter 4: Lake Assessment: Iron Gate I Reservoir

Chapter 4 is titled "Sediment retention in the Lower Iron Gate Reservoir: Effect of the Danube River Bays and the implications for nutrient retention". It has long been speculated that Iron Gate I reservoir was a significant cause of suspended solids and nutrient (silica) retention. The motivation of this study is an assessment to estimate the silica retention. Sediment retention causes downstream erosion of rivers, which can lead to bank instability and impact structures such a bridges. Furthermore, sediment retention is speculated to cause shoreline erosion at the Danube Delta, destroying wetlands and habitats. The retention of silica is thought to have cause a shift in algal species from diatoms to less desirable blue-green algae, which negatively impacts fisheries (Friedl et al. 2003).

Previous to this study, it was not clear if Iron Gate I stratified during the summer, which would lead to increased primary productivity and subsequent settling of silica frustules from settling diatoms. It was suspected, however, that if stratification did occur, it would likely be in the adjacent side bays, where flow conditions are more quiescent. Field data were collected estimate the sediment and nutrient retention and the extent of thermal stratification. Through data analysis and modeling, greater understanding of transport mechanisms in the Iron Gate I and its role in the sediment and nutrient retention reported at the mouth of the Danube Delta was achieved.

6. Conclusions

The general conclusion is that understanding the natural and man-made mixing mechanisms in lakes and reservoirs are highly important for any modeling applications. This is true regardless of whether it is basin-scale modeling, such as with a lake or reservoir model, modeling the local effects of a plume, or modeling specific regions, such as the role of side bays on sedimentation. Inflows (natural or man-made) and seiche-

generated currents drive the stratification and constituent distribution. However, they also affect the distribution and properties of inflows, outflows, and plumes, which in turn affect the background stratification and constituent distributions. With this in mind, the specific conclusions are listed below.

6.1 Chapter 2: Lake Hallwil

In Lake Hallwil, the importance of the selection of boundary conditions was identified for accurate plume modeling. Furthermore, it was found that the plume operation itself affected the boundary conditions, and the plume-lake interaction was much more complex then originally thought. Three distinct zones were identified with the following main findings for each:

1. Plume near-field. This is the zone directly influenced by the plume operation and fallback water, which ranged in tens of meters from the plume. It was determined that the plume properties are highly dependent on this zone, as this plume fallback water is a high percentage of the water that is entrained by the plume. It was further determined that due to the increased isothermal conditions resulting from the enhanced mixing, the fallback water reaches much deeper than previously expected, leading to further short-circuiting by the plume. The bubble-core inside the plume was also shown not to spread as rapidly as previously expected.
2. Seiche-enhanced near-field. Because Lake Hallwil is subject to intense, persistent seiching, the effects of the plume are distributed in a zone in the range of hundreds of meters. This acts to spread the effects more rapidly in the lateral direction. Plume performance is also affected because this seiching produces plume wandering, and the resulting plume cross-flow caused by the seiche current may cause multiple detrainment.
3. Far-field. Transport of the oxygenated plume water is limited by the short-circuiting that occurs in the near-field. It is estimated that only approximately 30 percent of the oxygenated plume water is returned to the far-field. Furthermore, there is an increase in the vertical apparent turbulent diffusivity in the far-field, leading to faster transport of nutrients and other constituents.

6.2 Chapter 3: Spring Hollow Reservoir

A linear plume model was written based on the circular plume model presented in Chapter 2. While the linear plume model is uncalibrated, a preliminary coupling was performed with CE-QUAL-W2. The entrainment coefficient and the bubble-core-to-plume ratio were obtained from literature. The preliminary coupling proved to be effective, and predicted the evolution of the temperature and dissolved oxygen profiles well for two separate data sets, and will be included in the CE-QUAL-W2 code. The only sensitive calibration parameter proved to be the coefficient of horizontal eddy viscosity and diffusivity. This value is currently temporally and spatially invariant in CE-QUAL-W2. Current work is underway to determine these values in Spring Hollow Reservoir. The program code is freely available and modular. Therefore, the next step will be to include an algorithm to calculate these parameters. However, even in the current form, the coupled model should prove a valuable tool for understanding and predicting not only the effect of the bubble plume, but also thermal plumes in lakes and reservoirs.

6.3 Chapter 4: Iron Gate I Reservoir

Based on the analysis and modeling, it was shown that Iron Gate I does not significantly stratify and therefore does not support primary productivity. Further analysis of data, as well as acoustic Doppler current profiler (ADCP) velocity measurements, also revealed a lack of primary productivity. There is a greater degree of stratification and limited primary productivity occurring in Orsova Bay, the largest side-bay in the study area, which is indicated in the temperature and ADCP measurements. Chlorophyll peaks were observed in the quiescent center of the bay during the summer season; however, due to the limited stratification and exchange with the Danube River, the contribution of Orsova Bay to nutrient retention is not expected to be significant. The exchange of water between Orsova Bay and the main branch is measured to be about 15 percent. The calculated sediment retention by the bay is between 50-70 percent, depending on the flow in the main branch.

Based on the study, it can be concluded that Orsova Bay is the only likely permanent sink of suspended solids in the immediate study area. Suspended solids retention was measured in the main branch during the low flow period in October; however, it appeared that resuspension occurred during the higher flow period in March. Therefore, it is likely that the permanent sink of sediments occurs in the larger side bays and that the amount estimated for the entire reservoir is almost an order of magnitude less than previously expected. Therefore, it is suggested that other sinks, such as upstream impoundments, be investigated. It has also been suggested that the weathering rates in the Danube drainage basin may have decreased (Friedl et al. 2003).

7. References

Beutel, M. W., and A. J. Horne. 1999. A review of the effects of hypolimnetic oxygenation on lake and reservoir water quality. Journal of Lake and Reservoir Management **15** (4): 285-297.

Cooke, G. D., E. B. Welch, S. A. Peterson, and P. R. Newroth. 1993. Restoration and Management of Lakes and Reservoirs, Second edition. Lewis Publishers, Boca Raton.

FERC. 2001. Report on hydroelectric licensing policies, procedures, and regulations. Comprehensive review and recommendations pursuant to section 603 of the Energy Act of 2000. Report submitted to the United States Congress by the Department of Energy. May 8, 2001.

Friedl, G., and A. Wüest. 2002. Disrupting biogeochemical cycles - Consequences of damming. Aquatic Science **64**: 55-65.

FWPCA. 2002. Federal Water Pollution Control Act. [As Amended Through P.L. 107-202, November 27, 2002]. http://www.epa.gov/region5/water/pdf/ecwa.pdf.

Galy-Lacaux, C., R. Delmas, G. Kouadio, S. Richard, and P. Gosse. 1999. Long-term greenhouse gas emissions from hydroelectric reservoir in tropical forest regions. Global Biogeochemical Cycles **13** (2): 503-517.

Hauser, G. E. 2000. Personal communication. TVA Engineering Lab, 129 Pine Rd, Norris, TN 37828.

HRC. 2003. Hydropower Dam Licenses - The Sweetheart Deal of the 20th Century. Hydropower Reform Coalition. www.hydroreform.org.

Jung, R., J. O. Sanders, and H. H. Lai. 1998. Improving water quality through lake oxygenation at Comanche Reservoir. Presentation at the Cal. Lake Manage. Soc., Corte Madera.

Little, J. C., and D. F. McGinnis. 2001. Hypolimnetic Oxygenation: Predicting Performance using a Discrete-Bubble Model. Water Science & Technology: Water Supply **1** (4): 185-191.

Mobley, M. H. 2001. Personal communication. Mobley Engineering, Inc., PO Box 600, Norris, TN 37828.

Sherman, B. 2000. Scoping options for mitigating cold water discharges from dams. CSIRO Land and Water, Canberra. Consultancy Report 00/21, May 2000. Report to: Agriculture, Fisheries and Forestry - Australia, NSW Fisheries, CRC for Freshwater Ecology and NSW Department of Land and Water Conservation as part of NHT Murray-Darling 2001 FishRehab Program.

Stephenson, K. 2000. Taking nature into account: Observations about the changing role of analysis and negotiation in hydropower re-licensing. William and Mary Environmental Law and Policy Review **25** (2): 473-498.

Truffer, B., J. Markard, C. Bratrich, and B. Wehrli. 2001. Green electricity from alpine hydropower plants. Mountain Research and Development **21** (1): 19-24.

USACE. 1998. 3.7.2 Habitat Replacement System. From the Draft Environmental Assessment of Finding of No Significant Impact. R. B. Russell Dam and Lake Project Pumped Storage, November 1998.

Wu, R. S. S., B. S. Zhou, D. J. Randall, N. Y. S. Woo, and P. K. S. Lam. 2003. Aquatic hypoxia is an endocrine disruptor and impairs fish reproduction. Environ. Sci. Technol. **37** (6): 1137-1141.

CHAPTER 2: THE INTERACTION BETWEEN BUBBLE PLUMES AND THE NEAR-FIELD IN LAKES AND RESERVOIRS: INFLUENCES ON PLUME TRANSPORT AND MODELING

D. F. McGinnis[1], A. Lorke[2], J. C. Little[1], A. Wüest[2] and A. Stöckli[3]

[1]*Department of Civil & Environmental Engineering, Virginia Polytechnic Institute and State University, Blacksburg, Virginia 24061-0246, USA*

[2]*Applied Aquatic Ecology, Federal Institute for Environmental Science and Technology (EAWAG), Kastanienbaum, CH-6047, Switzerland*

[3]*Baudepartement des Kantons Aargau, Abteilung für Umwelt, Sektion Gewässer und Betriebsabwasser, CH-5001, Switzerland*

Abstract

A steady-state bubble-plume model is evaluated using full-scale temperature and water quality data collected in a Swiss Lake. Preliminary inconsistencies in the model evaluation led to additional, high-resolution field data collection and careful re-examination of the plume dynamics and plume-lake interaction. The data revealed a plume-generated near-field environment that differed significantly from the ambient far-field water column properties, which were previously used as boundary conditions in the model simulations. The data also revealed that the plume fallback water penetrates much deeper than previously expected. The plume entrains a portion of the fallback water leading to short-circuiting and generating a complex plume-lake interaction. The integral model incorporates the entrainment hypothesis and is therefore highly sensitive to the near-field environmental constituents. It is shown that with the selection of the appropriate near-field boundary profiles, the model agrees well with the field data.

Keywords

Aeration; bubble plume; hypolimnion; transport; oxygen transfer; lake; buoyancy

1. Introduction

As the *in-situ* productivity in most lakes and reservoirs is phosphorus (P) limited (Arbuckle and Downing 2001), excess P loading increases the content of organic matter, which, through decomposition, leads to an elevated oxygen demand (Beutel and Horne 1999). Many stratified, eutrophic lakes do not contain a sufficient supply of hypolimnetic dissolved oxygen (DO) to meet this demand during the stratified season and become anoxic before the advent of deep-water convection in winter (Beutel and Horne 1999). As a result, anoxic products form, such as methane, CO_2, hydrogen sulfide, ammonia, and dissolved iron, manganese or phosphorus, which may further fuel the growth of algae and promote eutrophication under certain circumstances (Cooke et al. 1993, Galy-Lacaux et al. 1999, Gachter and Muller 2003). These pose environmental and drinking water treatment problems, which vary depending on the water body usage. For drinking water sources, oxygen depleted water may lead to taste and odor problems, increased treatment costs, and increase disinfection by-product formation (Cooke et al. 1993). For cold-water fisheries, low hypolimnetic DO stresses or eradicates fish populations, and eggs deposited in anoxic sediments may inhibit development. Furthermore, hypoxia itself has been shown to be an endocrine disruptor, which can disrupt fish reproduction (Wu et al. 2003). Eutrophication also negatively impacts downstream water quality resulting from anoxic reservoir releases (Beutel and Horne 1999). In the case of hydropower reservoirs, the U.S. Federal Energy Regulatory Committee (FERC), as an example, now requires hydropower operators to sustain 5 - 6 mg/L of DO in the turbine release water, which is commonly achieved with the installation of oxygenating bubble-plumes in the withdrawal zone (Mobley 1997) or comparable oxygenation systems such as the Speece Cone (Jung et al. 1998) or full-lift hypolimnetic oxygenator (Burris et al. 2002). Between the years 2000 and 2010, roughly 20% of hydropower plants in the US are required to apply for new FERC licenses (Stephenson 2000), raising the likelihood of significant continuing demand for new oxygenation systems.

The advantage of hypolimnetic oxygenation with bubble-plumes as a mitigation technique in lakes and reservoirs is the replenishment of DO while preserving the hypolimnetic stratification (Nakamura and Inoue 1996, Beutel and Horne 1999). Bubble-plume diffusers are either linear or circular and inject air or oxygen with a relatively weak gas flow rate using small (< 2 mm diameter) bubbles (Wüest et al. 1992, McGinnis et al. 2001). This application lends itself to deeper lakes where the bulk of the bubbles dissolve in the hypolimnion, and the momentum imparted to the plume by the introduction of gas is small enough to prevent intrusion into the thermocline, which could lead to excessive warming of the hypolimnion (Wüest et al. 1992). Furthermore, penetration of P-laden plume water into the photic zone can fuel algal growth. Plume operation will also inevitably increase the far-field vertical transport of P and other constituents (Nakamura and Inoue 1996, Moosmann et al. 2002). To prevent, or at least minimize these potential problems with plume operation, it is important to better understand and properly model the bubble plume, and its interaction with the lake or reservoir environment. Furthermore, for substantial plume operation, the effect of the plume on the lake, and in particular on its near-field environment, may to play a significant role for the plume behavior and related transport.

Specifically lacking in current research is the attention to the plume-lake interactions, and the impact of the near- and far-field bubble-plume effects on its own dynamics. To date, no thorough plume-lake studies have been undertaken which investigate these interactions. While many bubble-plume models have been developed and tested, most were in laboratory settings (McDougall 1978, Asaeda and Imberger 1993, Borchers et al. 1999, Brevik and Kristiansen 2002) or limited in-situ studies (Wüest et al. 1992, Lemckert and Imberger 1993, Johnson et al. 2000, McGinnis et al. 2001). Previous models typically assume steady-state conditions and therefore do not account for short- and long-term temporal and spatial alteration of the density structure or water quality and the ensuing change in plume dynamics and performance. Such changes, specifically in density structure, will result from seasonal (climactic) warming and cooling, reservoir operation (withdrawal), inflow, seiching, and more importantly for this study, the plume operation itself. The reservoir density structure significantly affects the predicted bubble-plume dynamics and the spatial and temporal variability are important considerations in selecting the proper boundary conditions for plume modeling. Furthermore, the altered temperature structure will affect the location of plume water withdrawal (entrainment) and return flow (detrainment) to the far-field environment. This work focuses on identifying and understanding these phenomena, and their impact on modeling bubble-plumes in lakes and reservoirs.

A new theory is suggested that a more complex plume-lake interaction exists than generally assumed, and knowledge of this complex interaction is necessary to correctly simulate the plume dynamics, the oxygen transfer efficiency, and the associated large-scale transport phenomena. This study attempts to resolve this theory using a combination of field-testing techniques and modeling. The primary thrust of this work, therefore, is 1) a detailed study of the bubble-plume and the plume-lake interaction in a Swiss lake, and 2) use this new understanding of the plume behavior for a 1:1 evaluation of the Wüest et al. (1992) bubble-plume model. An extensive background of the model is first presented listing key features, assumptions and uncertainties of the model. The research and testing approach is detailed next, listing features of the lake and bubble-plume diffuser, as well as the methods and specific equipment used. The results and discussion section presents the field study and modeling results in terms of the far-field and near-field plume regions leading to the final conclusions of this study.

2. Bubble-Plume Model

2.1 Assumptions and Key Features

While bubble-plumes are mechanically the least complex oxygenation devices their hydrodynamics are the most complicated (Wüest et al. 1992, McGinnis and Little 1998, Burris et al. 2002). Figure 1 shows the basic, conventional concepts of a bubble-plume in a lake. Gas bubbles are injected into the water column using a porous diffuser, creating a gas-water mixture that is less dense than the surrounding water, and imparting momentum due to a positive buoyancy flux. The positively buoyant mixture rises and entrains water at the boundaries, which increases the water flow rate and cross-sectional area while decreasing the momentum. The plume overcomes the vertical density gradient until the depth of maximum plume rise (DMPR) is reached, i.e. when the plume

momentum reaches zero and the plume cross-sectional area mathematically approaches infinity. At this stage, the plume water is negatively buoyant and falls back to the equilibrium depth (ED) where the plume density matches the ambient density. The fallback water, however, will entrain additional water as it approaches the ED, further decreasing the density. Upon reaching the ED, the plume water spreads horizontally into the far-field. In the far-field, there is a net downward advective transport of water below the ED due to water entrained by the plume below this point. The net advective transport above the ED will be upwards due to the water entrained by the rising plume above the ED and the fallback water.

A model that predicts the hydrodynamics and constituent concentrations in such circular bubble-plumes is investigated (Wüest et al. 1992). The plume model theory is based on the horizontally integrated equations of the conservation of mass, momentum and buoyancy (McDougall 1978). Entrainment is also considered in the model, so that the local entrainment velocity is proportional to the plume velocity and circumference at the same location (McDougall 1978). The plume model also includes the effects of stratification due to vertical temperature and salinity gradients. A key contribution of the Wüest et al. (1992) model was the use of a variable buoyancy flux to account for changing bubble size not only due to decompression and thermal expansion, but also gas dissolution and stripping. Previous studies neglected gas exchange, however this is particularly important in deep systems or weak plumes where gas transfer can be rapid. The variable buoyancy aspect of the plume model has been independently verified under wide ranging conditions, including discrete bubble tests in Tennessee Valley Authority (TVA) laboratories, and in a full-lift hypolimnetic aerator (Burris et al. 2002, McGinnis and Little 2002).

Table 1 lists the key variables of the plume model. Based on eight flux equations (Table 2) that are solved simultaneously, the model predicts water flow rate, water entrainment, gas transfer and constituent concentrations (DO, DN and TDS), DMPR, ED, under the given boundary conditions of the diffuser depth and diameter, applied gas flow rate, initial bubble size, and boundary profiles (temperature, DO, and salinity). The initial velocity is solved for based on a Froude number of 1.6 (Wüest et al. 1992), where

$$Fr = \frac{v}{\left[2\lambda bg\left(\rho_a - \rho_p\right)/\rho_p\right]^{1/2}}.$$

A summary of the key model assumptions is listed below; for a more detailed description, the reader is referred to Wüest et al. (1992). The Boussinesq assumption is used where the gas hold-up, $V_g << 1$ and the gas density is neglected in the momentum equation. A top hat distribution is used for water velocity, temperature, TDS, bubble velocity, and gaseous constituent concentrations. The plume radius for dissolved species and temperature is assumed to be equal to the radius b of the top hat plume velocity profile, while the bubbles occupy an inside core of radius, λb ($\lambda < 1$). Further assumptions are zero currents outside the plume and full turbulence inside the plume. Only advective constituent and momentum transport are considered; whereas transport from turbulent fluctuations is neglected. The bubble diffuser source is assumed to produce bubbles at a

constant rate that are uniformly distributed over the diffuser area, λb_o. Bubble coalescence is neglected, and all bubbles formed at the diffuser are assumed to be of uniform size. Water properties of the initial plume are the same as the ambient water at the diffuser depth. Gas exchange is neglected for gases other then oxygen and nitrogen, but can be easily incorporated by the addition of the appropriate gas conservation equations.

The plume hydrodynamics is strongly determined by the bubble size, the number flux of bubbles (i.e., gas flow rate), and rate of dissolution or expansion. The gas concentration (DO and DN) within the plume is governed by the ambient conditions at the diffuser depth, entrainment of dissolved gases, and the gas dissolution or stripping by bubbles within the plume. Table 2 gives the conservation equations for both the gaseous and dissolved oxygen and nitrogen, but other gasses may be easily included. The model also accounts for the variability of the gaseous concentrations within the bubbles as they rise. This affects the rate of gas transfer, as the concentration driving force is a function of the partial pressure of each gas species within the bubble. The model also uses bubble size dependent equations for bubble rise velocity and mass transfer coefficients, as well as a temperature dependent Henry's coefficient (Table 3). Multiple bubble sizes can also be incorporated by including an array in the gas conservation equations; however, McGinnis and Little (2002) demonstrated that using the Sauter mean diameter (Orsat et al. 1993) resulted in negligible lose in computational accuracy.

2.2 Shortcomings of the Current Model

During the initial evaluation of the model, several inconsistencies became apparent, primarily the substantial underprediction of the DMPR. The model could be calibrated to reach the observed DMPR, but only with large adjustments to the source diameter or initial bubble diameter. In fact, the authors reduced the diffuser diameter from an actual 7 meters to 5 meters for their standard case. However, both the diffuser diameter and initial bubble size should be treated as boundary conditions and not as calibration parameters. Furthermore, forcing the model to reach the measured DMPR by changing these two parameters generated further inconsistencies in predicted plume flow rate, plume temperature and DO during the simulations. Based on a sensitivity analysis, we concluded that the far-field ambient profiles were not adequate boundary conditions, and that near-field temperature and constituent profiles may be necessary to obtain close agreement between plume observations and model predictions. The importance of the location of the boundary profiles in relation to the plume had previously gone unrealized and consequently only ambient pre-diffuser installation, or far-field boundary profiles were used. However, based on the preliminary evaluation, it is evident that model simulations are highly sensitive to these boundary conditions.

3. Research Approach

For the establishment of adequate boundary conditions, a fine-scale spatial resolution of the near-plume environment is required. In order to gain better insight into the near-plume processes, an extensive plume-lake study and therefore, a high-resolution plume measurement campaign was undertaken. The focus of the study is to resolve the boundary conditions, determine the DMPR and in-plume constituent distributions, verify

the entrainment coefficient, and to better quantify the plume fallback behavior. The entrainment resulting in plume spreading is typically treated as a constant, an assumption that is somewhat counterintuitive given the variable nature of the plume flow conditions, namely changes in velocity resulting in different levels of turbulence at the plume-water column interface, interactions at strong density gradients, and mixing that may occur at the DMPR. Furthermore, the spreading rate (or lack of spreading) of the bubble core resulting from entrainment affects the plume rise height and the constituent concentration distributions in the plume (i.e. Gaussian versus top hat). The near-field placement and behavior of the plume return flow, or fallback water is not fully understood and is an area that is typically weakly addressed, but which may have significant interaction with the plume itself (Asaeda and Imberger 1993, Lemckert and Imberger 1993, Brevik and Kristiansen 2002). The far-field response to the plume entrainment (inflow) and detrainment (return flow) is also unclear, and will affect the ultimate location of oxygenated water in the lake and long term changes in plume characteristics.

The in-situ study was undertaken in Lake Hallwil, and the results are used for analysis of the bubble-plume model developed by Wüest et al. (1992). Lake Hallwil is a medium-sized lake located on the Swiss Plateau (Figure 2, Table 4) (Stöckli and Schmid 1987, Wüest et al. 1992, Scheidegger et al. 1994, Wehrli and Wüest 1996). Lake Hallwil is a P-limited, eutrophic lake that has experienced anoxia during the summer time for the past century (Stöckli and Schmid 1987). In 1985, the "Tanytarsus" diffuser system (Figure 3) was installed to combat anoxia and as an ultimate restoration technique (Stöckli and Schmid 1987, Wehrli and Wüest 1996). The system can be switched between artificial circulation mode using air and coarse bubbles, and hypolimnetic oxygenation mode using air or pure oxygen with fine bubbles. The six 6.5-m diameter diffusers in Lake Hallwil are configured in a 300-meter diameter circular arrangement near the center of the lake (Figure 2, Table 4). The diffuser is operated using air or oxygen during the summer season, and air for artificial circulation in the winter. See Table 5 for air and oxygen flow rates for 2001 and 2002.

The lake monitoring and testing program began in April 2001. Measurements primarily focused on the entire lake response to hypolimnetic oxygenation in 2001, and the near-field plume environment in 2002. During 2001, transects were measured weekly to monthly at 18 sampling locations along the long axis of Lake Hallwil (Figure 2) using a Seabird SBE19 CTD profiler. The SBE19 samples at 2 Hz and measures, besides conductivity, temperature and depth (CTD), also DO, light transmission and pH. In 2002, spatially high-resolution (1-2 m) transects were performed across an individual plume. Ropes where mounted on the water surface using existing heavy-duty buoys as well as anchors. A floating rope was placed directly over a single plume and the position of the rope was verified using GPS with no observed movement. 32 profiles were measured, with the 0-m point being located above what visually appeared to be the center of the plume. The profiles were measured every meter from 0 to 10 meters in either direction, then 2 meters from 10 to 20 meters.

During the monitoring program, two thermistor moorings were deployed 100 m from the diffuser ring (M1) and on the north end of Lake Hallwil (M2) (See Figure 2). Although

the thermistor configuration and type varied throughout the study, deployment was nearly constant. The thermistors were high resolution TR-1000 and TR-1050 (Richard Branker Research, LTD; Ottawa, Ontario, Canada), and 12- and 8-bit Vemco Minilog (Vemco, LTD; Nova Scotia, Canada). Additionally, a RD Instruments (RDI) Workhorse 600 kHz and a Nortek NDP 1.5 MHz Acoustic Doppler Current Profilers (ADCP) were deployed on the bottom of the lake facing upward. The ADCPs were positioned near the diffuser ring at M1 (Figure 2) throughout most of the study and measured the 3-dimensional velocity components within 50 cm vertical bins throughout most of the water column.

4. Observations and Model Comparisons

4.1 Far-Field Hypolimnetic Structure

The contour plots from 24 August, 2001 show typical temperature and oxygen contours (Figures 4 and 5, respectively) in Lake Hallwil during the 2001 stratification season when the plume was operated using pure oxygen at the flow rates listed in Table 4. The typical, two-dimensional nature of the mushroom-shaped plume is clearly depicted in the oxygen contours. In the lower region between 25 and 40 meters, the plume-induced structure is much broader than would be expected for the 300-m diameter diffuser ring. The depression of the isotherms in this deep central region indicates the presence of warmer water while the slightly convex isotherms in the shallower region indicate cooler water, demonstrating the plume impact on the lake temperature and DO structure.

The persistent warmer water at lower depths in this seiche-enhanced near-field may be explained by plume water fallback from either detrainment at the top of the plume, detrainment along the rising plume (multiple detrainment), or a combination of both. It was surprising to observe plume fallback water at depths lower then the estimated equilibrium depth (ED) or point of neutral buoyancy. This could also occur due to multiple detrainment, with some denser plume water detraining from lower in the plume. It is further hypothesized that as the higher than ambient density plume water detrains, momentum carries the fallback water past the point of neutral buoyancy (ED) and towards the lake bottom, before finally rising again to the ED, which is estimated to be between 20-30 meters based on the temperature and DO structure in Figures 4 and 5. This phenomenon was also observed to a lesser extent by Lemckert and Imberger (1993) in their plume testing.

A direct observation of the maximum fallback depth was acquired by the ADCP current measurements from June, 2002 (Figure 6). For this purpose, the ADCP was bottom-deployed (upward facing) on the north side of the diffuser ring approximately 30 meters from the northern-most diffuser (Figure 2). The contour plot in Figure 6 shows the measured downward velocity. There were no significant positive-upward velocities measured during this period and these values were omitted from the plot. Downward vertical velocities up to 18 mm/s - much higher then typical vertical velocities in a lake interior (Wüest and Lorke 2003) - were observed as deep as 40 meters. This observational fact is significant, because as the plume rises, it will entrain a large fraction of the fallback water, which has different properties than in the far-field, and may also result in the short-circuiting of plume return flow to the far-field.

Although the oxygen release was constant, the observed downward velocities showed a regular periodicity (Figure 6), which we interpret as the result of plume wandering due to basin-scale internal (baroclinic) seiching of the lake water body (Figure 7). This internal seiching motion explains well the horizontal dispersion of the signature of the plume, which reaches far beyond the extent that would be expected in still water. As indicated on the temperature and DO contour plots (Figures 4 and 5), the horizontal extent of the plume-influenced zone (higher temperature and DO) at the lower depths is approximately 1 km wide and slightly shifted to the right (north), which is much farther than what is expected for the 300-m diameter diffuser ring. Due to the geometry of the basin and a 24-hour wind forcing, rather intense and persistent seiching occurs, typically with a period of approximately 12 hours (Figure 7) (Gwaze 2003). Average hypolimnetic currents are 1 cm/s, and peak at up to approximately 3.5 cm/s during July, 2001 (Figure 7). As the pathway for water moving at 1 (3.5) cm/s over a 6-hour period is 220 (750) meters, seiching can significantly increase the horizontal dispersion of the localized plume signature. These observations further illustrate the complexity of the plume-lake interaction, and support the hypothesis that the plume generates a near-field environment, which strongly affects the plume hydrodynamics and constituent concentrations.

4.2 Compensation Flow in the Far-Field

Depending on operating conditions, a large portion of plume fallback water may be re-entrained by the plume, leading to short-circuiting (Figure 8). This short-circuiting is evident from the calculated plume-induced far-field vertical advective transport compared to the predicted plume entrainment with depth (Figure 9), which in the conventional case should be similar below the ED. The far-field vertical flow was calculated by balancing temperature in layers at different depths. The respective temporal and vertical gradients were determined using the high-resolution thermistor data collected at the mooring installed 100 meters north of the diffuser ring. The horizontally averaged vertical far-field transport is than given by

$$Q(z) = A_z(z)\frac{\partial T/\partial t(z)}{\partial T/\partial z(z)}$$

(positive Q is upward advective transport). To ensure the validity of this calculation, it was first necessary to determine the relative magnitude of the plume-induced mixing (apparent vertical turbulent diffusivity) with respect to the natural turbulent diffusivity. The apparent hypolimnetic turbulent diffusivity was calculated (Powell and Jassby 1974) by

$$k_t = \frac{\int_{z\,max}^{z} A(z')(\partial T(z',t)/\partial t)dz'}{A(z)\cdot(\partial T/\partial z)}.$$

for both the July 13-30, 2001 and May-June, 2002 data and found to be in the range of 0.16 – 17 $cm^2\ s^{-1}$. This range is much higher than the diapycnal diffusivity of approximately 0.03 $cm^2\ s^{-1}$ reported for Lake Alpnach, a Swiss lake of similar size with

stronger wind exposure but with no artificial oxygenation (Wüest et al. 2000). Therefore, the vertical transport induced by the plume is much greater than naturally occurring vertical turbulent diffusivity, so the latter can be considered negligible in the plume-affected hypolimnion. The predicted far-field plume entrainment flow rate at each depth was then estimated by calculating the expected vertical divergence $\partial Q/\partial z$ of the far-field transport from the plume model. This can then be directly compared to the observed far-field advective transport, as any water entrained by the upward plume at a particular depth below the ED should result in an equal amount flowing downward in the far-field to replace it. These estimates neglect plume fallback entrainment or further mixing at the DMPR.

Figure 9 shows the results of the observed far-field advective transport with depth compared to the predicted plume transport for the July 13-30, 2001 thermistor data. The plume was operated using pure oxygen at 5.1 t/d (at 25 $Nm^3\ hr^{-1}$ for each of the six diffusers), 80% of the June 2002 airflow rate (Table 5). The model underpredicts the DMPR due to the improper selection of boundary profiles, which is explained in more detail below. However, the predicted water flow rate below the ED should be close to the calculated range. For July 2001, while the shape of the observed and predicted curves do not closely match, the averaged integrated total flow below the minimum flow at 31 m for both the measured and predicted curves is within 10%. The differences in the shapes of these two curves will also be discussed in greater detail. It is thought that the point where the far-field flow Q = 0 at 23 meters is the upper extent of the ED with the bottom extent at around 31 meters, immediately above the minimum calculated Q. Where Q = 0 at 16 meters is the actual average DMPR over the 18-day period, while the model predicts a DMPR of 18.7 m.

Both the calculated and measured DMPRs, however, are well below the lower extent of the thermocline, which is at approximately 10 meters depth during this period. The depth from 16-23 meters shows a cooling, or upward flow of water, similar to observations during laboratory tests performed by McDougall (1978) for weak plumes. This upward flow is a result of plume entrainment above the ED plus further entrainment of the fallback water, effectively removing water from the far-field above the ED and placing it in the region of the ED. This suggests a weaker, well-defined plume flow and perhaps only a single detrainment at the top, limiting any short-circuiting to the zone above the lower extent of the ED at 31 meters.

The same analysis performed on the May-June, 2002 data when the plume was operated with air instead of pure oxygen at 30 x 6 $Nm^3\ hr^{-1}$ yield very different results (Figure 9). The observed far-field advective flow is significantly lower then that estimated from the plume model, with a nearly normal distribution in the observed flow rate versus depth. Furthermore, the area of upward advective flow is absent. Several important conclusions can be drawn from these results. The first is that the observed plume-induced advective far-field flow is much less then expected based on the plume model predictions, which is likely a result of short-circuiting of the plume fallback and ultimate return water. Secondly, the considerable underprediction in the observed far-field flow rate points to short-circuiting at all locations along the plume. These results suggest that either the

fallback water is almost reaching the lake bottom, multiple detrainment is occurring along the length of the plume similar to the observations of McDougall (1978) in lab experiments for strong plumes, or both.

Finally, there is an alteration in the isotherms near the plume due to enhanced mixing, with the near-field water being more vertically homogenous than the far-field temperature structure (Figure 9). That is, the temperature isopleths are much farther apart near the plume and at different depths than in the far-field. Assuming that the bulk advective transport from the far-field occurs along the isopycnals, this results in a somewhat normal distribution of advective vertical transport, rather then a linearly increasing flow rate as would be expected if the isotherms where truly horizontal and unaltered by the plume (see Figure 8). The more vigorous mixing resulting in a more homogeneous near-field density structure may allow the fallback water to reach greater depths as the fallback water encounters less density resistance. Additionally, the fact that there is no upward far-field advection, shown by the lack of an upward Q in Figure 9, indicates a warming in the entire hypolimnion due to plume penetration into and subsequent erosion of the themocline resulting in a net downward heat flux from the thermocline. This case can be thought of as a slow destratification of Lake Hallwil.

4.3 Plume-Affected Near-Field Environment

Based on the above observations, it was decided to probe the plume and its near-field at a much higher spatial resolution. Figures 10-12 show such high-resolution contour plots for temperature, DO and light transmission for July 18, 2002, when the diffuser load was air at 30 x 6 $Nm^3\ hr^{-1}$, corresponding to 1.3 t-O_2/d (Table 6). From the contour plots, the plume seems highly turbulent and inhomogeneous in nature. The high-resolution temperature contour plot (Figure 10) indicates an approximately normal distribution as expected. The maximum DMPR is 7.5 meters with the average DMPR of 9.4 meters taken at the 8°C contour line. Multiple detrainment occurs in the northerly (left) direction, as indicated by the temperature, DO and light transmission data (Figures 10-12). Such detrainment is probably the result of horizontal advective cross flow due to internal seiching. The depression in the temperature isopleths and the higher DO that penetrates almost to the lake bottom immediately to the left (north) of the plume is a result of either detrained water that passes the ED due to momentum, or local draw-down resulting from plume up flow.

Throughout the plume, the DO concentration is substantially lower than in the ambient lake water. The reason is that the plume initially entrains water from the anoxic bottom-boundary layer and the DO increase in the rising plume due to gas transfer from the air released from the diffuser (instead of oxygen) is only a small amount. Under this circumstance, the change in DO concentration within the plume is dominated by the initial conditions at the diffuser, and entrainment of surrounding water. This causes the plume to appear as though it is pumping anoxic water from the BBL into the hypolimnetic interior.

Another interesting feature shown on the light transmission contour are the spikes of low transmissivity within the plume. These spikes are a result of bubbles passing the light

transmission meter, suggesting the location of the bubble core (Figure 12). Lines where superimposed on Figure 12 to indicate the extent of the bubble core, which appears almost not to spread. The bubbles are travelling approximately 20 cm s^{-1} faster than the plume water, making them less subject to spreading due to entrainment as there is considerably less bubble contact time. While not conclusive, this almost non-expanding bubble core agrees with the laboratory observations of McDougall (1978), while the bubble-plume model of Wüest et al. (1992) assumes the bubble core expands in width at the same rate as the outer core, and occupies an area of λb. This issue will be addressed further in the discussion section.

It is obvious that the plume dynamics are highly complex, and non-homogeneous. It is clear from these observations that the appropriate boundary profiles and subsequent entrained water properties are also not homogenous or immediately obvious and will exhibit spatial and temporal variability from seiching, plume operation, and changes in the constituent properties of the water column. Additionally, the concentrated bubble core will result in a higher local rise height than the top-hat assumption, or even a Gaussian profile would yield. These conclusions lead to the need for further analysis of appropriate boundary conditions.

4.4 Plume Sensitivity to the Near-Field

Superimposed on the contour plots (Figures 10-12) are the plume model predictions for plume diameter as a function of depth, and the DMPR based on the averaged boundary profiles measured 5 meters on either side of the center of the plume and using the values listed in Table 6. Using the indicated profiles, the plume model predicts the DMPR and rate of spread extremely well given the top hat assumption versus the actual approximately Gaussian distribution. Figure 13 shows the averaged measured in-plume temperature and DO profile and the plume-model predictions. The predicted temperature profile fits reasonable well, but seems to diverge at 20 meters depth to approximately 0.3°C less than the measured temperature. This may be a result of using improper boundary profiles, because, depending on the direction and strength of the horizontal hypolimnetic current velocities and the plume interaction at the stronger temperature gradient, the plume may entrain and detrain water at different rates and with different properties around the plume.

Furthermore, the plume average is only based on the two-dimensional transect and the properties may also be laterally inhomogeneous. The diffuser geometry and bubble distribution may also be non-uniform. As evident in Figures 10-12, the plume boundaries are not well defined due to inhomogeneity from seiche and detrainment effects. Plume oxygen profiles are further evidence of the inhomogeneity, showing a slight underprediction of the DO concentration (Figure 13). It is clear from Figure 13 that using a single profile for the model calculation may not be appropriate under such inhomogeneous boundary conditions, and the average of several profiles from the plume boundary may yield better results.

Figure 14 shows the sensitivity analysis performed using different boundary profiles along the length of the transect (x-axis indicates distance of boundary profile from plume

centerline). As described above, the DMPR is shallower using profiles closest to the center, as the vertical density structure is more homogeneous. The predicted DMPR deepens sharply with boundary profiles farther then 5 meters from the plume center, particularly when using the southerly profiles, the direction from which the seiche current is suspected during the transect. The DMPR tends to become more stable with increasing distance from the diffuser due to more uniform vertical profiles.

As previously described, the ED is calculated by matching the final density of the plume water with the density at depth using the boundary profile. Variations occur because a small change in the final density of the plume water at the DMPR can result in a substantial difference in the ED placement in the less-stratified bottom water. Also, because the plume is reaching a strong temperature gradient as it stops rising, a small increase in predicted DMPR translates into a relatively large change in the predicted density, i.e., the higher the water rises, the less dense it becomes. It is important to note that the ED is based only on a density comparison, and that it assumes no further entrainment by the fallback water. The ED predictions are also less variable with increasing distance from the plume, and in reality, probably occur over a vertical zone because of multiple detrainment, through-flow, and entrainment by the fallback water.

5. Deficiencies of the Current Plume Model

A key assumption in the bubble-plume model is that entrainment is constant throughout the plume. This may not be the case, particularly at locations where the plume flow becomes more turbulent at the boundaries, or at the plume/thermocline interface at the DMPR (Brevik and Kristiansen 2002). This may account for the underprediction in the temperature and DO, particularly at shallower depths due to the fact that the plume is short-circuiting, re-entraining fallback water with higher DO and temperature than the ambient water, or enhanced turbulent mixing at the DMPR interface. Additionally, there is multiple detrainment, plume wandering and cross flow due to seiching; all of which may also enhance or alter the plume entrainment coefficient and the boundary conditions. Figures 10-12 indicate that there appears to be cross flow in the northerly (+) direction resulting in multiple detrainment. This is consistent with seiche observations in Lake Hallwil during 2001-2002. Currently, there is no method for the plume model to account for cross flow or plume wandering.

In summary, the following deficiencies of the model are obvious:

1. In reality, there is plume wandering, cross flow and multiple detrainment, all of which result in changing boundary conditions.
2. The entrained water is not from the far-field but from the near-field torus, which definitely has different properties than the far-field. Furthermore, fallback water is re-entrained by the plume resulting in short-circuiting and reducing return flow to the far-field.
3. The torus and seiche-enhanced near-field are much more mixed than the ambient, or far-field environment, with the deeper water being less dense and the upper water being more dense than the ambient.

Similar to the observations of McDougall (1978), and contradictory to the model assumptions, it appears from the light transmission contour plot (Figure 12) that the bubble core does not spread at the same rate as the plume. Due to the top hat assumption, the model is not sensitive to bubble spreading, and this will not change the plume predictions. However, this will result in a higher concentration of bubbles in the plume core and therefore a higher localized buoyancy flux, causing faster inner core water velocities and a higher local rise height. Also, if the inner bubble core does not spread, the positive buoyancy flux is less distributed across the width of the plume, and more concentrated in the core, making it more likely for the plume to detrain, or "peel away" at multiple locations, as the outer core will more rapidly become negatively buoyant and loose momentum.

6. Conclusions

A steady-state, horizontally averaged bubble-plume model was evaluated on a 1:1 scale using high-resolution CTD data collected in Lake Hallwil, Switzerland. This study was motivated by inconsistencies between the model and observations in lakes that have been exposed to aeration and artificial mixing by bubble plumes, and aimed at resolving the boundary conditions and the plume-lake interaction. Observations of the plume near-field revealed the following:

- The plume-lake interaction was found to be much more complex than previously believed. The plume creates its own local environment on two different scales: the plume torus, where the directly detrained water and fallback water are accumulated over tens of meters off the plume, while the seiche-enhanced near-field of the plume, clearly showing different water properties, reaches up to ½ km in either direction. This distance is governed by the internal seiche velocities and the corresponding horizontal cross flow.
- It is shown from the data that the plume fallback and mixing results in a more homogeneous density structure in the plume torus. This leads to a shallower plume rise height, as there is less of a density gradient to overcome. Therefore, to properly model the plume hydrodynamics, it was necessary to re-evaluate the appropriate model density boundary conditions.
- Because a significant portion of entrained plume water is from the torus itself, the plume temperature and constituent concentrations depend strongly on that region as well, which is created by the plume itself. Therefore, the plume properties and model predictions are strongly dependent on these continually changing near-field boundary conditions.
- Using the new boundary conditions rather than the far-field produced excellent agreement, with a higher predicted depth of maximum plume rise and closer constituent predictions.
- The data also show that the plume fallback is much deeper than expected and leads to considerable short-circuiting of the return flow, and a subsequent loss of oxygen transport to the entire lake as the fallback water is re-entrained by the plume. It is unclear whether the deep fallback is primarily due to multiple detrainment or the more isothermal plume torus. This fallback may alter the entrainment coefficient due to enhanced turbulence at the plume interface and

also reduces the mass flux of oxygen advectively transported to the far-field lake interior.

- While not affecting the model results, the bubble core was found not to spread, which requires particular attention to the interpretation of the model results as the bubble-plume will in reality rise locally higher then predicted, possibly penetrating the thermocline or photic zone. This will also increase the likelihood of multiple detrainment, as the positive buoyancy flux imparted by the gas bubbles is less distributed over the plume outer-core.
- Because the water flowing from the far-field to the plume travels along the isopycnals, the altered isotherms in the torus affect where water is withdrawn from the far-field into the plume.

Future work includes data collection over different gas flow conditions, and the use of pure oxygen versus air. Moreover, as initial bubble-size strongly affects the buoyancy and the dissolved gas concentrations, laboratory measurements of the initial bubble-size formed at the diffuser will be performed. It is evident, however, that a method needs to be made available to predict the altered near-field, short circuiting, and fallback past the equilibrium depth. One method currently being tested is a coupled plume-reservoir model using the Wüest et al. (1992) plume model described in this paper and a two-dimensional reservoir model, CE-QUAL-W2 (Cole and Wells 2000). This coupled model is currently under development to predict the plume dynamics, and the near- and far-field responses. It may, however, require the addition of a plume fallback model, to accurately predict the transport of water in the lake or reservoir. Using the now validated bubble-plume model with CE-QUAL-W2 should result in a fully predictive tool to aid in the design of new bubble-plume diffusers when appropriate boundary conditions are unavailable. A temperature and dissolved oxygen predictive version has been tested using a linear version of the bubble-plume model discussed in this work with good preliminary results (McGinnis et al. 2001, McGinnis et al. 2003). The coupled lake-reservoir model would then be used to further investigate the plume models in full-scale lake settings to better understand the plume-lake interaction, plume-enhanced mixing and warming, and other aspects such as variable entrainment, or nitrogen supersaturation in the case of air. The validated, coupled plume-reservoir model should also prove to be a valuable tool to operationally enhance existing systems, investigate the effectiveness of bubble-plumes in drinking water sources, perform economic optimizations for proposed or existing systems, and to identify future research needs.

7. Nomenclature

A	lake area, m^2.
b	plume diameter, m.
C	dissolved concentration, mol m^{-3}.
E	entrainment, m^2 s^{-1}.
F_D	dissolved species flux, mol s^{-1}.
F_G	gaseous species flux, mol s^{-1}.
Fr	Froude number, -.
F_S	salinity flux, g s^{-1}.
F_T	temperature flux, ^oC m^3 s^{-1}.

g	gravitational acceleration, m s^{-2}.
H	Henry's coefficient, mol m^{-3} bar^{-1}.
k_t	apparent vertical turbulent diffusivity, cm^2 s^{-1}.
K_L	mass transfer coefficient, m s^{-1}.
M	water momentum, m^4 s^{-2}.
N	number flux of bubbles, s^{-1}.
P	pressure, bar.
Q	plume or far-field flow rate, m^3 s^{-1}.
r	bubble radius, m.
S	salinity, g kg^{-1}.
t	time, s.
T	temperature, ^oC.
V_g	gas holdup, -.
v	velocity, m s^{-1}.
z	depth, m.

Greek letters

α	entrainment coefficient, -.
λ	plume radius ratio, -.
ρ	density, kg m^{-3}.

Subscripts

a	ambient water
b	bubble
i	gas species, oxygen or nitrogen
p	plume water and gas mixture
w	plume water

8. References

Arbuckle, K. E., and J. A. Downing. 2001. The influence of watershed land use on lake N:P in a predominantly agricultural landscape. Limnol. Oceanogr. **46** (4): 970-975.

Asaeda, T., and J. Imberger. 1993. Structure of bubble plumes in linearly stratified environments. J. Fluid Mech. **249**: 35-57.

Beutel, M. W., and A. J. Horne. 1999. A review of the effects of hypolimnetic oxygenation on lake and reservoir water quality. Journal of Lake and Reservoir Management **15** (4): 285-297.

Borchers, O., C. Busch, A. Sokolichin, and G. Eigenberger. 1999. Applicability of the standard k-e turbulence model to the dynamic simulation of bubble columns. Part II: Comparison of detailed experiments and flow simulations. Chemical Engineering Science **54**: 5927-5935.

Brevik, I., and Ø. Kristiansen. 2002. The flow in and around air-bubble plumes. International Journal of Multiphase Flow **28**: 617-634.

Burris, V. L., D. F. McGinnis, and J. C. Little. 2002. Predicting oxygen transfer rate and water flow rate in airlift aerators. Water Research **36**: 4605-4615.

Cole, T. M., and S. A. Wells. 2000. CE-QUAL-W2: A two-dimensional, laterally averaged, Hydrodynamic and Water Quality Model, Version 3.0, Instruction Report EL-2000-. US Army Engineering and Research Development Center, Vicksburg, MS.

Cooke, G. D., E. B. Welch, S. A. Peterson, and P. R. Newroth. 1993. Restoration and Management of Lakes and Reservoirs, Second edition. Lewis Publishers, Boca Raton.

Gachter, R., and B. Muller. 2003. Why the phosphorus retention of lakes does not necessarily depend on the oxygen supply to their sediment surface. Limnol. Oceanogr. **48** (2): 929-933.

Galy-Lacaux, C., R. Delmas, G. Kouadio, S. Richard, and P. Gosse. 1999. Long-term greenhouse gas emissions from hydroelectric reservoir in tropical forest regions. Global Biogeochemical Cycles **13** (2): 503-517.

Gwaze, S. 2003. Structure, Dynamics and Energetics of Internal Waves in Lake Hallwil. M.Sc. IHE-DELFT, Delft.

Johnson, G. P., N. J. Hornewer, D. M. Robertson, D. T. Olson, and J. Gioja. 2000. Methodology, data collection, and data analysis for determination of water-mixing patterns induced by aerators and mixers. Water-Resources Investigations Report 00-4101, U.S. Department of the Interior, U.S. Geological Survey, Urbana, Illinois.

Jung, R., J. O. Sanders, and H. H. Lai. 1998. Improving water quality through lake oxygenation at Comanche Reservoir. Presentation at the Cal. Lake Manage. Soc., Corte Madera.

Lemckert, C. J., and J. Imberger. 1993. Energetic bubble plumes in arbitrary stratification. Jour. Hyd. Eng. **119** (6): 680-703.

McDougall, T. J. 1978. Bubble plumes in stratified environments. J. Fluid Mech. **85** (4): 655-672.

McGinnis, D., J. C. Little, and A. Wüest. 2003. Coupling bubble-plume and reservoir models: plume-induced mixing and transport. **In preparation**.

McGinnis, D. F., and J. C. Little. 1998. Bubble dynamics and oxygen transfer in a Speece Cone. Water Science & Technology **37** (2): 285-292.

McGinnis, D. F., and J. C. Little. 2002. Predicting diffused-bubble oxygen transfer rate using the discrete-bubble model. Water Research **36**: 4627-4635.

McGinnis, D. F., J. C. Little, and A. Wüest. 2001. Hypolimnetic oxygenation: Coupling bubble-plume and reservoir models. Proceedings of Asian Waterqual 2001, First IWA Asia-Pacific Regional Conference, Fukuoka, Japan.

Mobley, M. H. 1997. TVA reservoir aeration diffuser system. TVA Technical Paper 97-3. ASCE Waterpower '97, Atlanta, GA, August 5-8.

Moosmann, L., D. McGinnis, and A. Wüest. 2002. Erhöhte Sauerstoffzehrung im Sommer 2001 im Hallwilersee - Ursachen und Handlungsmöglichkeiten. EAWAG Report to Canton Aargau.

Nakamura, Y., and T. Inoue. 1996. A theoretical study on operation condition of hypolimnetic aerators. Wat. Sci. Tech. **34** (7-8): 211-218.

Orsat, V., C. Vigneault, and G. S. V. Raghavan. 1993. Air diffusers characterization using a digitized image analysis system. Applied Engineering in Agriculture **9** (1): 115-121.

Powell, T., and A. Jassby. 1974. The estimation of vertical eddy diffusivities below the thermocline in lakes. Water Resour. Res. **10** (2): 191-198.

Scheidegger, A., A. Stöckli, and A. Wüest. 1994. Einfluss der internen Sanierungsmassnahman auf den Sauerstoffhaushalt im Hallwilersee. Wasser, Energie, Luft **86** (5/6): 126-131.

Stephenson, K. 2000. Taking nature into account: Observations about the changing role of analysis and negotiation in hydropower re-licensing. William and Mary Environmental Law and Policy Review **25** (2): 473-498.

Stöckli, A., and M. Schmid. 1987. Die Sanierung des Hallwilersees. Wasser, Energie, Luft **79** (7/8): 143 - 149.

Wehrli, B., and A. Wüest. 1996. Zehn Jahre Seenbelüftung: Erfahrungen und Optionen. Report for EAWAG, No. 9.

Wu, R. S. S., B. S. Zhou, D. J. Randall, N. Y. S. Woo, and P. K. S. Lam. 2003. Aquatic hypoxia is an endocrine disruptor and impairs fish reproduction. Environ. Sci. Technol. **37** (6): 1137-1141.

Wüest, A., N. H. Brooks, and D. M. Imboden. 1992. Bubble plume modeling for lake restoration. Water Resources Research **28**: 3235-3250.

Wüest, A., and A. Lorke. 2003. Small-Scale Hydrodynamics in Lakes. Annu. Rev. Fluid Mech. **35**: 373-412.

Wüest, A., G. Piepke, and D. C. Van Senden. 2000. Turbulent kinetic energy balance as a tool for estimating vertical diffusivity in wind-forced stratified waters. Limnol. Oceanogr. **45** (6): 1388-1400.

Table 1. Key plume model variables.

Variable	Formula	Units
Entrainment	$E = 2\alpha\pi bv$	$m^2\ s^{-1}$
Plume Water Volume Flux	$Q = \pi b^2 v$	$m^3\ s^{-1}$
Momentum Flux	$M = \pi b^2 v^2$	$m^4\ s^{-2}$
Temperature Flux	$F_T = QT_p$	$^oC\ m^3\ s^{-1}$
Dissolved Solids Flux	$F_S = QS\rho_W$	$g\ s^{-1}$
Dissolved O_2 and N_2 Fluxes	$F_{Di} = QC_i$	$mol\ s^{-1}$
Gaseous O_2 and N_2 Fluxes	$F_{Gi} = Q\lambda^2(v + v_b)y_i$	$mol\ s^{-1}$

Table 2. Non-linear differential flux equations.

Water Volume Flux	$\frac{dQ}{dz} = E$
Momentum Flux	$\frac{dM}{dz} = \frac{\rho_a - \rho_p}{\rho_p} g\pi b^2 \lambda^2 + \frac{\rho_a - \rho_w}{\rho_p} g\pi b^2 (1 - \lambda^2)$
Temperature Flux	$\frac{dF_T}{dz} = ET_a$
Salinity Flux	$\frac{dF_S}{dz} = E\rho_a S_a$
Dissolved Gas Flux (DO and DN)	$\frac{dF_{Di}}{dz} = EC_{ia} + \frac{4\pi r^2 N}{v + v_b} K_L (H_i P_i - C_i)$
Gas Flux (DO and DN)	$\frac{dF_{Gi}}{dz} = -\frac{4\pi r^2 N}{v + v_b} K_L (H_i P_i - C_i)$

Table 3. Correlation equations for Henry's constant, mass transfer coefficient, and bubble rise velocity (Wüest et al., 1992)

Equation	Range
$H_O = 2.125 - 5.021 \times 10^{-2}T + 5.77 \times 10^{-4}T^2$ (mol m^{-3} bar^{-1})	(T in Celsius)
$H_N = 1.042 - 2.450 \times 10^{-2}T + 3.171\times 10^{-4}T^2$ (mol m^{-3} bar^{-1})	
$K_L = 0.6r$ (m s^{-1})	$r < 6.67 \times 10^{-4}$ m
$K_L = 4 \times 10^{-4}$ (m s^{-1})	$r \geq 6.67 \times 10^{-4}$ m
$v_b = 4474r^{1.357}$ (m s^{-1})	$r < 7 \times 10^{-4}$ m
$v_b = 0.23$ (m s^{-1})	$7 \times 10^{-4} \leq r < 5.1 \times 10^{-3}$ m
$v_b = 4.202r^{0.547}$ (m s^{-1})	$r \geq 5.1 \times 10^{-3}$ m

Table 4. Characteristic features of Lake Hallwil and the diffuser system.

Maximum depth [m]	48
Mean depth [m]	28.9
Surface area [10^6 m^2]	9.9
Total water volume [10^6 m^3]	280
Diffuser geometry	circular
Number of diffusers [-]	6
Diffuser diameter [m]	6.5
Average diffuser depth [m]	47
Gas flow rate [Nm^3 h^{-1}]*	30 – 210 (O_2) 180 – 510 (air)

Table 5. Diffuser air and oxygen flowrates through 2001-2002 monitoring program

Start date	Mode	Q ($Nm^3\ hr^{-1}$)	O_2 input (tons day^{-1})
4/2/2001	aeration	180	1.3
5/7/2001	oxygenation	60	2.0
6/25/2001	aeration	180	1.3
7/2/2001	oxygenation	60	2.0
7/13/2001	oxygenation	150	5.1
8/22/2001	oxygenation	210	7.1
10/15/2001	oxygenation	150	5.1
10/23/2001	aeration	180	1.3
10/30/2001	circulation	510	3.6
1/20/2002	circulation	240	1.7
3/18/2002	aeration	180	1.3
7/22/2002	oxygenation	120	4.1
9/30/2002	aeration	180	1.3

Table 6. Model base line conditions for a single diffuser.

Parameter	Nomenclature	Value
Diffuser Depth, m	$z°$	47
Initial plume area, m^2	$\pi b°^2$	33.2
Entrainment factor	α	0.11
Plume radius ratio	λ	0.8
Initial Froude number	$Fr°$	1.6
Air flow rate, $Nm^3\ hr^{-1}$	$Q_g°$	30
Initial bubble diameter, mm	$r°$	2

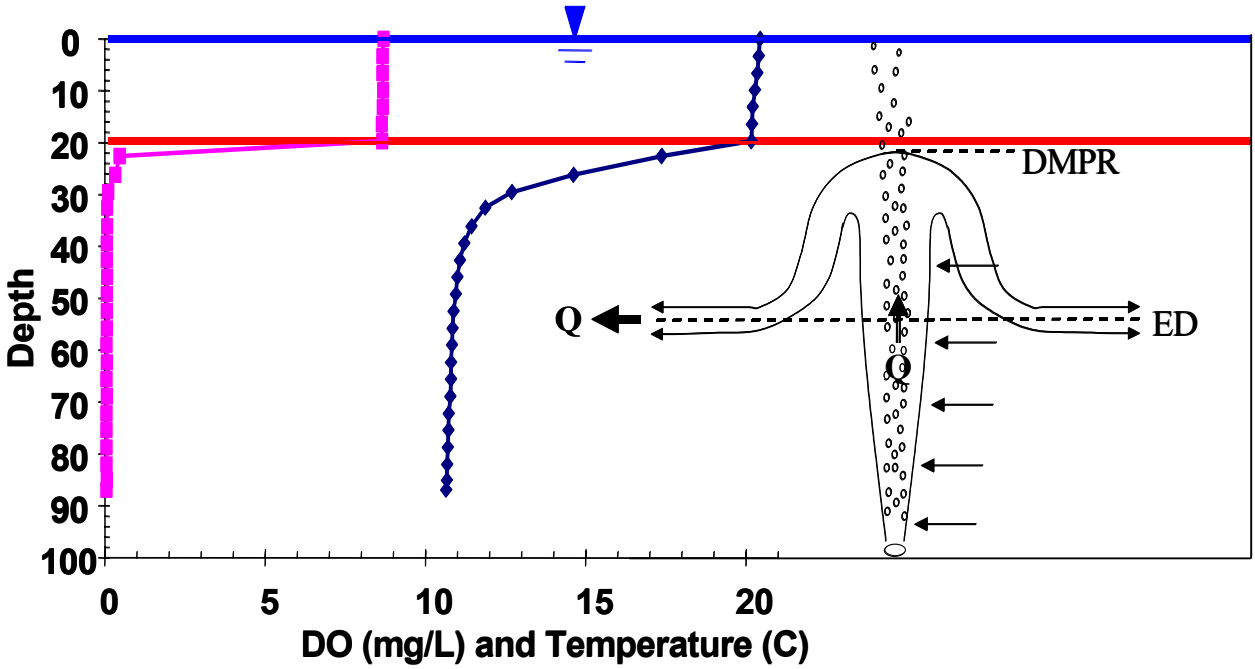

Figure 1. Schematic of bubble-plume in a lake.

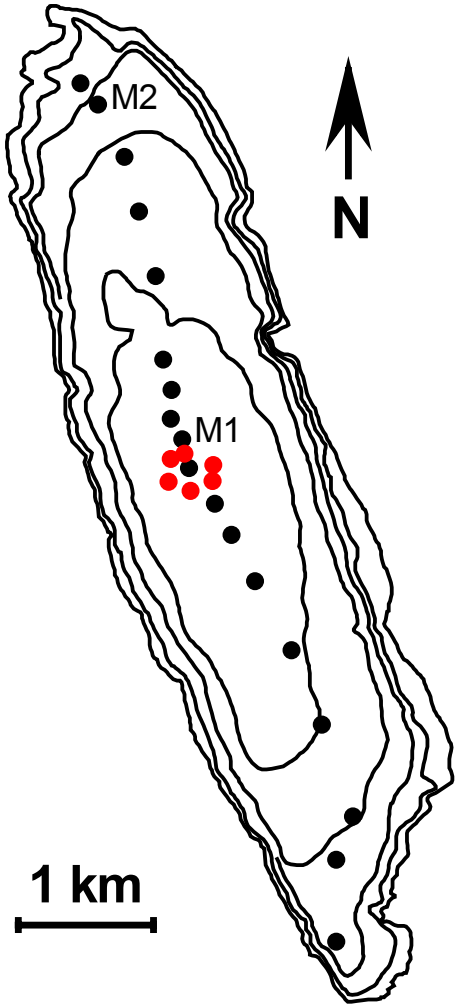

Figure 2. Lake Hallwil bathymetry showing sampling stations (black dots), diffuser locations (red dots), mooring 1 (M1) and mooring 2 (M2).

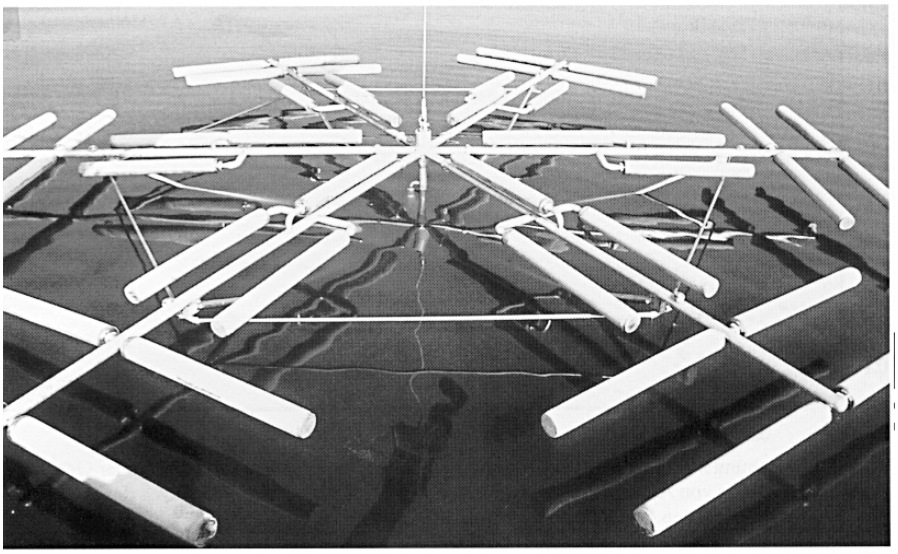

Figure 3. 6.5-m diameter Tanytarsus diffuser system.

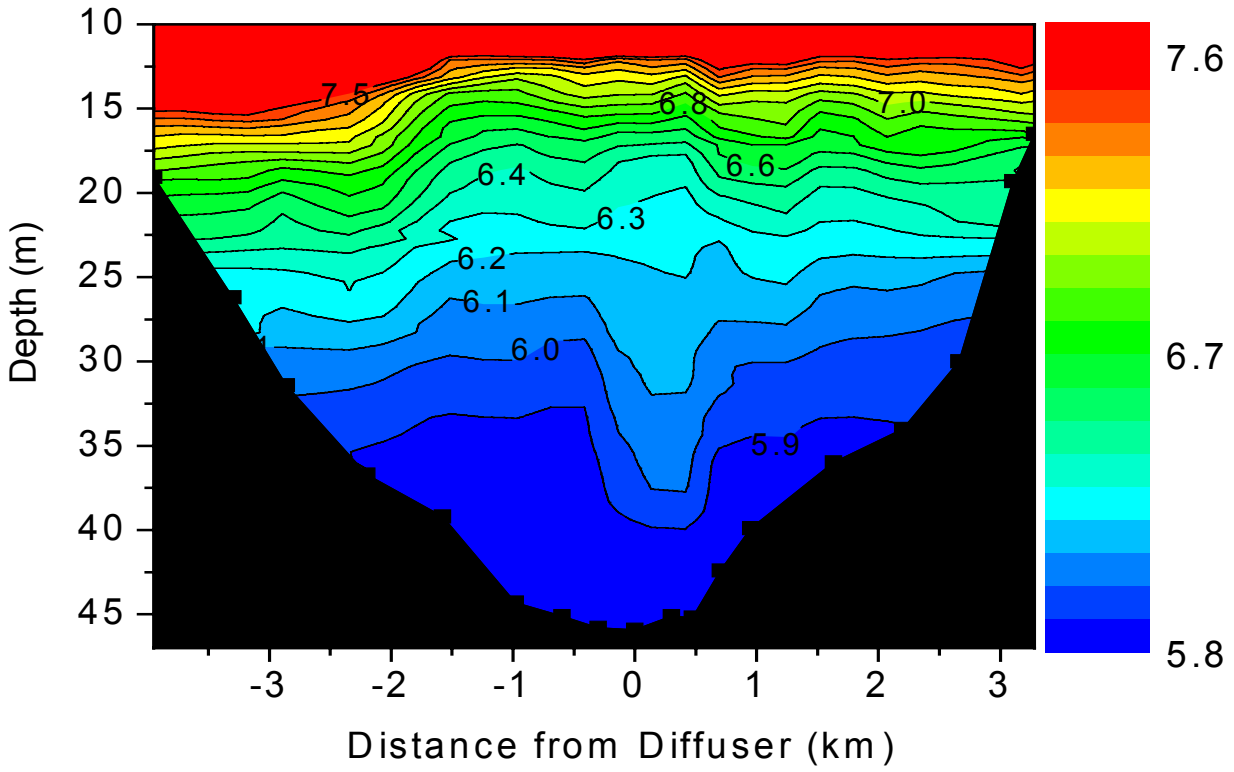

Figure 4. 24 July, 2001 temperature contours (°C). The x-axis zero point is located at the center of the 300-meter diameter diffuser ring. The contours were interpolated from 18 CTD profiles (locations indicated by black squares at the bottom of the plots) sampled along the centerline of the lake (Figure 2 – map showing sampling points).

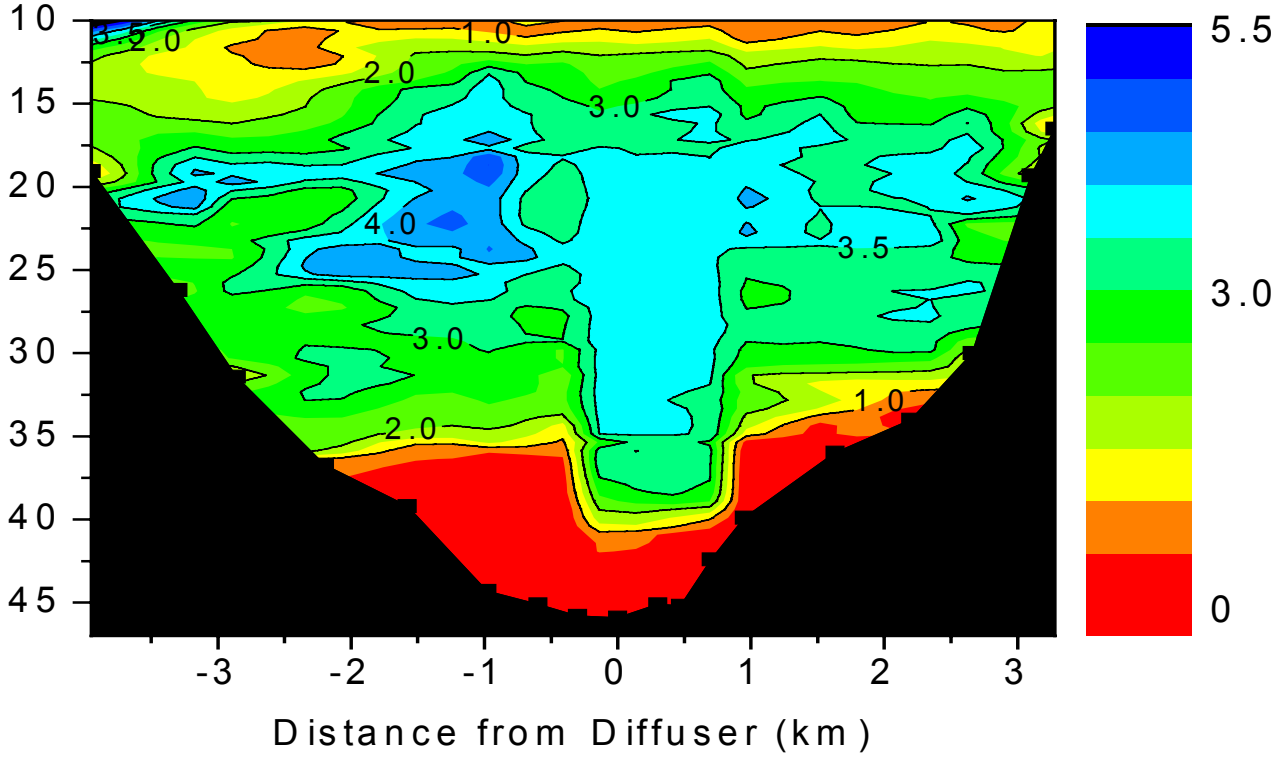

Figure 5. 24 July, 2001 DO contours (g m^{-3}). The x-axis zero point is located at the center of the 300-meter diameter diffuser ring. The contours were interpolated from 18 CTD profiles (locations indicated by black squares at the bottom of the plots) sampled along the centerline of the lake (Figure 2 – map showing sampling points).

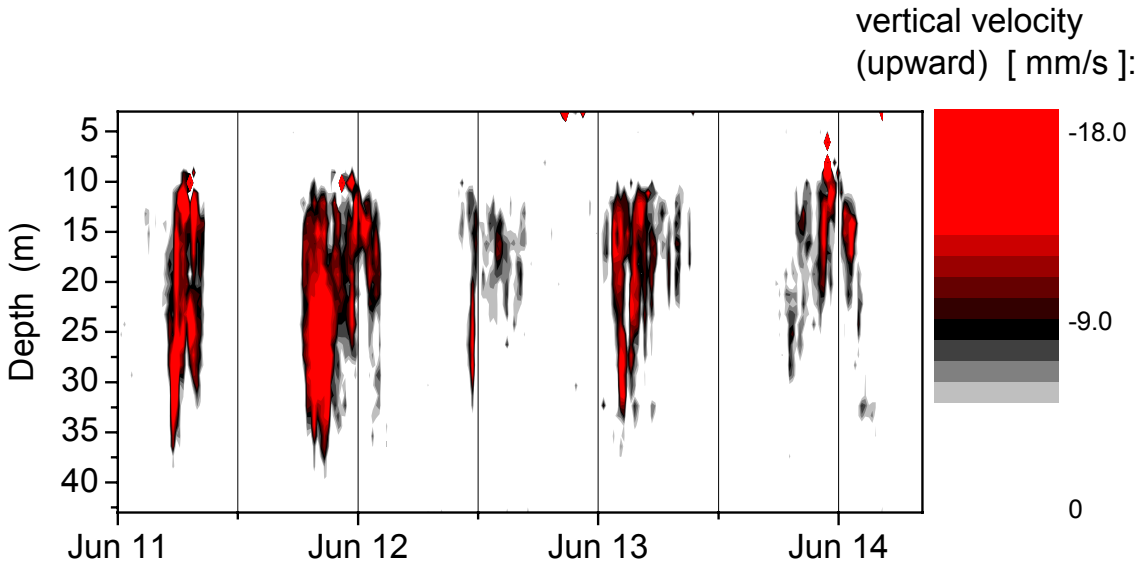

Figure 6. ADCP (RDI) measurements in June 2002 showing downward flowing water near the northern diffuser (M1 in Figure 2). For clarity, velocities greater then –5.0 mm/s are omitted from the plot. The 12-hour periodicity in downwelling measurements is plume wandering due to seiching.

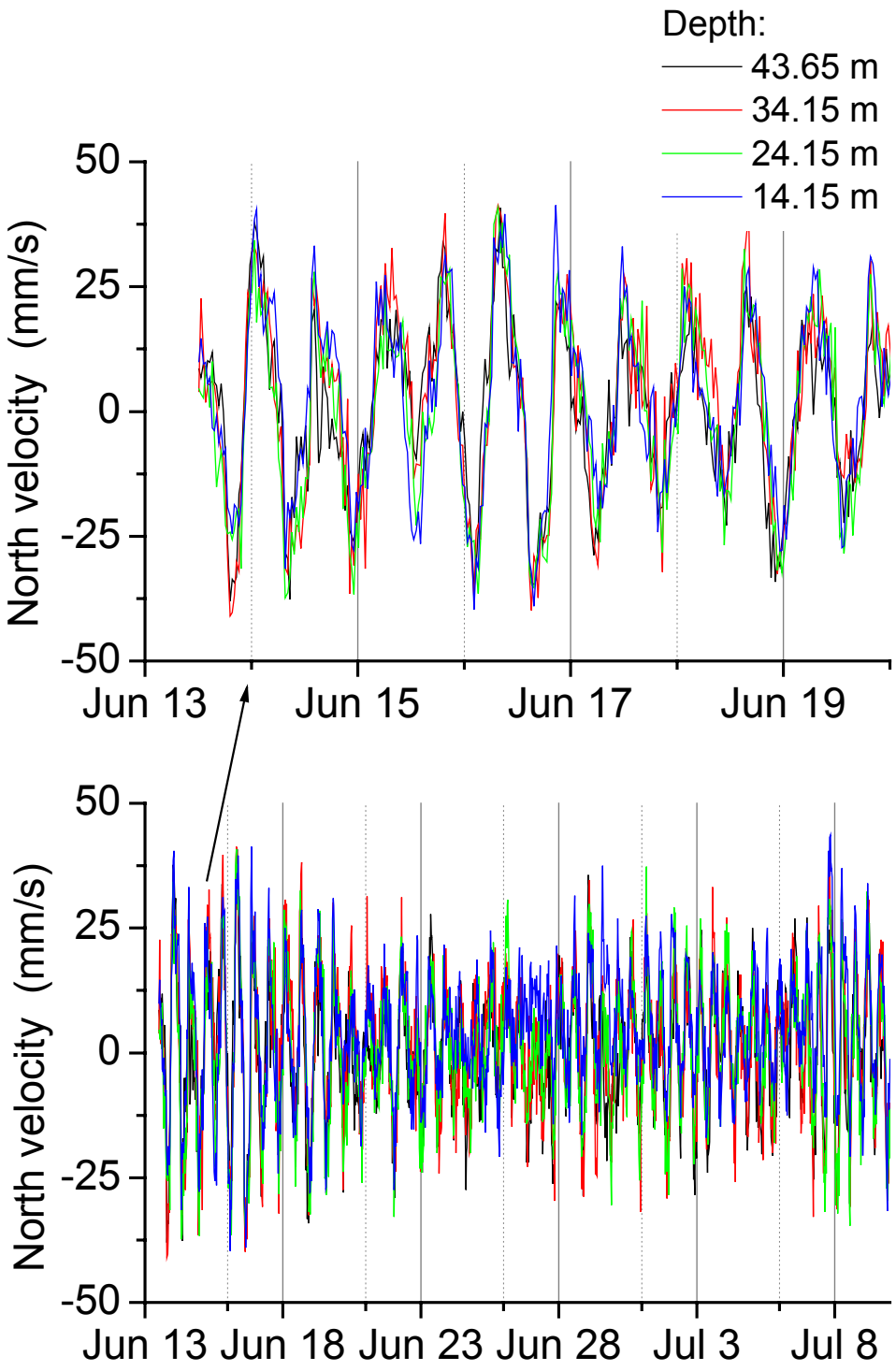

Figure 7. ADCP (NORTEK) measured in June-July 2002 showing hypolimnetic horizontal (northerly) current velocities. Current velocities are nearly constant with depth in the hypolimnion with a periodicity of approximately 12 hours.

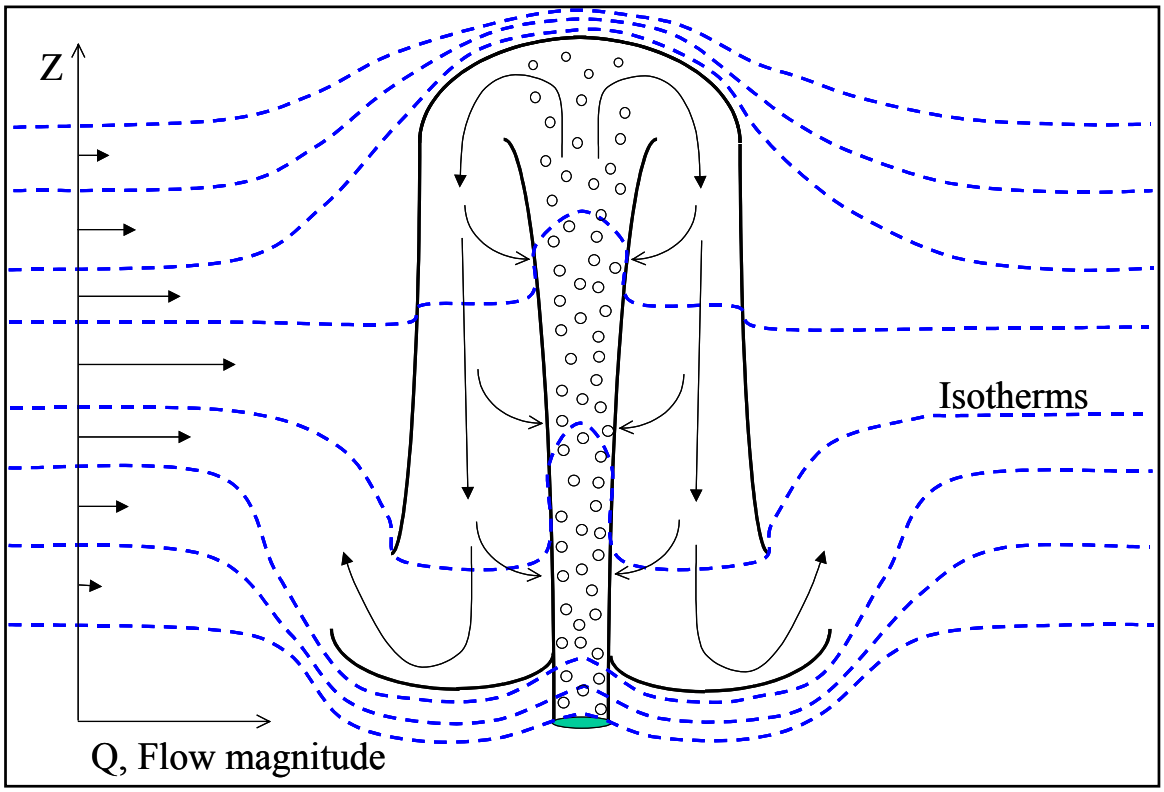

Figure 8. Conceptual drawing of plume behavior and short-circuiting in deep lakes. Blue dashed line indicated constant temperature isopleths demonstrating near-field alteration. Left axis shows estimated far-field flowrate distribution.

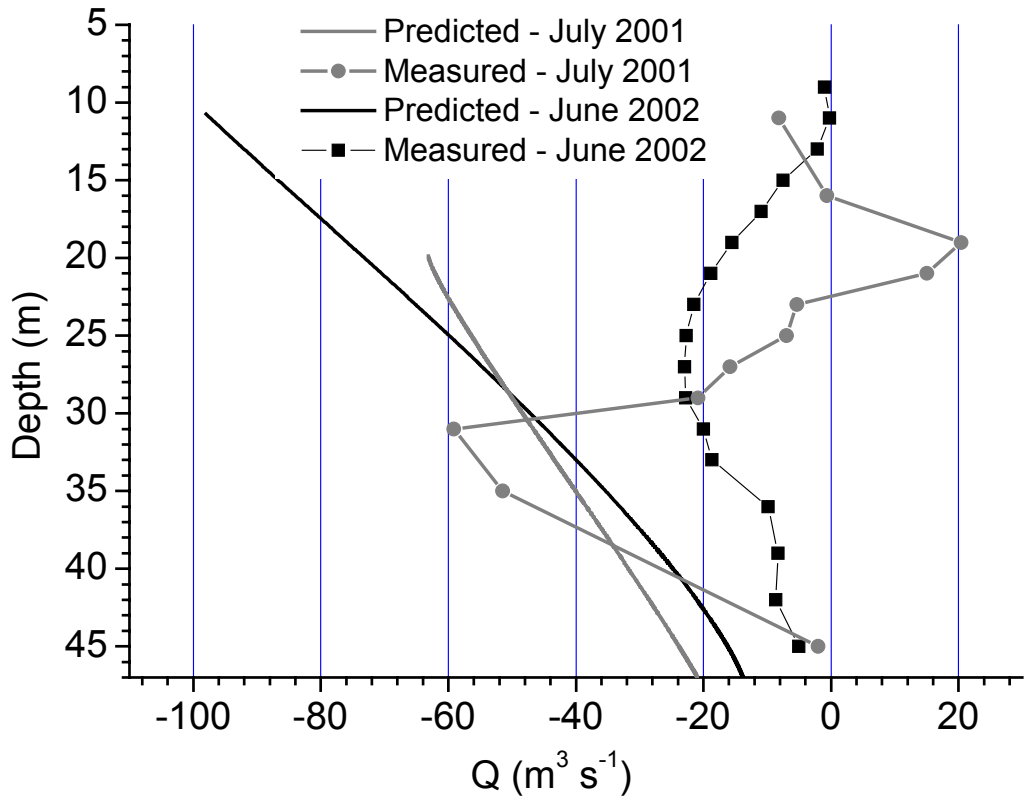

Figure 9. Predicted plume entrainment flowrate and observed far-field plume induced advective flowrate. Negative values indicate downward flow. The stop points for the predicted entrainment flowrate at approximately 20 meters for 2001 and 11 meters for 2002 indicate the modeled depth of maximum plume rise.

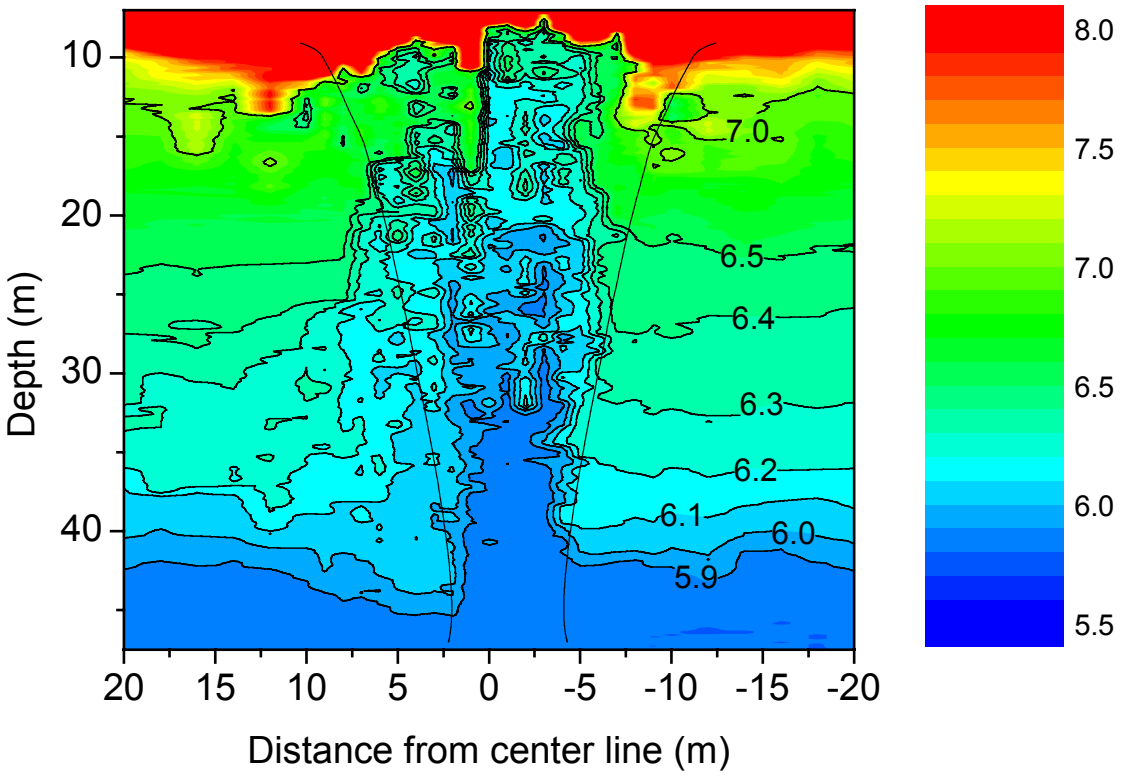

Figure 10. July 18, 2002 temperature (°C) with plume predictions overlaid. For clarity, the temperature contour was scaled to show only values in the range of 5.5 – 8 °C, with values above 8.0 shaded red and below 5.5 shaded blue.

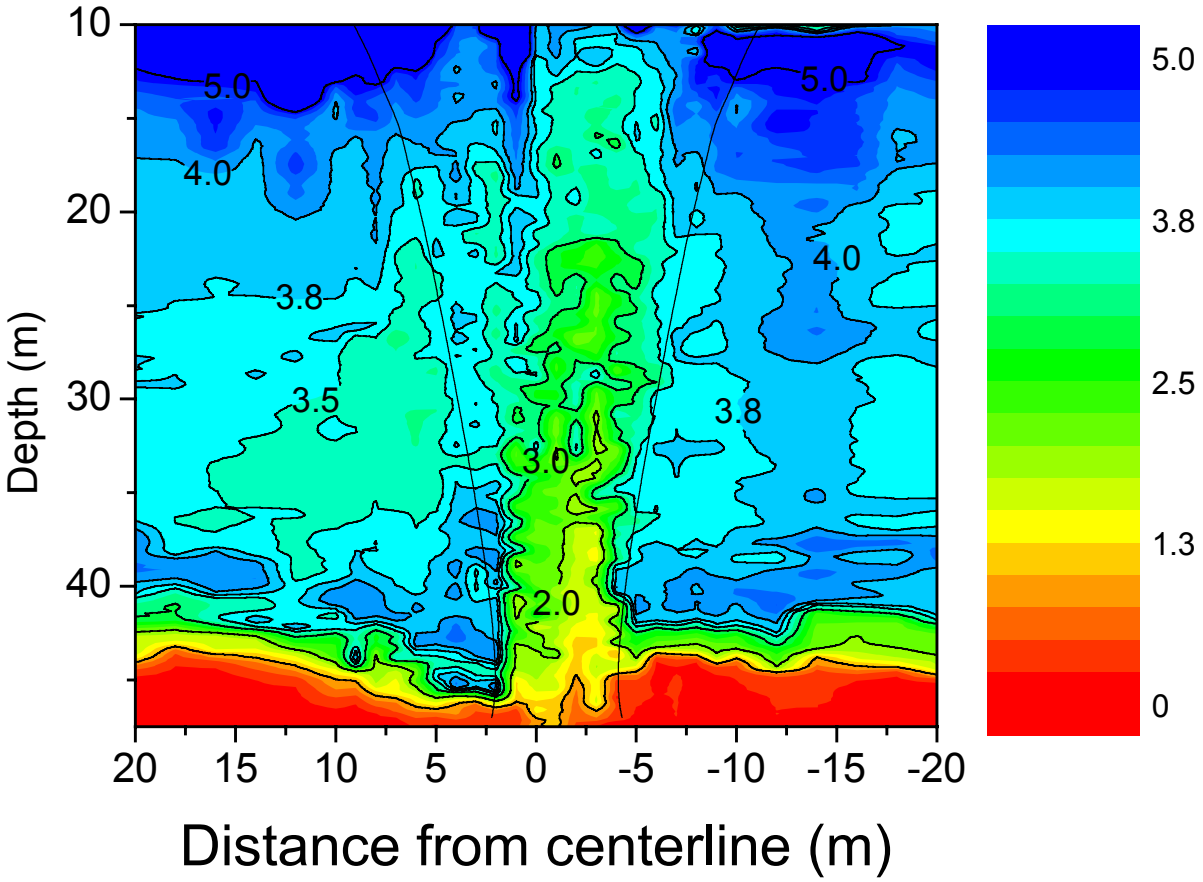

Figure 11. July 18, 2002 dissolved oxygen (g m^{-3}) with plume predictions overlaid. For clarity, the DO contour was scaled to show only the DO values in the range of 2.9 – 4.5 g m^{-3}, with values above 4.5 shaded blue and below 2.9 shaded red.

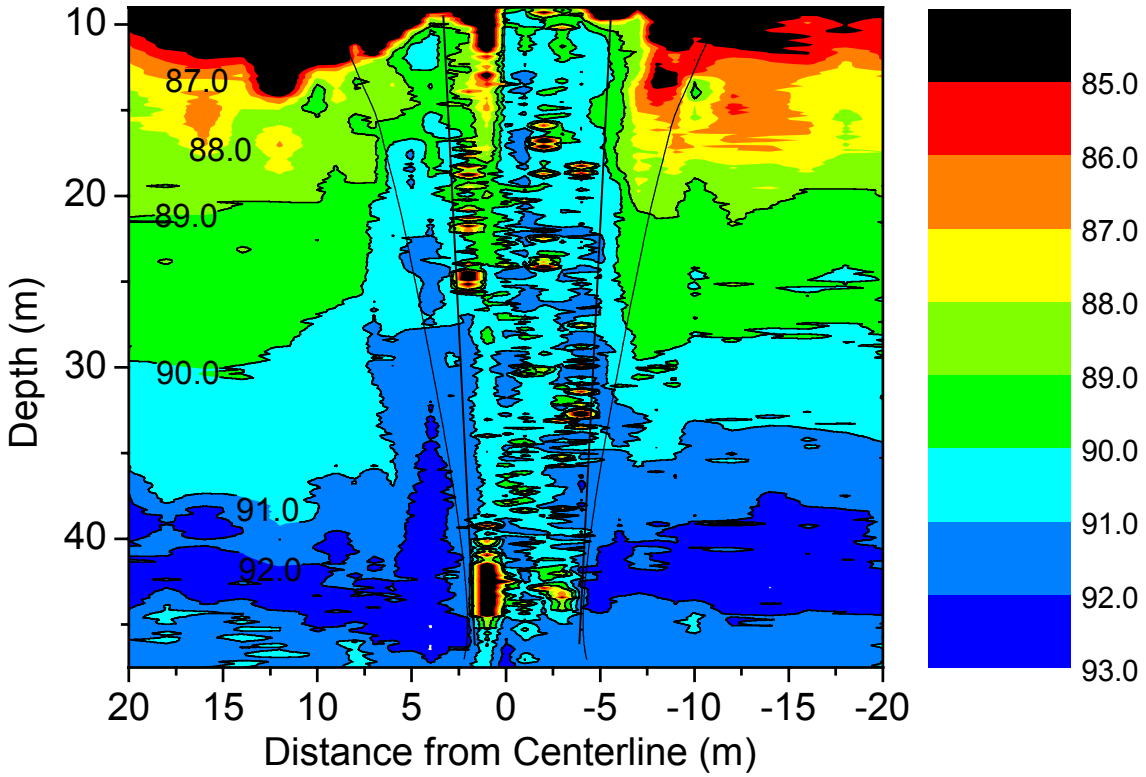

Figure 12. July 18, 2002 light transmission (%) with plume predictions overlaid with inside lines indicated extent of bubble core. For clarity, the light transmission contour was scaled to show only the values in the range of 85-93 %, with values above 93 shaded blue and below 85 shaded black.

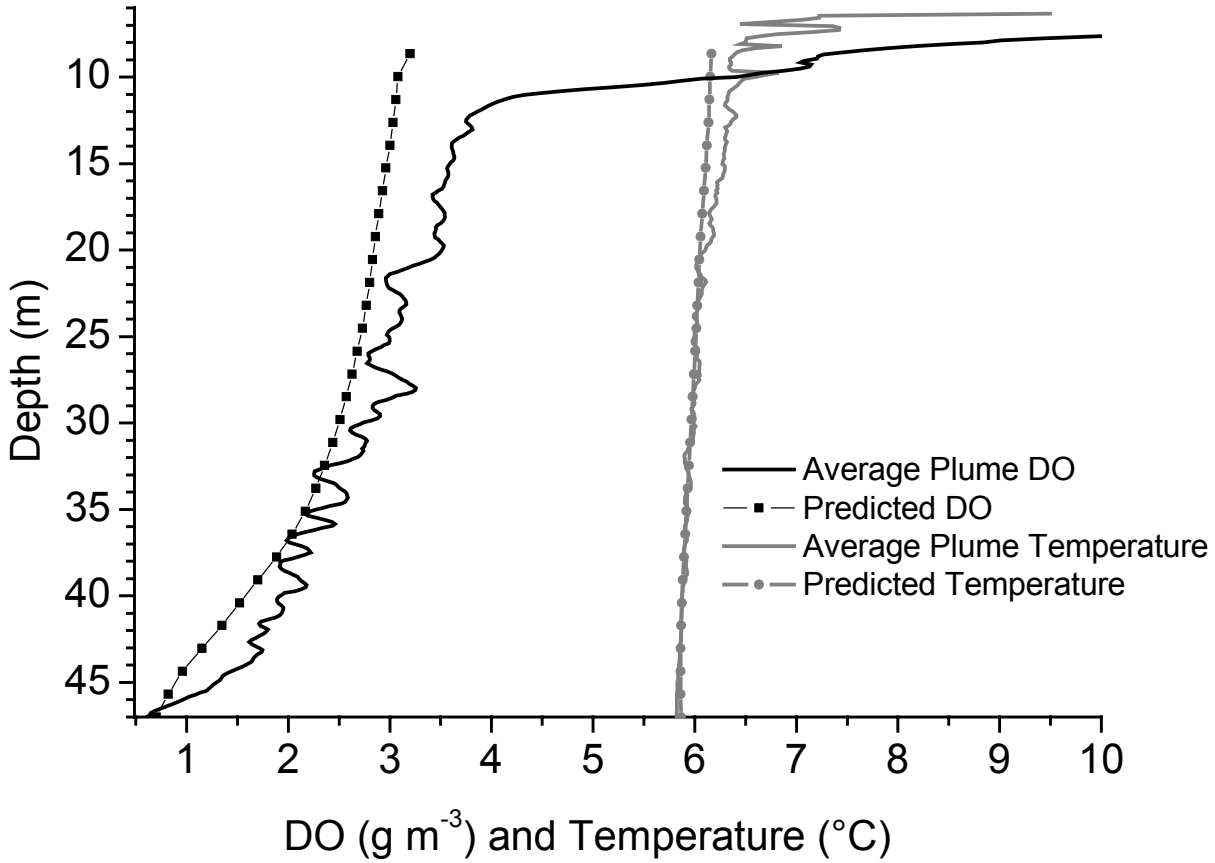

Figure 13. Averaged measured and predicted constituents

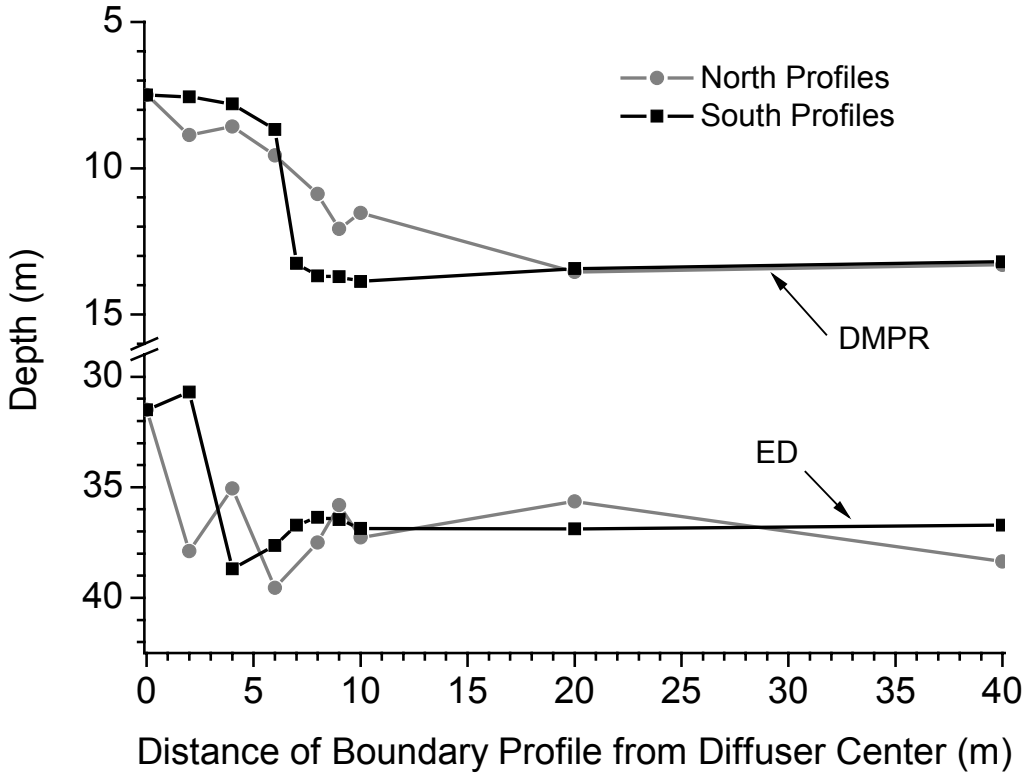

Figure 14. Predicted plume rise height (DMPR) and equilibrium depth (ED) as a function of boundary profile distance from diffuser (x-axis indicates profile distance from centerline of a single diffuser).

CHAPTER 3: HYPOLIMNETIC OXYGENATION: COUPLING BUBBLE-PLUME AND RESERVOIR MODELS

D. F. McGinnis[1], J. C. Little[1] and A. Wüest[2]

[1]*Department of Civil & Environmental Engineering, Virginia Polytechnic Institute and State University, Blacksburg, Virginia 24061-0246, USA*

[2]*Applied Aquatic Ecology, Federal Institute for Environmental Science and Technology (EAWAG), Kastanienbaum, CH-6047, Switzerland*

Abstract

Stratification of reservoirs may result in hypolimnetic oxygen depletion with negative consequences for water quality in hydropower reservoirs, water-supply reservoirs, and cold-water fisheries. Although bubble plumes are used to add oxygen to the hypolimnion without significantly disrupting thermal stratification, they nevertheless introduce energy, which causes mixing. The induced mixing changes the vertical density gradient, and hence the characteristics of the plume. To account for this effect, a bubble-plume model was coupled with a hydrodynamic reservoir model and then used to predict operational data obtained from Spring Hollow Reservoir in Virginia, USA. The coupled model was able to accurately predict the extent of hypolimnetic warming. With adjustments only to the coefficient of horizontal eddy diffusivity, the predictions followed the observed temperature and oxygen concentration profiles closely.

Keywords

Aeration; bubble plume; hypolimnion; mixing, oxygen transfer; reservoir

1. Introduction

Thermal stratification of lakes and reservoirs can result in substantial depletion of dissolved oxygen (DO) in the hypolimnion, which may have a negative impact on cold-water fisheries, the drinking-water treatment process, and hydropower operations (Little and McGinnis 2001). For drinking water sources, eutrophication may lead to taste and odor problems, increased treatment costs, and disinfection byproduct formation (Cooke et al. 1993). Eutrophication also negatively impacts downstream water quality resulting from anoxic reservoir releases (Beutel and Horne 1999). For example, hydrogen sulfide-rich dam releases, caused by hypolimnetic anoxia in Comanche Reservoir (California), resulted in a massive fishkill in a downstream hatchery (Jung et al. 1998, Beutel and Horne 1999). Furthermore, hypoxia itself has been shown to be an endocrine disruptor in fish that inhibits healthy reproduction (Wu et al. 2003). Under Section 401 of the U.S. Clean Water Act (CWA), the Federal Energy Regulatory Commission (FERC) may not license a hydropower project without first obtaining State water quality certification or a waiver (FERC 2001, EPA 2003, FERC 2003). This allows State agencies to regulate water quality, and generally means that hydropower operators are required to maintain DO at 5-6 g m^{-3} in the turbine releases (Stephenson 2000).

One common solution to replenish DO in the hypolimnion without destratifying the reservoir is to install a bubble-plume diffuser (Figure 1) (Wüest et al. 1992, Mobley 1997, Beutel and Horne 1999). Bubble-plume diffusers are either circular or linear, as is the case in this work (Figure 1), and use either air or oxygen with a relatively low gas flow rate and small (< 2 mm diameter) bubbles (Wüest et al. 1992, Mobley 1997, McGinnis and Little 2002). This technology lends itself to deeper lakes where the bulk of the bubbles dissolve in the hypolimnion and the momentum imparted to the plume by the introduction of gas is small enough to prevent significant intrusion into the thermocline, which leads to warming of the hypolimnion (Wüest et al. 1992). Furthermore, penetration of P-laden plume water into the euphotic zone can fuel algal growth. Plume operation will also inevitably increase the far-field upward vertical transport of nutrients and other constituents (Nakamura and Inoue 1996, Moosmann et al. 2002, McGinnis et al. 2003).

While bubble plumes are successful at adding oxygen, it is inevitable that the added energy will induce some degree of mixing in the hypolimnion, depending on diffuser design and operational characteristics. For example, increased advection, shear and turbulent diffusion may cause partial erosion of the thermocline and warming of the hypolimnion, ultimately resulting in premature destratification. The increased temperature, current velocity and turbulence may also be responsible for an increase in hypolimnetic oxygen demand (Little and McGinnis 2001) due to an increase in temperature-dependent oxidation kinetics and a decrease in the diffusive boundary layer thickness at the sediment-water interface (Nakamura and Stefan 1994, Lorke et al. 2003).

While plume operation changes the thermal structure of the reservoir, the performance of the bubble plume itself depends strongly on the vertical density gradient. The complex interaction between plume and reservoir needs to be accounted for in the design and operation of bubble plume diffusers. Modeling plume-enhanced mixing is also crucial

for the accurate prediction of DO and other constituent concentrations. To date, however, no thorough studies have been undertaken in which the bubble-plume and reservoir interaction were investigated. While many bubble-plume models have been developed, most were tested in laboratory settings (McDougall 1978, Asaeda and Imberger 1993, Borchers et al. 1999, Brevik and Kristiansen 2002) or in limited in-situ studies (Wüest et al. 1992, Lemckert and Imberger 1993, Johnson et al. 2000). Specifically lacking in past research is attention to the plume-reservoir interactions, and the effect of evolving water-column conditions on plume hydrodynamics. Most plume models assume steady-state far-field conditions and do not account for temporal and spatial alteration of the density structure or water quality and the ensuing impact on plume performance. Modifications to the density structure may result from seasonal (climatic) changes, changes due to reservoir operation (withdrawal), pumped water or river inflow, internal seiching, and more importantly for this study, the plume operation itself. Therefore, as the changing density structure significantly affects the bubble-plume performance, a study was undertaken to combine a bubble-plume model with a reservoir model.

The data used in this study were collected during 1997 and 1998 from Spring Hollow Reservoir (SHR) located in Roanoke County, Virginia, USA (Figure 2). Spring Hollow is a side-storage drinking water reservoir with an existing bubble-plume diffuser that uses air to add oxygen and improve drinking water quality (Little and McGinnis 2001). SHR tends to be mesotrophic and experiences periods of low DO towards the end of the stratified period. While it is only necessary to operate the diffuser for several weeks in the late summer to meet the DO demand, this short interval of plume operation resulted in not only an increase in DO, but also a substantial increase in the hypolimnetic temperature (Figure 3), particularly in 1997. Table 1 provides design and operational characteristics for both years and Figure 2 shows the bathymetry and diffuser location for 1997 and 1998. Note that the pool elevation, diffuser length, and applied air flow rate all differ substantially between 1997 and 1998.

Figures 3a and 3b show temperature and oxygen profiles, beginning on Nov 12, 1997 and Sept 28, 1998 immediately before diffuser start-up. The data illustrate the effects of the operational bubble-plume in SHR. In 1997, the system operated continuously from Nov 12 until November 24. Temperature and DO profiles were measured to evaluate the performance of the diffuser system. As shown in Figure 3b, it appears that oxygen is added to the hypolimnion fairly rapidly, although it is not clear what fraction is added by the aeration system and what fraction is added due to mixing with the well-oxygenated epilimnion. Furthermore, the surface mixed-layer was deepening during this period due to natural cooling. More importantly, the reservoir was at roughly half its normal operating level due to a drought earlier in the season and an estimated 350-m length of the 1070-m diffuser projected up through the thermocline and partially into the epilimnion (Figure 4). Clearly this situation would promote substantial mixing between the two layers, as shown in Figure 3a.

After the 1997 diffuser test, the line diffuser was shortened to the 360-m closest to the dam, in the deepest portion of the reservoir (Figures 2 and 4). The applied air flow was also reduced, and the water level was 5 meters higher (Table 1). Figures 3a and 3b show

temperature and oxygen profiles beginning immediately before diffuser start-up on Sep 28, 1998. The air supply was shut down on Oct 13, but unfortunately no data were collected on that day. The diffuser again successfully adds oxygen to the hypolimnion. Although some mixing and warming of the hypolimnion occurs, the extent of warming is considerably lower than during the 1997 diffuser operation. Following shut down, additional data were collected on Oct 21 and Oct 28 showing no further warming of the hypolimnion, but continued depletion of dissolved oxygen.

The two data sets demonstrate the need for a coupled bubble-plume/reservoir model to simultaneously predict the rate of oxygen addition and depletion, as well as the extent of thermocline erosion and hypolimnetic warming. As previously mentioned, bubble-plume performance is strongly influenced by the prevailing thermal gradient, further indicating the importance of developing a coupled model that predicts reservoir/plume interactions. Therefore, this work focuses on a preliminary coupling of a linear bubble-plume model with CE-QUAL-W2 (W2), a 2-D reservoir model, to investigate if the coupled model can properly quantify the plume-induced mixing and evolving dissolved oxygen concentration. To achieve this, W2 is first used to model SHR without the plume to investigate the effect of wind on mixing in the hypolimnion. A sensitivity analysis is conducted on the coupled model to determine which mixing mechanisms are most important. Finally, the formal coupling is performed using a calibrated value for the horizontal turbulent diffusivity, the only important mixing parameter identified during the sensitivity analysis. The rationale for modifying the horizontal diffusivity is discussed, and future work is identified. This work will provide the background for a formal embedding of the plume model within the W2 program.

2. Bubble-Plume Model

Figure 1 provides a schematic representation of a linear bubble-plume diffuser in a reservoir. Of the three commonly used hypolimnetic oxygenation devices (Speece Cone, airlift aerator and bubble-plume diffuser) (McGinnis and Little 1998, Burris et al. 2002, Wüest et al. 1992, respectively) bubble plumes are mechanically the simplest, but hydrodynamically the most complex. Gas bubbles are injected into the water column using a porous-hose diffuser (Mobley 1997), creating a gas-water mixture that is less dense than the surrounding water, and imparting momentum due to the positive buoyancy. The plume rises and entrains water at the boundaries, which increases the water flow rate and plume cross-sectional area while decreasing the plume velocity and momentum. The plume rises past the point of neutral buoyancy until the momentum reaches zero, at which point it has reached the depth of maximum plume rise (DMPR). At this stage, the plume water is typically negatively buoyant and will detrain and fall back until it reaches the equilibrium depth (ED) where the plume density matches the ambient density. During fallback, additional water will be entrained, further decreasing the density and resulting in a somewhat shallower ED. After reaching the ED, the plume water is transported to the far-field by advection and turbulent mixing.

A model for predicting the performance of circular bubble plumes has been developed by Wüest et al. (1992). Based on eight flux equations that are solved simultaneously, the model predicts water flow rate, gas transfer, and plume rise height, given the diffuser

depth, applied gas flow rate, initial bubble size, and diffuser geometry (Wüest et al. 1992). As shown in Tables 2 and 3, the eight model equations were modified to conform to linear, as opposed to circular, geometry. The plume model is based on horizontally integrated equations for the conservation of mass, momentum, and buoyancy (McDougall 1978). Entrainment is also considered, and the entrained flow is assumed to be proportional to the local plume velocity (McDougall 1978). The plume model also includes the effects of stratification due to vertical temperature and salinity gradients. The model does not distinguish between the region of flow establishment and fully developed flow (Wüest et al. 1992). This shortcoming is improved by the appropriate selection of the initial plume velocity. The plume should show a slight acceleration in flow velocity (i.e. $\partial v / \partial z \geq 0$) and a small decrease in plume width immediately above the source, as this slight contraction has been observed in tank testing (Wüest et al. 1992). Fortunately, the predicted plume behavior is relatively insensitive to the initial plume velocity.

A key contribution by Wüest et al. (1992) was the use of a variable buoyancy flux to account for changing bubble sizes. This is particularly important when pure oxygen is used or in high-pressure systems when the bubble dissolution rate is rapid. The variable buoyancy flux tracks the change in bubble size due to decompression and thermal expansion, as well as gas dissolution from the bubbles and stripping of dissolved gas from the water (Wüest et al. 1992). Although previous studies neglected gas exchange, plume hydrodynamics are strongly influenced by the initial bubble size, the number flux of bubbles (i.e., gas flow rate), and the rate of bubble dissolution or expansion. The dissolved gas concentration (DO and DN) within the plume is governed by the ambient conditions at the diffuser, entrainment of dissolved gas concentrations, and gas dissolution or stripping within the plume. Table 3 gives the conservation equations for both gaseous and dissolved oxygen and nitrogen. Other gasses may be easily included. The model also accounts for the variability of the gas partial pressure within the bubbles as they rise. This affects the rate of gas transfer, as the concentration driving force is a function of the partial pressure of each gas species in the bubble. The model uses bubble-size dependent equations for bubble rise velocity and the mass transfer coefficient, as well as a temperature dependent Henry's constant (Table 4). A distribution of bubble sizes can be incorporated although McGinnis and Little (2002) demonstrated that using the Sauter mean diameter (Chisti 1989) resulted in negligible loss in computational accuracy. The Sauter-mean diameter is the diameter of a sphere having the same surface-to-volume ratio as the entire distribution of bubbles and gives more weight to larger bubbles (Orsat et al. 1993). Therefore, it is more representative for mass transfer than the mean bubble diameter (Orsat et al. 1993). The gas-transfer aspect has been independently validated in discrete bubble oxygen transfer tests in a large 14-m high tank (McGinnis and Little 2002), and for a full-scale airlift aerator (Burris et al. 2002). As gas transfer and plume momentum are highly dependent on the initial bubble size and the change in bubble size as the plume rises, these independent validations increase overall confidence in the plume model.

Based on the eight flux equations in Table 3, the model predicts water flow rate, water entrainment with depth, gas transfer and plume constituent concentrations (DO, dissolved

nitrogen (DN) and total dissolved solids (TDS)), DMPR, and ED, given the diffuser depth and geometry, applied gas flow rate, initial bubble size, and boundary profiles (temperature, DO, and salinity). The predicted entrainment flow rate with depth and the final detrainment flow rate, the DMPR, as well as the final plume temperature and DO concentration are used as inputs to the reservoir model.

2.1 Key Assumptions

The key model assumptions are summarized below. For a more detailed description, the reader is referred to Wüest et al. (1992). The Boussinesq assumption is used because the gas hold-up is small ($V_g << 1$) and gas density is neglected in the momentum equation. A "top hat" distribution is used for water velocity, temperature, TDS, bubble rise velocity, and gaseous constituent concentrations within the plume. The plume width for dissolved species and temperature is assumed to be equal to the width of the top hat plume velocity profile, while the bubbles occupy an inside core of width, λW (where $\lambda < 1$). There is no cross flow of ambient water and flow within the plume is fully turbulent. Only advective constituent and momentum transport are considered, while transport by turbulent diffusion is neglected. The diffuser is assumed to produce uniformly-sized bubbles at a constant rate that are evenly distributed over the cross-sectional area. Because gas holdup is small, bubble coalescence is neglected. The properties of the influent and entrained water are the same as the ambient water at the appropriate depth. Gas exchange is neglected for gases other then oxygen and nitrogen, but can be easily incorporated if needed.

An entrainment coefficient, α, of 0.08 and a plume width ratio, λ, of 0.85 were chosen based on prior work by Fannelop et al. (1991) and Brevik and Kristiansen (2002) on linear plumes. The entrainment coefficient is treated as a constant, an assumption that is somewhat counterintuitive given the variable nature of the plume flow conditions, with a region of flow establishment, varying turbulence at the plume-water boundaries, variations in the ambient vertical density gradient, and complex mixing that may occur at the DMPR. Nevertheless, Brevik and Kristiansen (2002) showed that α is reasonably constant except near the source and lies near the value of 0.08 recommended by Fannelop et al. (1991). The computational procedure and other details are the same as for the circular plume model (Wüest et al. 1992).

3. Reservoir Model (W2)

W2 is a two-dimensional, laterally averaged, hydrodynamic and water quality model (Cole and Buchak 1995, Cole and Wells 2000, 2002). W2 includes horizontal, but not vertical momentum, and accounts for momentum transfer from inflowing branches and the associated shear stress imparted to the surrounding water. An important aspect of the model is the ability, within the constraints of the laterally averaged assumption, to accurately calculate the two-dimensional velocity field in stratified reservoirs. The ability to simulate transport accurately is critical for predicting the influence of the bubble-plume on the temperature and constituent concentrations. W2 employs a finite difference solution of a set of six equations for hydrodynamics and constituent transport. The equations are for x- and z-momentum and continuity, as well as an equation of state, and equations for the free water surface elevation, and constituent transport (Cole and

Wells 2002). The z-momentum is set equal to zero by invoking the hydrostatic pressure assumption. The equation of state gives water density as a function of temperature and solids concentration. The unknown parameters for the six equations are the free water surface elevation, pressure, horizontal velocity, vertical velocity, constituent concentrations, and density. The solution of six equations with six unknowns comprises the basic structure of W2 (Cole and Wells 2002).

The following input data are required for model application: geometric data (bathymetry), initial conditions, boundary conditions, hydraulic parameters, kinetic parameters, and calibration data. The main components of the geometric data are longitudinal spacing, vertical spacing, average cross-sectional width, and slope. Initial conditions that must be specified are the start and end time, and the corresponding initial temperature profile (or other constituents). Boundary conditions include inflows, outflows, and meteorological data. The most critical inputs for the surface boundary conditions are meteorological data (wind speed, wind direction, air temperature, dew point temperature, and cloud cover).

The hydraulic parameters are the turbulent eddy viscosity, turbulent diffusion and bottom friction coefficients. Vertical turbulent diffusion coefficients for momentum and temperature/constituents vary temporally and spatially and are calculated by the model. The bottom friction coefficient (either Chezy or Manning) may be varied longitudinally. Horizontal turbulent diffusion coefficients for momentum and temperature/constituents are time and space invariant in Version 3.1 of W2. Sensitivity analyses have shown that the model is relatively insensitive to variations in the default values for reservoirs (Cole and Wells 2002), although this may not be true for the coupled plume model.

3.1 Wind- and Plume-Induced Mixing

Because no water was pumped into the reservoir during the two bubble-plume test periods, the dominant mixing mechanisms will be those induced by the wind and by the bubble plume itself. The W2 algorithms through which both wind- and plume-induced mixing are activated are briefly described below. The results of a sensitivity analysis on these mixing mechanisms are discussed in Section 5.

The wind speed and direction are used to calculate the surface shear stress. The shear imparted to the water surface is defined as

$$\tau_{wx} = C_D \rho_a v_w^2 \cos\Theta; \tau_{wy} = C_D \rho_a v_w^2 \sin\Theta$$

where τ_{wx} is the wind surface shear stress along the x-axis, and τ_{wy} is in the lateral direction. The default values for the surface drag coefficient, C_D, were changed to those given by Wüest and Lorke (2003). W2 sets the drag coefficient to zero for winds less then 1 m s^{-1}. However, according to Wüest and Lorke (2003), weak winds have drag coefficients that are larger than those at a wind speed of 25 m s^{-1}. Therefore, the W2 code was modified for winds below 3 m s^{-1} to:

$$C_D = 0.0044 v_w^{-1.15}.$$

The wind speed is multiplied by the wind sheltering coefficient (WSC), which allows the user to either increase or decrease the wind speed, and therefore the energy added. The WSC is variable both spatially and temporally and accounts for the effects of different terrain and summer foliage.

The bottom shear stress is defined as

$$\tau_b = \frac{\rho g}{C_B^2} v_b |v_b|$$

where C_B is the Chezy friction factor, which may be varied spatially. This term accounts for stress due to flow at the reservoir boundaries and is applied where cells are in contact with the bottom and the sides of the reservoir. The calculated shear stresses are included in the horizontal momentum equation.

W2 has five turbulence closure schemes for calculating vertical diffusivity (Cole and Wells 2002). The W2 and W2N (W2 plus Nickaradse's mixing-length formulation) algorithms are the only two that incorporate cross shear from lateral inflows (τ_l) and wind (τ_{wy}) in the lateral direction (Cole and Wells 2002). W2 uses a fixed mixing length that is defined by the cell thickness, while W2N uses Nickaradse's mixing length model, which is a more appropriate formulation as it decreases the mixing length with depth. Cole and Wells (2002) recommend these two formulations for stratified, deep water bodies, while the other three are recommended for estuaries and rivers.

Since there is no momentum transfer from lateral inflows to the main branch and vertical momentum is neglected, the mixing resulting from the inflowing water is accounted for as cross-shear in the W2 and W2N vertical eddy viscosity (A_z) algorithms by increasing the cross-shear velocity gradient (Cole and Wells 2002). This process is similar to the addition of cross flow wind shear in the lateral direction, as previously described, by including a new shear term, τ_l, in the calculation of A_z, or

$$A_Z = \kappa \left(\frac{l^2}{2} \right) \sqrt{\left(\frac{\partial v}{\partial z} \right)^2 + \left(\frac{\tau_{wy} e^{-2kz} + \tau_l}{\rho A_Z} \right)^2} \, e^{(-1.5Ri)}$$

where the lateral inflow shear is $\tau_l \cong \rho \frac{f_i}{8} v^2$ and $v = \frac{\sum Q_l}{\Delta z \Delta x}$. The internal friction factor, f_i, has a default value of 0.01, and is listed as a calibration parameter in W2. It is evident that the cell entrainment and detrainment area may also affect the estimated shear contribution, where the area, $\Delta z \Delta x$, is defined by the inflow (detrainment) cell layer height and length, respectively. The mixing length in the W2N algorithm, l, is given by Nickaradse's mixing length model,

$$l = D\left[0.14 - 0.08\left(1 - \frac{z}{D}\right)^2 - 0.06\left(1 - \frac{z}{D}\right)^4\right]$$

where D is the total depth, and z is the vertical distance measured from the bottom (Cole and Wells 2002).

In Version 2 of the W2 model, the vertical eddy viscosity was solved explicitly with A_{Zmax} set to 1.0 x 10^{-5} m^2 s^{-1} (Cole and Wells 2002). This, however, resulted in insufficient vertical mixing with preliminary coupling attempts using Version 2. With the W2 and W2N formulations in Version 3, the user can specify a maximum coefficient of vertical eddy viscosity (A_{Zmax}), and select between the implicit and explicit solution techniques. The A_{Zmax} is in fact leftover from the explicit solution technique and was used because it reduced the timestep required for maintaining numerical stability when solving the momentum equations explicitly (Cole and Wells 2002, Wells 2003). A_Z is typically low in stratified lakes and reservoirs, but will increase in rivers and estuaries. For rivers and estuaries, Cole and Wells (2002) recommend using the implicit solution technique with A_{Zmax} set to 1 m^2 s^{-1} and it is recommended to use the same for the coupling and allow the model to calculate A_Z (Wells 2003). This will be discussed in greater detail later.

Longitudinal turbulent shear stress is defined in W2 as

$$\frac{\tau_x}{\rho} = A_x \frac{\partial v}{\partial x}$$

where A_x, the horizontal eddy viscosity, or D_x, the horizontal turbulent diffusivity, is spatially and temporally invariant in Version 3.1 of W2 and is user-defined with a default value of 1 m^2 s^{-1}. While A_x and D_x do not directly affect vertical mixing, they do indirectly affect it by spreading momentum, heat and constituents more rapidly in the horizontal direction and hence produce a "far-field" effect. Although treated independently in W2, A_x and D_x are considered to be equal in lakes and reservoirs (Peeters et al. 1996), and are hereafter both referred to as A_x. In typical lake applications, this term is very low, except at boundaries such as dam walls where there are higher velocity gradients due to the rapid deceleration of flow velocity (Cole and Wells 2002). However, this will also be significant in the application of a bubble plume diffuser, which could conceivably produce relatively intense horizontal velocity gradients in the hypolimnion, particularly in the near-field and for a strong plume with high velocities that decay rapidly with distance from the diffuser.

4. Coupling of Bubble-Plume and Reservoir Model

W2 was applied to SHR for the years 1997 and 1998 when the aeration system was operated. The main branch of the reservoir is discretized into eighteen 76-m long segments along the x-axis (centerline), and the segments are then divided into 1-m cells along the z-axis. A cell in W2 is treated as a well-mixed volume, and has the dimensions listed above, with a lateral length (y-axis) that varies with the reservoir width. Surface

reaeration and sediment oxygen demand using the zero-order sediment compartment (Cole and Wells 2002) were included in the simulations. No other water quality constituents were modeled. The meteorological data for W2 were supplied by the National Oceanic and Atmospheric Administration for the Woodrum Airport in Roanoke, VA. The data are collected at hourly intervals and include air temperature, dew point temperature, cloud cover, and the wind speed and direction. A temperature calibration was first performed adjusting only the wind-sheltering coefficient to a value of 0.7 for both years, or 70% of the measured wind velocity from Woodrum Airport. SHR is relatively wind protected given the mountainous terrain, and Woodrum Airport is located in a relatively flat valley approximately 15-km away. The model was calibrated for the periods of Sept 29 – Nov 25, 1997 and July 31 – October 31, 1998. These periods correspond to no inflow periods due to low flow in the North Fork of the Roanoke River. Roanoke County pumps water into SHR through a pipe that points vertically up at approximately 26 meters deep depending on the reservoir elevation. Because this inflow water would also form a plume, it was decided to neglect the periods of inflow at this time due to the additional modeling complexity. Based on the calibrated model, and without diffuser operation, slight warming of the hypolimnion (<0.1°C) is expected during the 1997 test period due to the onset of destratification, and essentially no warming is predicted during the 1998 test period due to the more stable stratification. When compared to the actual hypolimnetic temperature changes during the two test periods shown in Figure 3a, the model predictions show that plume-induced mixing dominates and that hypolimnetic mixing induced by the wind is close to negligible during both test periods.

Within W2, plume entrainment is handled as a lateral outflow while plume detrainment is handled as a lateral inflow. Lateral flows are advantageous as the outflow or inflow zone can be specified for a specific area within a segment. This area can range from the entire segment depth down to only a fraction of an individual 1 × 76-m cell. The plume entrains ambient water as it rises. The entrained volume of water accumulates within the plume until the entire volume detrains at the DMPR, and flows back into W2. For the purpose of coupling, the plume model is used to compute the flow rate of ambient water entrained as the plume rises, and the flow rate, temperature, and oxygen concentration of the water that is detrained upon reaching the DMPR. Entrainment therefore removes water of known temperature and oxygen concentration from a range of depths, while detrainment returns the sum of all the entrained water at the specified discharge location. This plume action is simulated within W2 by withdrawing water from the "entrainment" cells (outflows from W2) and discharging it at the "detrainment" cell (inflows into W2). With each lateral flow specification, the user specifies a flow rate file (negative for entrainment and positive for detrainment), a temperature file, and a constituent concentration file. The constituent concentration files allow the user to specify the concentrations of any of the available W2 constituents (see Cole and Wells 2002).

The "manual" coupling procedure was handled as follows. First, the initial reservoir temperature and DO profiles immediately prior to aeration were used as boundary conditions in the plume model to predict the flow rate of entrained and detrained water, and the final temperature and DO concentrations. This procedure was performed for each

of the 76-m long discretized diffuser segments, 14 segments for 1997 and 5 for 1998. Then, starting when the plume was turned on, and using the sets of predicted inflow data (14 for 1997 and 5 for 1998), the coupled plume/W2 model was run for 6 hours. The predicted ambient temperature and DO profiles obtained at the end of this 6-hour period were then used as input to the plume model to generate a new set of plume entrainment and detrainment data for each of the plume segments. The entire procedure was repeated for each 6-hour interval until the diffuser was turned off (Nov. 24, 1997 at 12h00 and Oct. 9, 1998 at 12h00). Because of the changing temperature gradient, the plume rise height also changes and it was necessary in some cases to specify new detrainment cells during the course of the simulation.

5. Results

Before the coupling was performed, a preliminary sensitivity analysis and parameter calibration was carried out with and without the coupled plume model. To ensure more representative conditions for the sensitivity analysis for W2, the coupling was done in a slightly different way than previously described. Instead of using the predicted water column temperature and DO profiles at the end of each 6-hour period as inputs to the plume model, the actual measured temperature and oxygen concentration profiles obtained during the diffuser operation were used. This gave a more accurate response of W2 itself and provided a better basis for the sensitivity analysis. The sensitivity analysis was then carried out to determine the extent to which the various plume-induced mixing mechanisms influence the model predictions. Surprisingly, for this sensitivity analysis, it is shown that horizontal diffusivity is the only parameter having a significant impact on the coupled model predictions. Based on this result, the value of A_x was calibrated using the 1997 diffuser conditions. Finally, using the calibrated value of A_x, the formal coupling was performed using the predicted (as opposed to measured) reservoir profiles for the plume model boundary conditions. The results of the sensitivity analysis are discussed in greater detail in Section 6.

5.1 Coupling for 1997

The full coupling using the procedure described in Section 4 was performed using the W2N turbulence closure scheme and the default values listed in Table 5, with the exception that A_x was set to the previously calibrated value of 36 m^2 s^{-1}. The results are shown in Figure 5. The coupled model captures both the evolution of T and DO very well, particularly in the hypolimnion, although mixing between the depths of 15 and 25 m is overestimated, resulting in a deeper thermocline. This may be due to overestimation of the plume rise height. The observed data exhibit a slight thermal gradient in the hypolimnion, which would result in the plume losing momentum due to overcoming the constant density increase. W2, however, predicts an almost isothermal hypolimnion between 30 and 46 meters, allowing the plume to conserve momentum in this region and hence reach a shallower depth. The situation may be exacerbated by the exclusion of total dissolved solids (TDS) as a modeled constituent, as this would contribute to a more stable density structure. The plume entrainment coefficient used was taken from the literature and could also be a source of error. Furthermore, decreasing A_{Zmax} will also typically increase the density gradient in the hypolimnion by limiting vertical mixing, however doing so also inhibits mixing in the thermocline, resulting in less overall

warming. Also, it could be a shortcoming of W2 in the mixing calculations due to the laterally averaged assumption or the lack of vertical momentum. The mixing energy may be improperly distributed in the horizontal and vertical directions, specifically in the upstream location where the plume starts and stops within the thermocline. In the two upstream segments, the total plume rise height is less then 2 meters during the simulation. This means that the entire entrainment and detrainment are occurring within two adjacent cells, a situation where properly quantifying the generated shear stress and subsequent vertical and horizontal distributions become increasingly important.

The evolution of the DO is predicted well, with the exception of Nov 13, which was the day after system start-up. After the compressor is turned on, it takes about a day for the air flow rate through the diffuser to reach a steady rate because the water that is initially present in the line has to be forced out through the diffuser. In the simulation, however, the air flow rate through the diffuser is assumed to reach the operational level immediately, and this could to some extent account for the overestimated mixing and oxygen transfer during the initial day or so of operation. As shown in Figure 5, the 1997 diffuser operation resulted in a considerable amount of mixing. The diffuser was 1070-m long, and due to large diffuser elevational changes resulting from the bottom topography (over 30 m) and the exceptionally low water level during 1997, the diffuser protruded into the thermocline and epilimnion, resulting in highly efficient mixing (Figures 2 and 4). Obviously, 1997 is a complicated case to model, due to the more extreme conditions. Therefore, the coupled model was verified using the 1998 data, where the diffuser is shorter, more level, and the plume is less hydrodynamically complicated.

5.2 Coupling for 1998

The 360-m long diffuser in 1998 also changes in elevation with its deepest point being closest to the dam wall (Figures 2 and 4), but is overall more level then in 1997. A_x was determined to be 5 m^2 s^{-1} by scaling the 1997 value of 36 m^2 s^{-1}, as described below in Section 6. Other than A_x, the coupling was performed with the default values listed in Table 5, with results shown in Figure 6. The coupled model again predicts the data well for both T and DO, including the region below the diffuser. The model slightly underpredicts the temperature profiles, however this occurs mainly during the first 2 days of the simulation, with the subsequent profiles exhibiting the correct change in temperature, only shifted by approximately 0.1°C. This may again be due to the slow build-up in air flow rate during system start-up. The DO profiles also fit extremely well, with a slight overprediction, which is likely a result of excluding water column BOD.

5.3 Summary of Results

Figures 5 and 6 show that the coupled model predicts mixing and warming induced by plume operation quite accurately. The plume penetrates the thermocline and epilimnion through the entire 1997 simulation, however, during the 1998 simulation the plume only partially penetrates the lower region of the thermocline. Although all oxygen sinks except sediment oxygen demand (SOD) are turned off in the W2 model, Figures 5 and 6 demonstrate that the coupled model predicts the evolution of hypolimnetic DO fairly well. The SOD is a simple zero-order rate that can be spatially adjusted in W2. The SOD was measured in SHR to be approximately 0.6 g m^{-2} day^{-1} (Gantzer 2002), however

it was fairly insensitive over the range of 0.1 – 1 g m^{-2} day^{-1} during the simulations, which is the range suggested by Cole and Wells (2002). Once the other oxygen demands are correctly incorporated in W2, the predicted oxygen concentrations will not increase as rapidly. The 1997 DO predictions are possibly more accurate because the rate of addition of oxygen is much more rapid, and the DO sinks have less effect on the DO concentration. Further mixing and oxygen transfer may be induced by secondary plume formation for both years when the plume stops below the thermocline. Because bubbles continue to rise from this point, a secondary plume may form.

6. Discussion

6.1 Sensitivity Analysis

Before the coupling was performed, a sensitivity analysis was carried out (with and without the embedded plume model) on the vertical diffusivity, as well as the other hydraulic parameters described in Section 3 and listed in Table 5. The sensitivity was investigated using the listed range for each parameter to determine the dominant mixing mechanisms. As already described, the plume inputs for the sensitivity analysis were obtained from the measured profiles, as opposed to using those predicted by the model. It is important that the hydraulic parameters are properly quantified, as a slight under or over prediction in mixing early on in the coupling procedure could significantly affect the results towards the end of the simulation. From Section 3, the mixing parameters examined include the turbulence algorithm for vertical eddy viscosity, A_z, the internal friction factor, f_i, the detrainment cell area, $\Delta z \Delta x$ (plume detrainment area), the horizontal eddy viscosity, A_x, the wind-sheltering coefficient (WSC), and the bottom friction coefficient, C_B. In addition, the maximum vertical eddy viscosity (A_{Zmax}) was investigated. While the coupled model was insensitive to A_{Zmax} using the predetermined plume inputs, a course coupling sensitivity analysis found that it does affect the plume model results, which will subsequently change the W2 predictions. This will be discussed in Section 6.3. These include all the user-adjustable mixing mechanisms activated by the coupling procedure. Investigating other mechanisms that may influence mixing (for example, vertical momentum is neglected in W2) involve major modifications to the source code, and are beyond the scope of this work.

Each turbulence closure scheme was tested using the plume inputs, and surprisingly, no significant differences in the predicted DO and T profiles were observed. Furthermore, only minor differences (not shown) were observed when varying the internal friction factor, f_i, the maximum vertical diffusivity, A_{Zmax}, the bottom friction coefficient, C_B, and the detrainment cell depth, which was varied from a thickness of Δz = 0.1 to 1 m (Table 5). However, there were significant changes when varying the horizontal eddy viscosity, A_x. The results of the sensitivity analysis are shown in Figure 7. A_x has a default value of 1 m^2 s^{-1}, however, the coupled model temperature and DO predictions were improved with A_x adjusted to 36 m^2 s^{-1}. The temperature predictions below the diffuser are substantially improved, exhibiting less mixing when the value for A_x is increased. This is perhaps a result of the local velocities and resulting shear being spread laterally at a much faster rate, more effectively distributing the mixing energy in the horizontal direction. The DO prediction is also improved due to enhanced horizontal diffusion of DO. Low A_x values result in a longer time for the warmer water and DO to travel the 160 m to the dam

wall, and cause a higher concentration and temperature above the diffuser. Figure 8 demonstrates this effect. Remembering that water is entrained (effectively removed) above the diffuser, this means that the mass of oxygen and heat removed is too large, changing the overall hypolimnetic DO and thermal balance. In addition, due to the laterally averaged assumption, plume water containing higher DO and higher temperature is instantly mixed in the lateral direction and then transported longitudinally, whereas in reality, this higher DO and temperature water would be transported longitudinally more rapidly. Therefore, it was necessary to estimate more appropriate values for A_x. Figure 8 shows the effect of this parameter on the predicted temperature and DO in the hypolimnion.

6.2 Estimating Horizontal Eddy Viscosity and Diffusivity

Horizontal mixing occurs due to velocity field fluctuations and shear resulting from mean advective currents (Peeters et al. 1996). Typically, very little energy is necessary for the rapid horizontal transport of constituents in reservoirs and is several orders of magnitude higher then vertical transport (Imboden and Wüest 1995). The distinction between horizontal advective and horizontal turbulent mixing is not significant, particularly because of the scales involved. In the case of enhanced plume mixing in Spring Hollow Reservoir, the eddy size covers a length scale from the reservoir scale down to the dissipation scale. The hypolimnetic velocities averaged over a long period are typically very small, however, over short time scales plume-enhanced horizontal velocities can significantly contribute to advection, particularly in the near-field where constituents are transported rapidly away from the diffuser. According to Imboden and Wüest (1995) and Peeters et al. (1996), a hypothetical tracer cloud injected into the hypolimnion is moved primarily by advection caused by eddies that are larger than the cloud, while smaller eddies, or turbulent diffusion, would generate mixing only within the patch. It is assumed, due to the nature of the hypolimnetic currents resulting from plume operation, particularly in the near-field, that advective transport dominates and that turbulent diffusion can be included in the computation of the overall effective diffusivity, which is quantified by the rate of growth of the tracer cloud. While there is currently no well-substantiated theory for horizontal diffusion, there are several empirical models available including the Diffusion Velocity, Fickian, and Shear Diffusion models (Imboden and Wüest 1995). Using a Fickian diffusion local closure scheme, the apparent horizontal diffusivity can be estimated by

$$A_x = \frac{1}{4}\frac{d\sigma^2}{dt}$$

where σ^2 is the cloud size (Imboden and Wüest 1995). From the sensitivity analysis and calibration for the 1997 conditions, A_x was estimated to be 36 m^2 s^{-1}. The average predicted plume detrainment flow rate is approximately 80 m^3 s^{-1}, which results in a hydraulic turnover time in the hypolimnion of less then 8 hours, a condition that comes close to approximating 1-D behavior with respect to horizontal mixing. In a true 1-D case, A_x approaches infinity. For 1998, the predicted plume detrainment flowrate is 30 m^3 s^{-1}. This detrainment flow rate results in a hydraulic turnover rate of approximately 1 day, or three times longer than the 1997 case. To obtain a coarse estimate for 1998, the

value for A_x is scaled using the equation given above and the 1997 and 1998 detrainment flowrates. Assuming the same time scales and detrainment areas for both years, A_x was estimated to be 5 $m^2 s^{-1}$. As shown in Figure 6, this value gave very good results. Using the Fickian approach this term is assumed to be constant, although this is contrary to field observations (Lerman et al. 1995). Fortunately, as the velocity gradients decrease rapidly away from the diffuser and the laterally averaged effect becomes less significant, the value of these terms also has less impact in the far-field. Note, however, that for 1997 there is no predicted difference when using an A_x value above 36 $m^2 s^{-1}$, as indicated in Figure 7. For 1998, a sensitivity analysis was performed varying A_x from 1 to 10 $m^2 s^{-1}$ (not shown). There were no significant differences except that mixing below the diffuser was overpredicted with A_x = 1 $m^2 s^{-1}$, providing further justification for the increase in this value. A_x values in the literature range from 0.02 to 17.1 $m^2 s^{-1}$ for lakes (Imboden and Wüest 1995, Peeters et al. 1996, Stocker and Imberger 2003), and from 0.3 to over 1000 $m^2 s^{-1}$ in fjords and the ocean (Sundermeyer and Price 1998). The estimated values of 5 and 36 $m^2 s^{-1}$ therefore appear reasonable, given the significant additional mixing imparted by the plume.

6.3 Maximum Eddy Viscosity (A_{Zmax})

Due to the extensive time required for this coupling procedure, it was not feasible to perform a sensitivity analysis on all the parameters during the actual coupling. However, a course analysis was performed on the effects of adjusting A_{Zmax}, the maximum eddy viscosity. This coefficient was previously discussed in Section 3.1. It was found that the plume rise height and final flowrate (and therefore temperature and DO) do depend on the value of A_{Zmax}. As mentioned previously, using the default A_{Zmax} of $1x10^{-3}$ $m^2 s^{-1}$ increases the thermal gradient in the hypolimnion, which reduces the plume rise height. Because the plume model is uncalibrated, it is currently impossible to determine the proper rise height, however, the need to increase the A_{Zmax} from the W2 default value is apparent to achieve proper mixing.

The W2 default is to use the explicit solution technique with A_{Zmax} set to $1x10^{-3}$ $m^2 s^{-1}$ for deep, stratified lakes and reservoirs, however Cole and Wells (2002) recommend the implicit solution technique with A_{Zmax} set to 1 $m^2 s^{-1}$ for rivers and estuaries, and in coupled model (Wells 2003). In fact, according to Cole and Wells (2002), using the explicit solution technique with a value for A_{Zmax} above $1x10^{-2}$ $m^2 s^{-1}$ results in prohibitively slow run times, which was indeed found to be the case. In natural lakes, vertical eddy viscosities have been measured to be in the range of $3x10^{-6}$ $m^2 s^{-1}$ (Wüest et al. 2000) to 0.1 $m^2 s^{-1}$ measured in Zugersee (Switzerland) during an extremely strong storm (Lerman et al. 1995). In Hallwilersee (Switzerland), a natural lake that uses a bubble-plume diffuser, the apparent eddy viscosity was measured by McGinnis et al. (2003) to be as high as $1.7x10^{-3}$ $m^2 s^{-1}$. Hallwilersee uses approximately the same airflow rate at the same depth as SHR, however the volume of the hypolimnion is around 200 times larger. This translates to 200 times more energy per unit volume in the hypolimnion of SHR. Assuming direct scalability, this results in an A_{Zmax} of up to 0.3 $m^2 s^{-1}$ in SHR, two orders of magnitude larger than values typically seen in natural lakes without artificial oxygenation. If computational speed is not an issue, and since the A_Z is

calculated for each cell, it is recommended that the implicit solution technique be used with removal of the restrictions on A_{Zmax} (Wells 2003).

6.4 W2 Assumptions

The entire plume discharge is mixed into the detrainment cell due to the laterally averaged assumption. Because the theoretical plume width at the point of detrainment approaches infinity, this instantaneous mixing appears reasonable to a first approximation, particularly in a narrow reservoir such as SHR. However, it is also clear that the laterally averaged assumption inhibits the proper longitudinal transport of constituents, particularly in 1997 where the water flowrate is higher. As shown in Figure 8, the model predicts a higher zone of oxygen and temperature above the diffuser and slightly upstream with $A_x = 1\ m^2\ s^{-1}$. Data from 1997, 1998 and the current (2003) diffuser testing show that SHR is much more well-mixed than the model predicts in this case. Based on the sensitivity analysis, the dominant parameter controlling the mixing is the horizontal eddy viscosity. To compensate for this, A_x was estimated for 1997 based on the calibration, and scaled to 1998 using a Fickian diffusion local closure scheme. This results in better mixing of the water column as shown in Figure 8. This also has the effect of distributing the velocities and resulting shear stress more uniformly, resulting in the proper extent of mixing below the diffuser.

There are very few studies on horizontal transport in lakes and reservoirs, and the mechanisms remain poorly understood (Lerman et al. 1995, Stocker and Imberger 2003). Horizontal diffusivity and eddy viscosity are currently time and space invariant, however it is suggested that a more appropriate method for calculating these values should be established. One of the goals of the ongoing research is to determine these values, both with and without diffuser operation, and to formulate such a method.

W2 also invokes the hydrostatic pressure assumption, which means that there is no vertical momentum. This prevents accurate modeling of vertical accelerations, such as convective cooling (Cole and Wells 2002). It is currently unclear what impact this assumption has on the coupled plume model. It is felt, however, that the shear forces are accurately parameterized so that the right amount of warming takes place, and that the dominant mixing still occurs in the horizontal direction. The case where this may be important is if there is substantial mixing within the detrained plume water (McGinnis et al. 2003). If the density of the detrained plume water is high enough to result in substantial momentum in the fallback water, the fallback water could pass the point of the ED, resulting in significant additional entrainment below the point of neutral buoyancy (ED). This will also result in more mixing at deeper depths before the fallback water finally reaches a point of neutral buoyancy.

While it is true that the W2N turbulence algorithm has been positively tested on many waterbodies, it's ability to accurately handle the mixing resulting from the bubble-plume should be further tested, as this is a novel application of W2 and the incorporated turbulence algorithms. While the results are encouraging, further investigation into the available turbulence algorithms is desirable once the formal coupling is completed. A k-epsilon turbulence algorithm should be available for W2 in the near future where all of

the available turbulence closure models collapse to a single model (Cole and Wells 2002).

6.5 Plume Model Assumptions

The primary assumption is that, given that the linear-plume model in uncalibrated at this point, using the values obtained in literature for the entrainment coefficient and the plume width ratio provide reasonable estimates of the DMPR, and other crucial plume properties. Furthermore, plume cross-flow and multiple detrainment are also neglected, which may have a significant impact on constituent transport. A top hat distribution is used for water velocity, temperature, TDS, bubble velocity, and gaseous constituent concentrations within the plume. In reality, a Gaussian velocity distribution probably exists. This leads to an underprediction of the plume rise height, and the subsequent underprediction of mixing in W2, particularly when the plume reaches the thermocline. The entrainment coefficient is also not well understood for linear plumes. It is currently treated as a constant, but has been suggested to change, particularly due to enhanced turbulent mixing between the plume fall back water, and the rising plume boundary (Brevik and Kristiansen 2002).

While the effects of density stratification are included in the plume model, the behavior of the plume model in the 1997 case is uncertain in the upstream-most segments where the diffuser is located in or very close to the thermocline. Due to the strong temperature gradient, the plume rise height is less than two meters in each of the upstream-most segments where the diffuser is actually in the thermocline. This is likely to prevent an established flow field from developing, however no data currently exist to verify plume behavior with such extreme boundary conditions. Furthermore, secondary plume formation is neglected. This may have a substantial effect, particularly if the primary plume stops early due to such a strong density gradient, as in the case of the plume in the thermocline. Bubbles from the primary plume continue to rise forming a second plume that would promote further, perhaps relatively vigorous, mixing.

7. Conclusions

The goal in this study was to explore the viability of W2 to handle plume-enhanced mixing and transport. While the preliminary results of the coupled model are encouraging, the iterative "manual" coupling procedure is time consuming. Given the preliminary, positive results, the plume model will therefore be incorporated as a subroutine in W2 so that the computation can be performed automatically. The sensitivity of various parameters can then be investigated more thoroughly. For example, the location of the boundary condition profiles with respect to the plume predictions will be important, particularly if there is a large degree of spatial variability (McGinnis et al. 2003). Additionally, W2 should be modified to include an algorithm for the horizontal eddy viscosity and diffusivity, allowing these parameters to vary both spatially and temporally. It may also necessary to increase or eliminate the A_{Zmax} restriction to achieve proper mixing. Further testing and calibration of the linear plume model, W2 and the coupled model are being carried out with new data currently being collected at Spring Hollow Reservoir in Virginia as well as at Lake Hallwil in Switzerland. The values of horizontal and vertical diffusivity, as well as the plume rise height, will be established

using data from thermistor arrays as well as from measured temperature and oxygen concentration profiles.

The coupled model is promising as W2 seems to accurately predict the mixing mechanisms induced by plume operation, and the current research will further enhance the understanding of the plume behavior and the plume-reservoir interaction. The coupled model should then prove to be a valuable tool for the design and optimization of bubble-plume diffusers in lakes and reservoirs. The natural extension of this work is to incorporate other hypolimnetic oxygenation devices, such as the full-lift hypolimnetic aerator and the Speece Cone. The coupled model can also easily be extended to include thermal plumes resulting from pumped inflow, and is likely necessary to accurately model the pumped inflow from the vertical influent pipe in Spring Hollow Reservoir.

8. Nomenclature

A_x horizontal eddy viscosity, $m^2\ s^{-1}$.
A_z vertical eddy viscosity, $m^2\ s^{-1}$.
C dissolved concentration, mol m^{-3}.
C_B Chezy friction factor, -.
C_D surface drag coefficient, -.
D depth, m.
D_x horizontal diffusivity, $m^2\ s^{-1}$.
E entrainment, $m^2\ s^{-1}$.
f_i internal friction factor, -.
F_D dissolved species flux, mol s^{-1}.
F_G gaseous species flux, mol s^{-1}.
F_S salinity flux, g s^{-1}.
F_T temperature flux, $^oC\ m^3\ s^{-1}$.
g gravitational acceleration, m s^{-2}.
H Henry's coefficient, mol m^{-3} bar^{-1}.
k wave number, m^{-1}.
K_L mass transfer coefficient, m s^{-1}.
l vertical length scale, m.
L plume length, m.
M water momentum, $m^4\ s^{-2}$.
N number flux of bubbles, s^{-1}.
P pressure, bar.
Q flow rate, $m^3\ s^{-1}$.
r bubble radius, m.
Ri Richardson number, -.
S salinity, g kg^{-1}.
T temperature, ^oC.
v velocity, m s^{-1}.
V_g gas holdup, -.
W plume width, m.
y gaseous concentration, mol m^{-3}.
z depth, m.

Greek letters

α	entrainment coefficient, -.
Θ	wind direction, rad.
κ	von Kerman constant, -.
λ	spreading coefficient, -.
ρ	density, kg m^{-3}.
σ	cloud radius, m.
τ	shear stress, N m^{-2}.

Subscripts

a	ambient water, air
b	bubble, bottom
i	gas species, oxygen or nitrogen
l	lateral inflow
p	plume water and gas mixture
w	plume water, wind
x	x-axis of lake
y	y-axis of lake

9. References

Asaeda, T., and J. Imberger. 1993. Structure of bubble plumes in linearly stratified environments. J. Fluid Mech. **249**: 35-57.

Beutel, M. W., and A. J. Horne. 1999. A review of the effects of hypolimnetic oxygenation on lake and reservoir water quality. Journal of Lake and Reservoir Management **15** (4): 285-297.

Borchers, O., C. Busch, A. Sokolichin, and G. Eigenberger. 1999. Applicability of the standard k-e turbulence model to the dynamic simulation of bubble columns. Part II: Comparison of detailed experiments and flow simulations. Chemical Engineering Science **54**: 5927-5935.

Brevik, I., and Ø. Kristiansen. 2002. The flow in and around air-bubble plumes. International Journal of Multiphase Flow **28**: 617-634.

Burris, V. L., D. F. McGinnis, and J. C. Little. 2002. Predicting oxygen transfer rate and water flow rate in airlift aerators. Water Research **36**: 4605-4615.

Chisti, M. Y. 1989. Airlift Bioreactors. Elsevier Science Publishing, New York.

Cole, T. M., and E. M. Buchak. 1995. CE-QUAL-W2: A two-dimensional, laterally averaged, Hydrodynamic and Water Quality Model, Version 2.0, Instruction Report EL-95-. US Army Engineering Waterways Experiment Station, Vicksburg, MS.

Cole, T. M., and S. A. Wells. 2000. CE-QUAL-W2: A two-dimensional, laterally averaged, Hydrodynamic and Water Quality Model, Version 3.0, Instruction Report EL-2000-. US Army Engineering and Research Development Center, Vicksburg, MS.

Cole, T. M., and S. A. Wells. 2002. CE-QUAL-W2: A two-dimensional, laterally averaged, Hydrodynamic and Water Quality Model, Version 3.1, Instruction Report EL-2002-1. US Army Engineering and Research Development Center, Vicksburg, MS.

Cooke, G. D., E. B. Welch, S. A. Peterson, and P. R. Newroth. 1993. Restoration and Management of Lakes and Reservoirs, Second Edition. Lewis Publishers, Boca Raton.

EPA. 2003. Clean Water Act. US Environmental Protection Agency. Laws & Regulations. http://www.epa.gov/region5/water/cwa.htm February 20, 2003.

Fannelop, T. K., S. Hirschberg, and J. Kuffer. 1991. Surface current and recirculating cells generated by bubble curtains and jets. Journal of Fluid Mechanics **229**: 629-657.

FERC. 2001. Report on hydroelectric licensing policies, procedures, and regulations. Comprehensive review and recommendations pursuant to section 603 of the Energy Act of 2000. Report submitted to the United States Congress by the Department of Energy. May 8, 2001.

FERC. 2003. Water power - Use and regulation of a renewable resource. http://www.ferc.gov/hydro/docs/waterpwr.htm.

Imboden, D. M., and A. Wüest. 1995. Mixing mechanisms in lakes. *in* A. Lerman, D. M. Imboden, and J. R. Gat, editors. Physics and Chemistry of Lakes. Springer-Verlag, Berlin.

Johnson, G. P., N. J. Hornewer, D. M. Robertson, D. T. Olson, and J. Gioja. 2000. Methodology, data collection, and data analysis for determination of water-

mixing patterns induced by aerators and mixers. Water-Resources Investigations Report 00-4101, U.S. Department of the Interior, U.S. Geological Survey, Urbana, Illinois.

Jung, R., J. O. Sanders, and H. H. Lai. 1998. Improving water quality through lake oxygenation at Comanche Reservoir. Presentation at the Cal. Lake Manage. Soc., Corte Madera.

Lemckert, C. J., and J. Imberger. 1993. Energetic bubble plumes in arbitrary stratification. Jour. Hyd. Eng. **119** (6): 680-703.

Lerman, A., D. M. Imboden, and J. R. Gat, editors. 1995. Physics and Chemistry of Lakes. Springer-Verlag, Berlin.

Little, J. C., and D. F. McGinnis. 2001. Hypolimnetic oxygenation: Predicting performance using a discrete-bubble model. Water Science & Technology: Water Supply **1** (4): 185-191.

Lorke, A., B. Müller, M. Maerki, and A. Wüest. 2003. Breathing sediments: The control of diffusive transport across the sediment-water interface by periodic boundary-layer turbulence. Limnol. Oceanogr. **accepted**.

McDougall, T. J. 1978. Bubble plumes in stratified environments. J. Fluid Mech. **85** (4): 655-672.

McGinnis, D., A. Lorke, J. C. Little, and A. Wüest. 2003. The interaction between bubble plumes and their near-field environment: Influences on plume transport and modeling. **In preparation**.

McGinnis, D. F., and J. C. Little. 1998. Bubble dynamics and oxygen transfer in a Speece Cone. Water Science & Technology **37** (2): 285-292.

McGinnis, D. F., and J. C. Little. 2002. Predicting diffused-bubble oxygen transfer rate using the discrete-bubble model. Water Research **36**: 4627-4635.

Mobley, M. H. 1997. TVA reservoir aeration diffuser system. TVA Technical Paper 97-3. ASCE Waterpower '97, Atlanta, GA, August 5-8.

Moosmann, L., D. McGinnis, and A. Wüest. 2002. Erhöhte Sauerstoffzehrung im Sommer 2001 im Hallwilersee - Ursachen und Handlungsmöglichkeiten. EAWAG Report to Canton Aargau.

Nakamura, Y., and H. G. Stefan. 1994. Effect of flow velocity on sediment oxygen demand: Theory. Journal of Environmental Engineering **120** (5): 996-1016.

Orsat, V., C. Vigneault, and G. S. V. Raghavan. 1993. Air diffusers characterization using a digitized image analysis system. Applied Engineering in Agriculture **9** (1): 115-121.

Peeters, F., A. Wüest, G. Piepke, and D. M. Imboden. 1996. Horizontal mixing in lakes. Journal of Geophysical Research **101** (C8): 18,361-318,375.

Stephenson, K. 2000. Taking nature into account: Observations about the changing role of analysis and negotiation in hydropower re-licensing. William and Mary Environmental Law and Policy Review **25** (2): 473-498.

Stocker, R., and J. Imberger. 2003. Horizontal transport and dispersion in the surface layer of a medium-sized lake. Limnol. Oceanogr. **48** (3): 971-982.

Sundermeyer, M. A., and J. F. Price. 1998. Lateral mixing in the North Atlantic tracer release experiment: Observations and numeric simulations of Lagrangian particles and a passive tracer. Journal of Geophysical Research **103** (C10): 21,481-421,497.

Wu, R. S. S., B. S. Zhou, D. J. Randall, N. Y. S. Woo, and P. K. S. Lam. 2003. Aquatic hypoxia is an endocrine disruptor and impairs fish reproduction. Environ. Sci. Technol. **37** (6): 1137-1141.

Wüest, A., N. H. Brooks, and D. M. Imboden. 1992. Bubble plume modeling for lake restoration. Water Resources Research **28**: 3235-3250.

Wüest, A., and A. Lorke. 2003. Small-Scale Hydrodynamics in Lakes. Annu. Rev. Fluid Mech. **35**: 373-412.

Table 1. Operating conditions for bubble-plume diffuser in Spring Hollow Reservoir.

Parameter	1997	1998
Maximum depth [m]	50	55
Surface area [10^6 m^2]	0.36	0.4
Total water volume [10^6 m^3]	6.1	7.2
Active diffuser length [m]	1070	360
Average diffuser depth [m]	32	43
Air flow rate [Nm^3 h^{-1}]*	192	43

*1 Nm^3 denotes 1 m^3 of gas at 1 bar and 0 ^oC

Table 2. Key model variables.

Variable	Formula	Units
Entrainment	$E = 2(L + W)\alpha v$	$m^2\ s^{-1}$
Plume Water Volume Flux	$Q = LWv$	$m^3\ s^{-1}$
Momentum Flux	$M = LWv^2$	$m^4\ s^{-2}$
Temperature Flux	$F_T = QT_p$	$^oC\ m^3\ s^{-1}$
Dissolved Solids Flux	$F_s = QS\rho_w$	$g\ s^{-1}$
Dissolved O_2 and N_2 Fluxes	$F_{Di} = QC_i$	$mol\ s^{-1}$
Gaseous O_2 and N_2 Fluxes	$F_{Gi} = LW\lambda^2(v + v_b)y_i$	$mol\ s^{-1}$

Table 3. Non-linear differential flux equations.

Water Volume Flux	$\frac{dQ}{dz} = E$
Momentum Flux	$\frac{dM}{dz} = \frac{\rho_a - \rho_p}{\rho_p} gLW\lambda^2 + \frac{\rho_a - \rho_w}{\rho_p} gLW(1-\lambda^2)$
Temperature Flux	$\frac{dF_T}{dz} = ET_a$
Salinity Flux	$\frac{dF_s}{dz} = E\rho_a S_a$
Dissolved Gas Flux	$\frac{dF_{Di}}{dz} = EC_i + \frac{4\pi r^2 N}{v + v_b} K_L (H_i P_i - C_i)$
Gas Flux	$\frac{dF_{Gi}}{dz} = -\frac{4\pi r^2 N}{v + v_b} K_L (H_i P_i - C_i)$

Table 4. Correlation equations for Henry's constant, mass transfer coefficient, and bubble rise velocity (Wüest et al., 1992).

Equation	**Range**
$H_O = 2.125 - 5.021 \times 10^{-2}T + 5.77 \times 10^{-4}T^2$ (mol m^{-3} bar^{-1}) $H_N = 1.042 - 2.450 \times 10^{-2}T + 3.171 \times 10^{-4}T^2$ (mol m^{-3} bar^{-1})	(T in ^oC)
$K_L = 0.6r$ (m s^{-1})	$r < 6.67 \times 10^{-4}$ m
$K_L = 4 \times 10^{-4}$ (m s^{-1})	$r \geq 6.67 \times 10^{-4}$ m
$v_b = 4474r^{1.357}$ (m s^{-1})	$r < 7 \times 10^{-4}$ m
$v_b = 0.23$ (m s^{-1})	$7 \times 10^{-4} \leq r < 5.1 \times 10^{-3}$ m
$v_b = 4.202r^{0.547}$ (m s^{-1})	$r \geq 5.1 \times 10^{-3}$ m

Table 5. Default hydraulic parameters in W2, and the ranges investigated for the sensitivity analysis.

Parameter, and W2 variable	**Units**	**Default**	**Range**
Maximum vertical eddy viscosity, Az_{max}	$m^2\ s^{-1}$	1.0E-1	1.0E-3 – 1.0E3
Longitudinal eddy viscosity, A_x	$m^2\ s^{-1}$	1	0.1 – 50
Longitudinal eddy diffusivity, D_x	$m^2\ s^{-1}$	1	0.2 – 50
Chezy coefficient, C_B	$m^2\ s^{-1}$	70	0 – 70
Internal friction factor, f_i	-	0.01	0.01 – 1
Wind sheltering coefficient, WSC	-	1	0 – 1

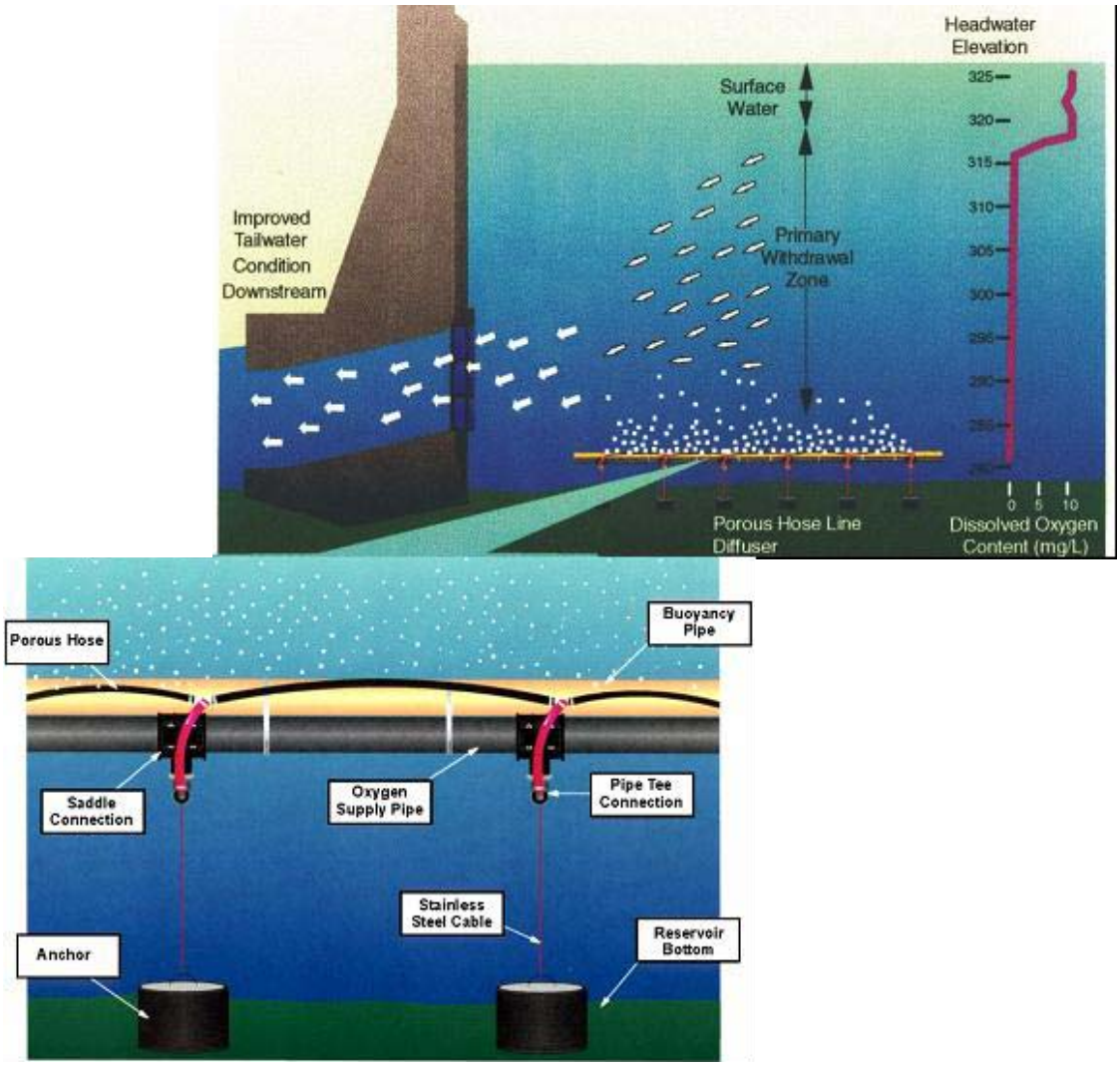

Figure 1. Schematic of linear diffuser in Spring Hollow reservoir, and typical configuration for hydropower reservoir installations. Figure courtesy of M. Mobley (Mobley 1997).

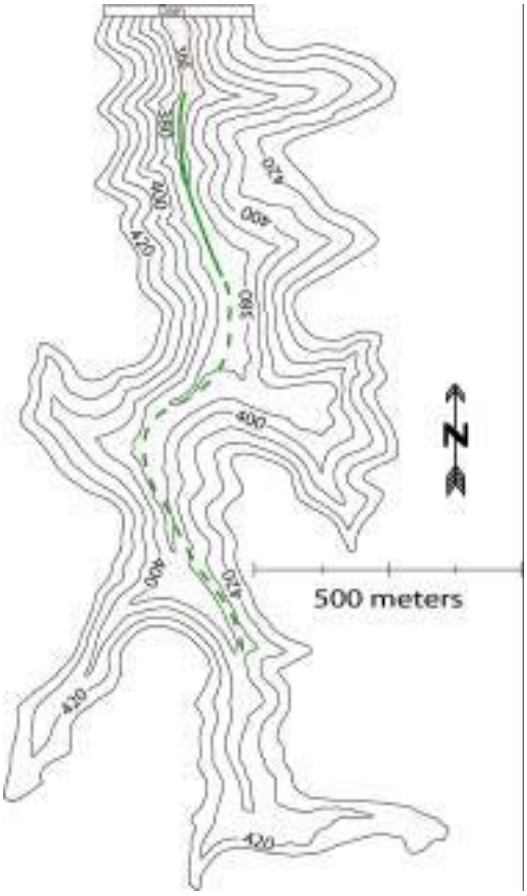

Figure 2. Spring Hollow Reservoir bathymetry (10 meter contours) and line diffuser location. The solid and dashed lines represent the total diffuser length for 1997, while the solid line represents the length for 1998.

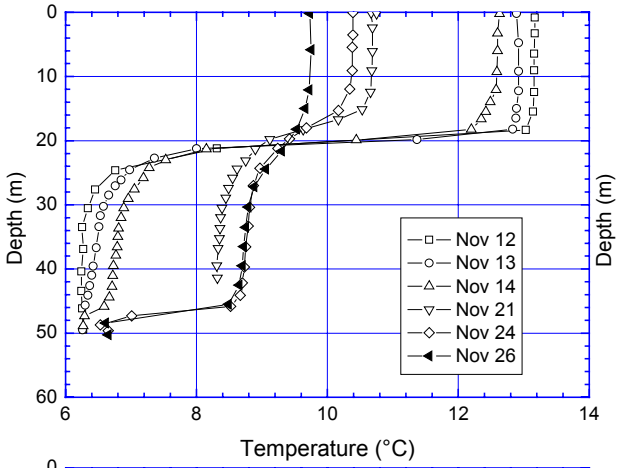

Figure 3a. Observed temperature profiles in Spring Hollow Reservoir for 1997 (above) and 1998 (below).

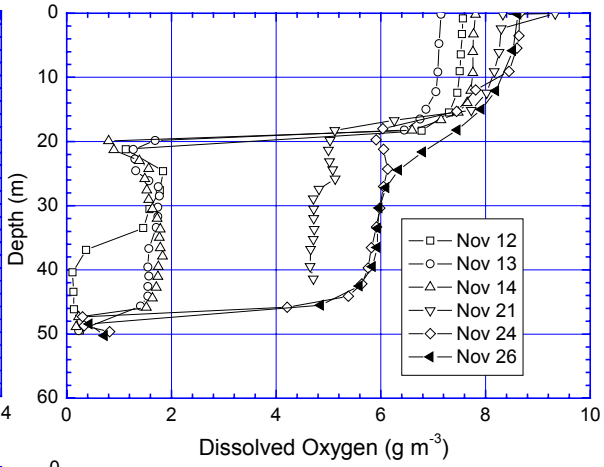

Figure 3b. Observed oxygen profiles in Spring Hollow Reservoir for 1997 (above) and 1998 (below).

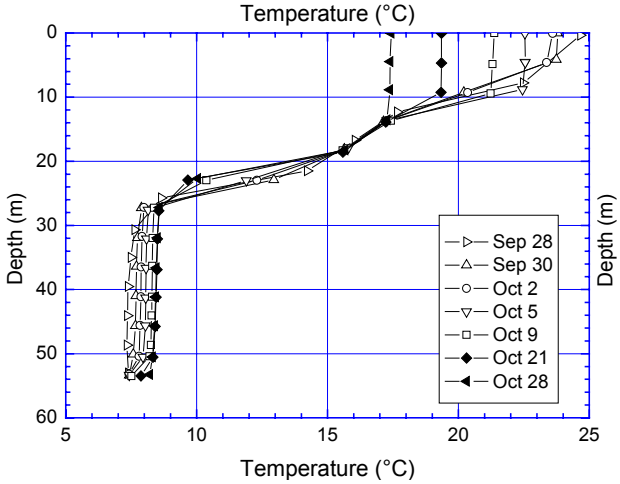

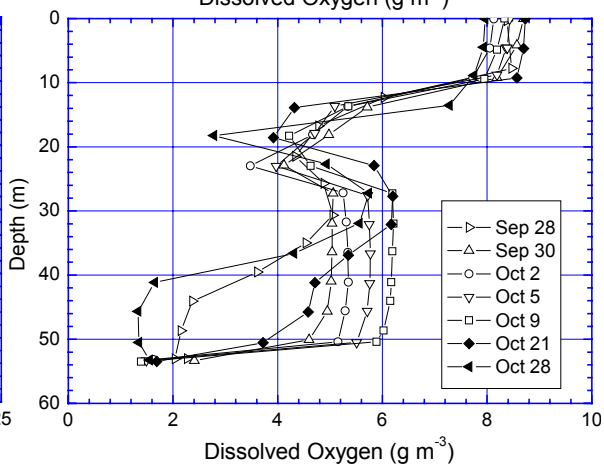

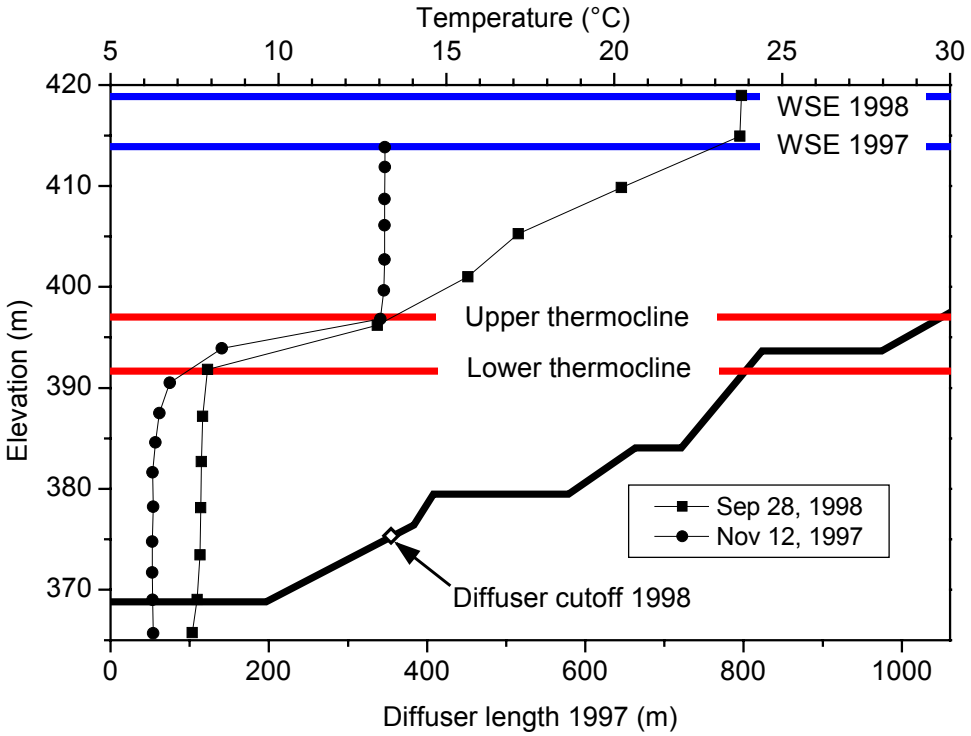

Figure 4. Diffuser elevation in 1997 and 1998. The diffuser was shortened in 1998 so that only the deepest portion was operated. Also shown are the water surface elevations (WSE) for 1997 and 1998, the approximate thermocline location, and the temperature profiles at the time of diffuser startup.

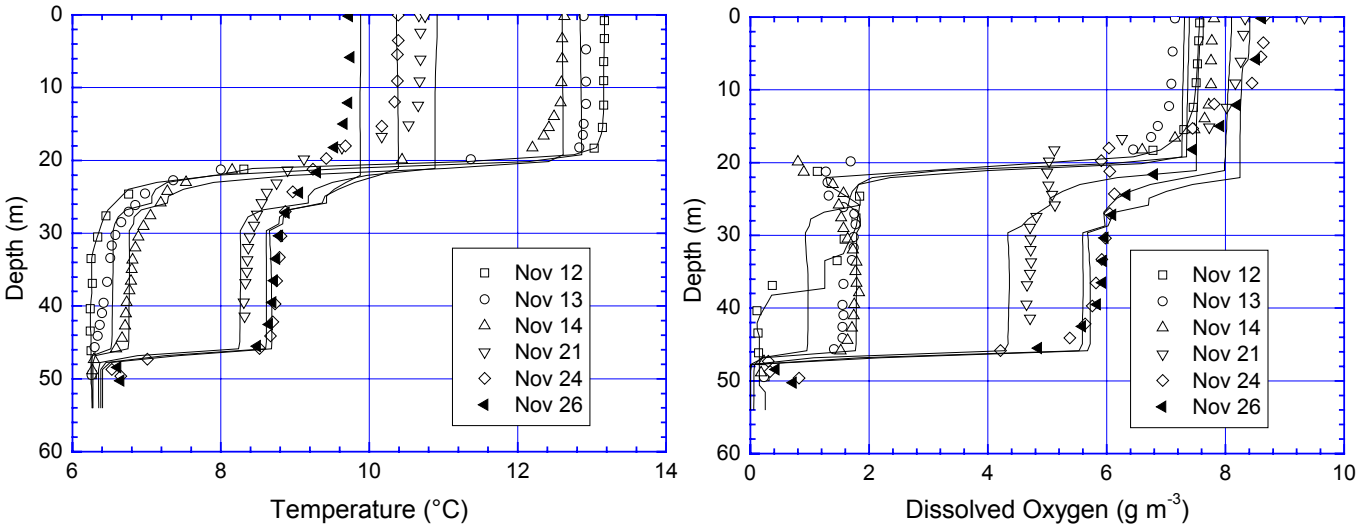

Figure 5. Results from 1997 full manual coupling.

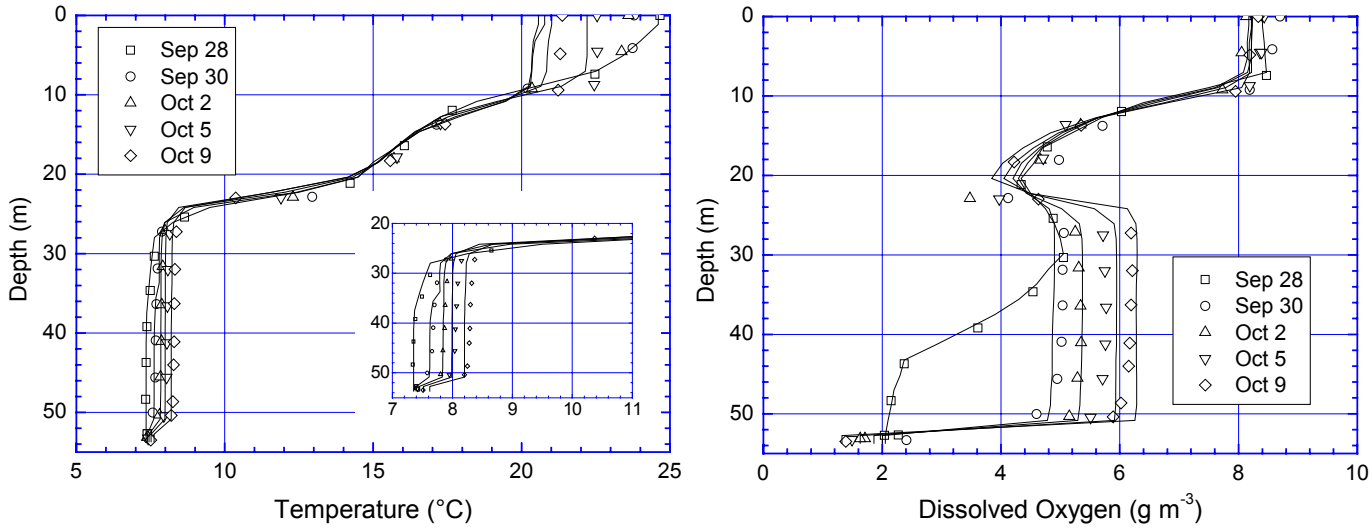

Figure 6. Results from 1998 full manual coupling.

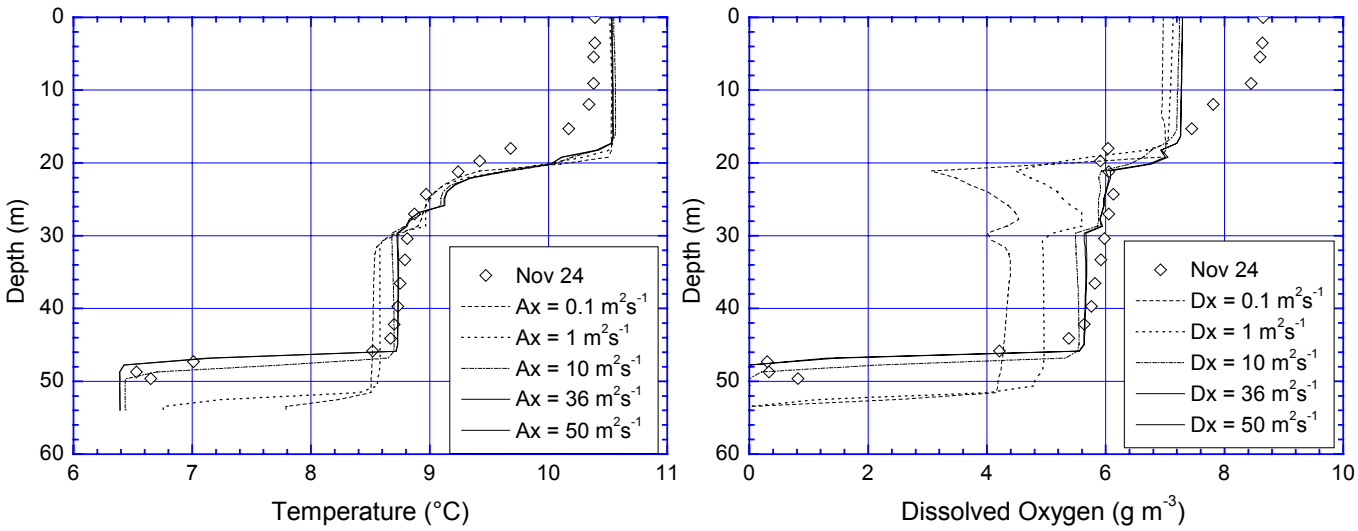

Figure 7. Sensitivity analysis for the longitudinal eddy viscosity, A_x.

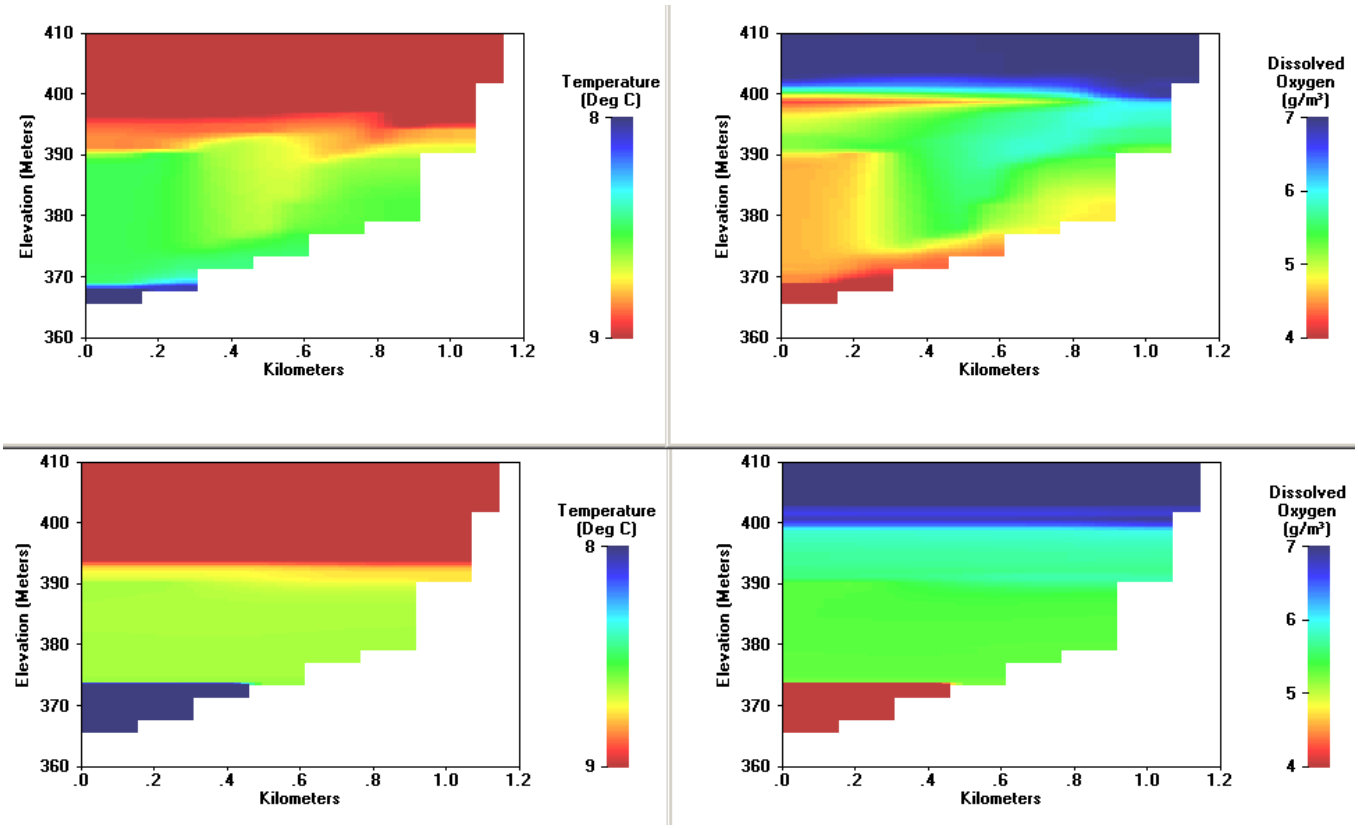

Figure 8. W2 predicted DO and temperature contours for November 23, 1997 for the case of $A_x = 1\ m^2\ s^{-1}$ (top) and $A_x = 50\ m^2\ s^{-1}$ (bottom).

CHAPTER 4: SEDIMENT RETENTION IN THE IRON GATE I RESERVOIR: EFFECT OF THE DANUBE RIVER BAYS AND THE IMPLICATIONS FOR NUTRIENT RETENTION

D. McGinnis[1], S. Bocaniov[2], C. Teodoru[2], G. Friedl[2], A. Lorke[2] and J. Wüest[2]

[1] *Department of Civil and Environmental Engineering, Virginia Tech, Blacksburg, USA*
[2] *Applied Aquatic Ecology, EAWAG, Kastanienbaum, Switzerland*

Abstract

Constructed in 1972, Iron Gate I Reservoir is the largest impoundment on the Danube River. Previous nutrient studies applied to the Danube River show large differences between nutrient and sediment loads to the Danube River and the loads that enter the Danube Delta and the Black Sea. Dissolved silica measurements in the coastal Black Sea in the vicinity of the Danube Delta indicate a 60% reduction since 1972. Additionally, measurements revealed an enormous reduction in the amount of sediment reaching the Danube Delta in the mid 1970s, the years immediately following the Iron Gate I construction. Iron Gate I, therefore, has been hypothesized as a possible sediment trap and nutrient sink due to increased primary productivity associated with damming the river. To assess the role as a sediment and nutrient sink, a reservoir model, CE-QUAL-W2, was applied to Iron Gate I. Additionally, a sediment balance was performed using suspended solids data on the lower reach of the Iron Gate I, and a thermal balance was performed on the adjoining bays to assess their roles as possible sinks. The main findings of this study are that (i) there is a significant lack of thermal stratification and associated primary productivity in the main branch; (ii) Orsova Bay is the only suspected permanent sediment trap within the study area; (iii) it is estimated that only 1100 to 6400 kt yr^{-1} (3 – 19%) of suspended solids entering the system are trapped; and (iv) the possible annual retention of suspended solids-related silica is between 2.5 – 15 kt yr^{-1}, or 3.5 – 21%. The higher values assume that no sediment resuspension occurs in the main branch, which in reality is unlikely. Therefore, it is suggested that upstream sources, such as other impoundments, may be responsible for the reported sediment and nutrient reductions.

Keywords

Danube, Bays, Dams, Nutrient retention, Sedimentation, Modeling, Suspended solids

1. Introduction and Motivation

The Danube River is the largest river in Europe. Originating in the Black Forest region in Germany, it flows east for approximately 2850 km, drains approximately 1/12 of the European landmass and discharges in the Black Sea shelf. The drainage basin is the largest in Western Europe at 800,000 km^2 and includes at least parts of 14 countries (ICPDR 2001). The average yearly outflow at the Danube Delta is approximately 5,600 $m^3 s^{-1}$ (Friedl et al. 2003). Several dams have been developed on the Danube in different countries for hydropower generation, water supply, irrigation and flood control. The Iron Gate project is the largest of these and is located in Orsova, Romania. It is jointly operated by Romania and the Federal Republic of Yugoslavia and consists of the upper Iron Gate I Dam (1972) and the lower Iron Gate II Dam (1984). The generation capacities are 2100 and 432 MW, respectively (NR, 1998). Iron Gate I is the largest project on the Danube both in terms of reservoir capacity and hydropower generation. The riverine reservoir at full-pool conditions stores 3.2 billion m^3, is 117 km in length and has a surface area of about 100 km^2 (Friedl et al. 2003).

There are several concerns emerging about the environmental effects of the Iron Gate project, as well as dams in general (Friedl and Wüest 2002). The primary concern of this work is the effect of damming on the local and downstream suspended solids and nutrient budgets (Humborg et al. 1997, Humborg et al. 2000). As the largest reservoir system in Western Europe, Iron Gate has great potential for trans-boundary environmental impacts. There are several indications that Iron Gate I is a significant sink for sediments and nutrients, particularly silica (Si) and phosphorus (P), and to a lesser extent nitrogen (N) (Friedl et al. 2003). A preliminary nutrient balance performed by Zessner and Kroiss (1998) shows a significant difference between estimated Si loads in the surface waters to the Danube Basin and those measured entering the Danube Delta and the Black Sea. For example, the total annual loads of N and P to the surface waters of the basin are estimated to be 1,150 – 1,400 kt yr^{-1} (1 kt is 1000 metric tons) and 140 – 190 kt yr^{-1}, respectively, while measurements at the mouth of the Danube indicated only 400 kt yr^{-1} and 20 – 50 kt yr^{-1}, respectively (DARP 1997). One explanation for these enormous reductions in the nutrient load is that retention, due largely to sedimentation, plays an important role in the Iron Gate system. More important for this study, Iron Gate I is suspected to have caused 80% of the total reduction of Si in the form of settled diatom frustules (approximately 600 kt yr^{-1}) seen in the Black Sea at the shelf, and the project may have caused a dramatic shift in the algal species composition from diatoms to nuisance blue-green algae, resulting in a reduction in fisheries (Humborg et al. 1997, SCOPE 1999, Humborg et al. 2000, Friedl et al. 2003). Additionally, a reduction of 30,000 kt yr^{-1} of sediment load has been documented since the construction of the Iron Gate system, resulting in coastline erosion at the Danube Delta (Panin et al. 1999, WCD 2001, Friedl et al. 2003).

To study the role of Iron Gate I as a sink for nutrients and sediments, the Swiss Federal Institute for Environmental Science and Technology (EAWAG), in co-operation with the Romanian National Institute of Marine Geology and Geo-ecology (GeoEcoMar) and the University of Geneva (Institute F.-A. Forel), implemented a 2-year project in February 2001 titled "Nutrients and Metal Retention Capacity of the Iron Gate Reservoirs (Danube River, Romania)". The present study is only a partial contribution to that work, and

continued analysis is being performed to improve understanding of the system. The particular focus of this work is suspended-solids related nutrient and sediment retention in the lower reach of Iron Gate I, particularly the two most downstream bays, Orsova and Eselnita (Figure 1). The somewhat limited scope of this study does not classify all of the sources of nutrient and sediment retention, but the study attempts to determine the degree to which sediment and nutrient retention is occurring by determining 1) if Iron Gate I is stably stratified so that primary productivity is supported, and 2) the contribution of the lower reach of the reservoir and two adjacent bays to sediment retention.

To aid in understanding the sediment and nutrient retention processes, the lower reach of Iron Gate I is firstly modeled with a 2-dimensional lake and reservoir model. Thermal and sediment mass balances are then performed to estimate the sediment deposition rate in the lower reach of the main branch and two adjacent bays, Orsova Bay and Eselnita Bay. Finally, estimates are made for total annual suspended solids retention at each site and the whole system, and any potential zones of primary productivity are identified.

2. Equipment and Methods

The first year of the project was devoted primarily to data collection from February 2001 until October 2001. There were two scientific cruises (March 18-28 and October 14-19) consisting of velocity and backscatter profiles using a boat-mounted acoustic Doppler current profiler (ADCP), water sampling, conductivity-temperature-depth (CTD) profiles, and sediment coring and sampling. Additionally, a meteorological station was installed at Orsova Bay, and several thermistor and sediment trap moorings were deployed.

The meteorological station (Aanderra) was installed March 26, 2001 near Orsova Bay. The measured parameters were 20-minute averages and included wind speed and direction, maximum wind gust, air temperature, incoming solar radiation, net radiation, and relative humidity. CTD profiles were measured during the two cruises with a Seabird SBE19 high-resolution profiler. The SBE19 samples at 2 Hz and measures temperature, pressure, DO, light transmission, pH and conductivity. The temperature loggers (thermistors), Vemco Minilog 12- and 8-bit manufactured by Vemco, LTD, were installed at the bottom (3.25 m above bottom) and at the surface (0.6 m below water surface) approximately 0.8 km upstream of the dam, and in Orsova and Eselnita Bays. The thermistors collected data from March 27 to October 19, 2001.

The ADCP measurements were performed using an RD Instruments Workhorse 600 kHz, which was attached to the boat facing downwards. The boat was driven slowly (2 km hr^{-1}) as the ADCP recorded the 3-dimensional velocity components within 50-cm vertical bins throughout the water column. The ADCP measurements were taken at different places, namely 1.2 km, 6 km and 15.5 km upstream of the dam and in Orsova Bay.

Using the collected data, the lower reach of Iron Gate I is modeled using CE-QUAL-W2 (W2), a 2-dimensional (2-D), laterally-averaged, hydrodynamic and water quality reservoir model (Cole and Buchak 1995, Cole and Wells 2000, 2002). W2 includes horizontal, but not vertical, momentum and accounts for momentum transfer from influent streams and the associated shear stress imparted to the water. The model is

calibrated using water level elevations, temperature, and water velocities measured during two scientific cruises. The calibrated model is then used to identify potential zones of sedimentation in the lower reach of Iron Gate I. This will provide a basis for the evaluation of sediment-related transport phenomena in the reservoir.

3. Lower Reach of the Main Branch

3.1 CE-QUAL-W2 Modeling

Objectives of the modeling part of this study were to simulate water level elevations, thermal structure, and hydrodynamics in Iron Gate I using W2, to aid in the prediction of zones of sedimentation and stratification, which supports primary productivity. The model results were then compared with collected data; particularly thermistor data and velocity profiles from the ADCP. Iron Gate I is a relatively narrow, riverine reservoir and, for modeling purposes, laterally homogeneous, making it ideal to model with W2 (Cole and Wells 2000). It should be noted that a significant portion of the sediment/nutrient and hydrodynamic processes, such as settling of suspended solids and increased primary productivity due to lower velocities and quiescent conditions, occur in bays (Bale and Giorgino 1998). There are two bays in the study area that exhibit complex hydrodynamics, namely Eselnita Bay and Orsova Bay (Figure 1). Due to 2-D limitations, it is not possible to effectively include these bays in W2; nevertheless, their effects need to be considered. Therefore, it was decided to use an analytical approach to quantify the impacts of the bays, including water exchange rate, to determine the sediment retention. This analysis was performed for both Eselnita and Orsova Bay.

The geometry of Iron Gate I is discretized into a series of longitudinal segments. Each segment is then further divided into vertical layers. The total length of Iron Gate I is 117 km; however, due to the lack of adequate boundary conditions and to focus the study on the downstream reach, the model is only applied for a distance of 20.5 km upstream of the dam (Figure 1). The discretized bathymetry consists of 44 active computational segments along the main branch. All segments are 500 m long except the first six segments from the dam, which range in length from 200 to 300 m. Each layer was 1 m thick for the shallowest 13 layers, and 0.5 m thick for the rest to more accurately represent the bathymetry. The simulation time was from March 19 – October 19, 2001.

3.1.1 Boundary Conditions

Upstream boundary conditions include measured water temperature every 30 minutes from the thermistor mooring and daily water levels from two gauging stations, Moldova Veche (river km 1048.9) and Orsova (river km 953.3), which were obtained from the Hungarian National Hydrological Forecasting Service. The river inflows were estimated by programming calculations based on the known water levels, geometry and outflow data. Outflow volume and temperatures were obtained from the Iron Gate I Dam Administration. The meteorological data was input into W2 at 20-minute intervals.

3.1.2 Model Results

Model calibration was achieved by performing a sensitivity analysis using the inflow, bathymetry (grid resolutions), wind speed and light extinction coefficient. Calibration data (i.e. field data) included CTD temperature profiles, thermistor data, and ADCP

velocity profiles. The model was then validated using data from the high flow period (March) and the low flow period (October). Both periods are generally in good agreement with the model predictions.

Simulated water levels were sensitive to inflow rates, and only small adjustments were required to obtain good agreement (Figure 2). Simulated near-surface and bottom water temperatures compared well with the thermistor data (Figures 3 and 4). Simulated near-bottom temperatures (approximately 3.25 meters above bottom) were within a maximum deviation of less than 0.5°C (Figure 4). The surface temperatures were overpredicted for the entire period, with the largest differences occurring during daytime (up to 2°C), and the smallest at night. The model underestimates the mixing intensity in the water column, and overpredicts daytime warming. The heat reaching the surface during the daytime hours is probably not adequately dispersed by mixing, resulting in temperatures that are too high. Further investigations into mixing and model light extinction coefficients are necessary to improve the surface temperature predictions.

Figures 5 a-c show the modeled water velocities compared to the measured values on the October 17 and 18, 2001 at 1.2, 6 and 15.5 km upstream of the dam. The ADCP measured vertical velocity profiles through the water column in the lateral direction. Each velocity component of the lateral profiles was then averaged and compared to the model predictions. The model reproduces reasonable water velocities within the range of measured values. However, the model fails to predict the rather uniform velocities measured in the water column. It is apparent from the results that the model is currently unable to represent the extent of mixing in the water column.

3.2 Thermal Stratification

An important nutrient sink can be relatively high rates of primary production. Relatively quiescent conditions are required for this to occur, indicated by the extent of thermal stratification. Thermal stratification is determined from the two thermistors moored 0.8 km upstream from the dam near the bottom and water surface. Figure 6 shows the extent of stratification. The average bi-monthly near-bottom and near-surface temperature differences are quite small for the entire period with a maximum value of about 0.3 °C, leading to the conclusion that the water column is relatively well mixed for the entire monitored period. The development of stratification is inhibited by the high flow to volume ratio, leading to the conclusion that Iron Gate I is continuously well mixed, which would limit primary productivity in the main branch.

3.3 Hydraulic Residence Time in Front of the Dam

The lower reach of the reservoir is defined as the 11-km long section between the dam and Orsova Bay, which has a total volume of 304 million m^3 (Figure 1). The hydraulic residence time (HRT) strongly influences limnological processes in lakes and reservoirs (Straškraba et al. 1993), including retention rates of dissolved and particulate matter, modifications to thermal structure and impacts on the size and composition of algal communities (Straškraba and Straškrabova 1975, Straškraba et al. 1993, Kennedy 1999). The HRT values for the warm period of the year (April – October) are between 0.4 and 1.5 days for the lower reach. This is a short residence time that would have a minimal

influence on water quality and allows little time for algae to increase their population. However, Ryding and Rast (1989) suggest that impoundment-related changes in water quality will occur when algal doubling times are less than the HRT. The generation time of algae (time for the population to double) is relatively short; the mean generation time for *Scenedesmus* is as little as 0.3 days (Jørgensen and Bendoricchio 2001). Also, Reynolds (1997) suggests that algal doubling rates are in the range of 0.5 to 1.5 day^{-1}. It is clear that nutrient-retention by algal uptake and the settling of algae are possible even at low HRTs; however, this is unlikely in Iron Gate I given the well-mixed nature of this reach of the reservoir.

3.4 Identification of Potential Zones of Sedimentation

According to Håkanson and Jansson (1983), sediment deposition for most grain sizes occurs at water velocities less than 10 cm s^{-1}. W2 was used to simulate horizontal water velocities from March 19 to October 19, 2001. The model predicts a large eddy formation during the entire simulation at river km 949 (7.5 km upstream of the dam) (Figure 7). The formation of this eddy corresponds to a submerged island and former Turkish village, Bahna. In this zone, the water flow reverses direction, and the velocities decrease to almost zero in some regions. Suspended solids may be drawn and deposited into this zone where the water velocity gradients are much lower than those in the rest of the reservoir. Thus, the Bahna region can be identified as a potential zone of sedimentation.

4. Eselnita Bay

Eselnita Bay, located approximately 17 km upstream from the dam on the Romanian side of Iron Gate I (Figure 1), is the second largest bay within the selected system boundaries (20.5 km from the dam). The basic morphological characteristics of the bay were calculated from the maps and transects obtained during the March 2001 cruise (Table 1). The surface area and volume of the bay vary considerably depending on the water level in the reservoir.

4.1 Calculation of the Exchange Rate with the Danube

Measured temperature is used to balance the thermal energy in the bay. A crucial contribution to this balance is the exchange of water between the Danube River and the bay, characterized by the water exchange rate (Q, m^3 s^{-1}). Temperature data were recorded in the bay (both at the surface and at the bottom) as well as in the Danube and can be used to estimate the water exchange rate between the Danube and the bay.

To calculate the water exchange rate, the heat-budget method was applied. The bay was considered to be a well-mixed reactor interacting only with the river water and the atmosphere. The sediment heat exchange was neglected. The heat balance can be written as:

$$\rho c_w \cdot V \cdot \frac{\partial T_E}{\partial t} = c_w \cdot \rho \cdot Q \cdot (T_D - T_E) + H_{net} \cdot A \qquad (1)$$

where ρc_w is the specific heat capacity for water, [J $(m^3 \cdot K)^{-1}$], V is the volume of Eselnita Bay (m^3) (Table 1), T_E is the average water temperature in the bay (K), t is the time interval (s), T_D is the water temperature measured in the Danube River (K), H_{net} is the heat flux from the atmosphere (W m^{-2}), and A is the surface area of the bay (m^2). The diurnal temperature fluctuation in the Danube reflects the daily changes in the atmospheric heat flux. Therefore, by calculating the heat attributed to those daily temperature fluctuations for a given time interval, the atmospheric heat flux can be determined. The following equation was used to calculate the atmospheric heat flux:

$$H_{net} = \frac{dT}{dt} \cdot z_{aver} \cdot \rho c_w \qquad (2)$$

where T is the difference in temperature between daily temperature fluctuations and the baseline (minimum) temperature (K) and z_{aver} is the average depth of the Danube River (m). The heat flux from the atmosphere was calculated as the five-day average for the time interval from May 3-7, 2001 using the diurnal temperature fluctuations in the Danube (Figure 8). The temperature fluctuations were averaged for each 30-minute time step (Figure 9). Two slopes representing dT/dt were then calculated for the heat gain and loss intervals (heat gain: from 8:00 to 18:00, and heat loss: from 18:00 to 7.30). The slopes are 0.0216 K s^{-1} (heat gain) and -0.0178 K s^{-1} (heat loss). Assuming heating occurs over 8 hours, it was reasonable to consider z_{aver} within the distance of water travel during this period. This was assumed to be approximately 9 km upstream, where ν = 0.32 m s^{-1} and z_{aver} = 18.53 m. The heat flux, H_{net}, can then be calculated for the heating and cooling intervals from Equation 2 as 469 W m^{-2} and -386 W m^{-2}, respectively.

The next step is to calculate the temperature in Eselnita Bay for different water exchange rates, Q, and to compare the calculated temperatures with the measured values (taken as the average of the measured bottom and surface temperatures). From Equation 1 it is possible to calculate $\partial T/\partial t$:

$$\partial T_E/\partial t = (Q/V) \cdot (T_D - T_E) + H_{net} \cdot (A/V)/\rho c_w. \qquad (3)$$

By assuming an arbitrary Q of 55 m^3 s^{-1}, $\partial T/\partial t$ is estimated for each 30-minute time step. The predicted temperature for the Eselnita Bay can then be found by:

$$T_{Eselnita\ Bay}(t_i) = T_{Eselnita\ Bay}(t_{i-1}) + (\Delta T/\Delta t) \times (t_i - t_{i-1}) \qquad (4)$$

This is repeated for different exchange rates from Q = 55 m^3 s^{-1} to Q = 95 m^3 s^{-1} (Figure 10). From Figure 10, it can be concluded that calculated temperatures for Q = 75 m^3 s^{-1} provide the closest fit for temperature. The corresponding HRT is 0.4 day. The weighted least-squares method is selected for a more precise estimation of Q between Eselnita Bay and the Danube. The values of sum of squares were calculated for Q of 50-100 m^3 s^{-1}, with the minimum also corresponding to an exchange rate Q = 75 m^3 s^{-1}.

4.2 Thermal Stratification in Eselnita Bay

The temperature data from the two thermistors deployed in Eselnita Bay were used to determine the extent of stratification. The differences between the top and bottom thermistors were plotted for each month, and the results are summarized in Table 2. The water column is nearly isothermal in early spring with diurnal stratification becoming apparent later in the spring. Table 2 indicates that the average daily stratification is lowest in March (0.1ºC) and September (0.03 ºC). The highest stratification is observed from May to July. Apart from daily stratification, the thermistor data indicate the development of a stable weak stratification (determined in this study as more than three days in duration) in the following time periods; mid-March (5 day stratification period); the entire month of May (one month stratification period); mid-June (7 day stratification period); and approximately half of August.

From the above calculations, it can be concluded that the overall effect of the hydrodynamics and sedimentation in the bay is not significant for the Danube. This is because both the HRT (0.4 day) and the percentage of the Danube water diverted to the bay (less than 1 %) are rather low, limiting sedimentation and nutrient uptake by primary productivity.

5. Orsova Bay

Orsova Bay, approximately 11 km upstream from the dam (Figure 1), is the largest bay within the study area. The basic morphometric characteristics of the bay were determined from the maps and transects obtained during the March 2001 cruise (Table 3). Unlike Eselnita Bay, a 5-meter high sill was measured with the bottom-tracking feature of the ADCP that separates Orsova Bay from the Danube River (Figure 11). The mouth of the bay is about 13 to 15 m deep depending on the water level in the reservoir.

5.1 Calculation of the Exchange Rate with the Danube

Calculation of the exchange rate was performed as described for Eselnita Bay for the same time interval (May 3-7, 2001). The heat flux is also assumed to be the same for the bay and for the Danube. According to Equation 2, H_{net} depends on the average depth of the Danube River for the 8-hour travel time distance from upstream to the bay. The average depth, z_{aver}, was determined to be 19.9 km. The atmospheric heat flux, H_{net}, was then calculated from Equation 2 as 502 W m^{-2} from 8:00 to 18:00 and -414 W m^{-2} from 18:00 to 8:00. From Equation 1, the average temperature in Orsova Bay is calculated for different water exchange rates (800 to 1450 m^3 s^{-1}). The bottom thermistor in Orsova Bay was lost, so no temperature data is available for this location. Therefore, the bottom temperatures in Orsova Bay are assumed to be close to those measured at the bottom of Eselnita Bay. Accounting for the different depths of the two bays (Orsova Bay is twice as deep as Eselnita Bay) and using existing temperature profiles taken in Orsova Bay, the bottom temperature for Orsova Bay was estimated to be 0.5 ˚C less than the corresponding bottom temperature in Eselnita Bay. The least-squares estimation of the temperatures calculated for the water exchange rate yielded Q = 1150 m^3 s^{-1}, which corresponds to a residence time of 0.5 day. This compares to a residence time of 0.4 day for Eselnita Bay.

5.2 Comparison of Calculated and Measured Exchange Rates

An analysis was performed to compare the calculated water exchange rate with the measured ADCP current velocities. During the October 2001 cruise, ADCP velocity profiles were performed in Orsova Bay (Figures 12 and 13a-c). Figure 13a shows the direction of flow, with a northerly inflow on the east side of the bay and a southerly outflow at the west side of the bay. From Figure 13c, the average water velocity for the lateral transects was determined for October 18 as υ_{in} = 8.11 cm s^{-1} and υ_{out} = 8.57 cm s^{-1}, with an average of υ_{avg} = 8.34 m s^{-1}. From the ADCP bottom tracking feature, the cross sectional area was calculated to be A = 24,355 m^2 with a corresponding water exchange rate of $Q_{measured}$ = 1000 m^3 s^{-1}. This results in a difference of only 12% between $Q_{measured}$ and $Q_{calculated}$, which is surprisingly consistent considering the different flow periods and measurement errors such as incomplete transects. (The boat was unable to measure completely from bank to bank, as water depth became too shallow). The water velocity was calculated as 9.5 cm s^{-1} using the 5-day average water exchange rate (May 3-7, 2001) and the average cross sectional area of the entire transect. The difference, therefore, between the measured and calculated water velocities is 14 %.

5.3 Thermal Stratification in the Bay

Initially, two thermistors were installed at 1 and 6.1 m depth in Orsova Bay. Unfortunately, the thermistor installed closest to the bottom was lost. Temperature data obtained only from one surface thermistor were not enough to describe the thermal stratification.

5.4 Orsova Bay as a Sediment and Nutrient Trap

It is obvious from the calculated exchange rate that Orsova Bay plays an important role in both the hydrodynamics and sediment transport in the Danube, as approximately 15% of the total Danube flow is diverted into the bay. Despite the low HRT of 0.5 days, Orsova Bay may play an important role in the sedimentation process and nutrient uptake by primary productivity. The average water velocities in the Danube at the mouth of Orsova Bay are in the range of 32 to 35 cm/s. As a fraction of the Danube water enters Orsova Bay, the average water velocities drop to values below 10 cm/s (Figure 13c). Many studies have been performed using flow velocity to estimate sedimentation. For example, Postma (1967) determined a critical value of 10 cm s^{-1} where river action begins to inhibit sedimentation. Therefore, deposition of sediments can be expected to occur in Orsova Bay where the average water velocity is typically below 9.5 cm/s.

Deposition is further supported by measurements of sediment concentrations taken along the Danube River in October at 4 m depth (except near Orsova Bay, where it was taken at 1 m depth) at different locations (Figure 14) (Teodoru 2002). The particle concentrations in the Danube drop in front of Orsova Bay by approximately 11 % (from 7.3 to 6.5 mg/L; Figure 14). This figure is in good agreement with the 15 % of the Danube discharge diverted to the bay. From these two values (11 % and 15 %), it is estimated that the bay traps about 70 % of the suspended particles from the Danube water entering the bay. This assumes that there is no removal in the river stretch between Eselnita Bay and Orsova Bay.

ADCP particle backscatter measurements were also taken together with suspended solids measurements at different locations along the Danube during the October cruise. The relationship between the ADCP particle backscatter (dB) and actual particle concentration (mg l^{-1}) was then estimated (Figure 15). The ADCP backscatter measurements were performed at the transect shown in Figure 12 in Orsova Bay on October 18, 2001. The average backscatter for inflow and outflow water was 65 dB and 68 dB, respectively (Figure 13b), corresponding to 5.3 mg/L and 7 mg/L, or about 25% increase. This is in direct contradiction to the previous sedimentation estimates for Orsova Bay. It is likely during the warmer weather and lower flowrates that some primary productivity may be occurring in the quiescent middle zone of the bay. The increase in the outflowing particle concentration may therefore be flushed algae, which is supported by the higher backscatter signal near the surface of the outflowing water in Figure 13b and by chlorophyll peaks observed in the center of Orsova Bay during Summer 2001 (Teodoru 2002; unpublished data). Furthermore, the higher backscatter signal does not necessarily translate to higher suspended solids. In the presence of several different types of particles, the ADCP backscatter signal may be stronger for one type of particle, such as algae, versus inorganic suspended solids making it difficult to distinguish individual particle types and concentrations. This is because the backscatter signal strength is highly dependent on particle size and composition. The ADCP backscatter signal has also been shown to be affected by the presence of algae air vesicles (Lorke et al. 2003).

However, the assumption that Orsova Bay is a significant sink for sediments is further supported by the measured particle concentrations with depth at four locations in October 2001 (Table 4). The average increase in the concentration per meter of depth is (in mg l^{-1}): 0.26 (Orsova Bay), 0.08 (Orsova), 0.07 (Bahna) and 0.04 (dam). The percent increase in particle concentration per meter of depth is: 4.9% (Orsova Bay), 1.17% (Orsova), 1.16% (Bahna) and 0.7% (dam). These calculations indicate the presence of a higher suspended solids gradient in Orsova Bay, while the other locations are more homogeneously distributed. This suspended solids gradient, taken together with the relatively small velocities, indicates that a higher rate of deposition takes place in Orsova Bay. This is reasonable in that if the vertical mixing (turbulent diffusivity) is low, the particle gradient becomes steeper.

Figures 16a-c show the results of the ADCP profiles taken in Orsova Bay (Figure 12) during the March 2001 cruise. The profiles indicate the flow direction (Figure 16a), backscatter signal strength (Figure 16b), and velocity magnitude (Figure 16c). The velocity direction (Figure 16a) clearly demonstrates a flow vortex in Orsova Bay similar to the October profiles (Figure 13a). However, contrary to the backscatter profiles in October (Figure 13b), there is a corresponding higher particle concentration flowing in (i.e. high backscatter signal, Figure 16b), corresponding with zones of higher velocity (Figure 16c). Note that, in general, the backscatter signal was much stronger during the March cruise (Figure 16b) than during the October cruise (Figure 13b) indicating a higher suspended solids concentration and larger particle sizes due to the higher flow rate in March. Based on a correlation developed between the backscatter signal and the measured suspended solids concentrations (not shown), it was estimated that the bay

retains 50% of the inflowing suspended solids in March 2001 (Figure 16b). This is reasonable given the estimated 70% retention at the lower flow rates during the October cruise.

6. Main Branch Sediment Balance

A simple mass balance was performed to estimate the suspended particle removal in the lower reach of the Danube. The ADCP backscatter measurements (i.e. suspended particle concentration) taken upstream and downstream of the bay (Figure 12) during the October 2001 cruise are used in conjunction with the correlation curve to estimate the suspended solids concentration (Figure 15). For the upstream (river km 959) and downstream (river km 949) transect, the average ADCP backscatter is 68.3 and 64.57 dB, respectively, which corresponds to a suspended particle concentration of 7.24 mg/L and 5.02 mg/L, respectively. This implies about 30 % suspended solids removal. Orsova Bay is estimated to be responsible for 8 to 11 % removal of particulate matter, leaving an additional 20% removal within the very short distance of 3 km from Orsova Bay to the downstream transect. It is suspected that the large, submerged, 15 - 20 meter high island of the former village of Bahna, located 2 km downstream of Orsova Bay, may be trapping suspended solids during this period (Figure 17). Sediment transport and the spread of the sediment plume depend on morphometric features such as bluffs or islands (Håkanson and Jansson 1983). Figure 17 shows the bottom cross-section along the transect at river km 951, showing the submerged island and village. While the estimated 20% removal is very uncertain because the balance is based on the removal in Orsova Bay, which is also somewhat uncertain, it is obvious that Bahna Island removes suspended particles by sedimentation among old trees, houses and infrastructure.

However, Figure 18 shows the particle concentrations taken at 4 m depth at different locations during the March 2001 cruise (March 24 and 25, 2001). Although Figure 18 shows a decrease in particle concentration from river km 970 to 960, the data shows some inconsistencies when compared to particle concentration in October 2001 (Figure 14). In October, the measurements indicate a continuous reduction in sediment concentration from Orsova Bay towards the dam with an increase downstream of the dam. The spring data show that there is no reduction (less than 0.4%) within the 16 km river section upstream of the dam. The degree of particle removal and the high exchange rate in Orsova Bay (approximately 15% of the Danube discharge) should reduce the downstream sediment concentration; however, this did not appear to occur. The constant suspended solids concentrations on either side of Orsova Bay, coupled with the estimated 7% removal by the bay, suggest sediment resuspension. This was possibly the result of unusual hydraulic conditions on March 24 and 25, caused by a high rate of discharge from the dam (50% more than the average annual discharge from the dam) and a sharp decline in the reservoir water level (the water level decreased by 1 meter). It appears reasonable that sediment deposition does occur in this reach during lower flow periods, but that flushing in the main branch during high discharge results in significant sediment resuspension.

Using the above estimates for sedimentation during the October period, the annual average flow for the Danube of 5,600 m^3 s^{-1} (NR 1998), and the measured suspended

particle concentrations at the two transects, the deposition rate is determined to be 12.4 kg s^{-1} for both Orsova Bay and Bahna Island. The average annual deposition rate, taking into account a removal efficiency of 30%, is therefore 390 kt yr^{-1}. Orsova Bay is responsible for one-third (130 kt yr^{-1}) of the removal, and Bahna Island is responsible for up to two-thirds (260 kt yr^{-1}) of the sediment removal within this 10 km long river section. Based on these values, the sediment removal rates are summarized in Table 5. There is considerable uncertainty in this estimation, particularly due to possible sediment resuspension in the main branch during the high flow periods.

Another mass balance was performed to estimate the deposition rate in the lower part of the reservoir immediately in front of the dam. The river section is taken between the previous downstream transect (river km 949) and at river km 944.5, located 2.5 km of the dam. The downstream ADCP measurements indicate an average backscatter of 61.23 dB. This corresponds to a suspended solids concentration of 3.06 mg L^{-1} (Figure 15). Applying the same calculation procedure as for the previous mass balance, the deposition rate is determined to be 11.9 kg s^{-1}. The results of the calculations are summarized in Table 5.

The total sedimentation rate in the entire 14.5 km stretch of the main branch including the bays is therefore up to 24 kg s^{-1} (or 770 kt y^{-1}); however, based on the March 2001 data, it is speculated that in the main branch a large portion of this will be resuspended during high flow events. According to the National Reviews report (NR 1998), due to the construction of the Iron Gate I, the average transport of suspended matter has been diminished from 1400 kg s^{-1} (measured in 1948 –1970) to 350 kg s^{-1} (measured in 1971 – 1974 downstream of the dam). Assuming that resuspension does (not) occur, then the calculated 4.1 kg s^{-1} (24 kg s^{-1}) corresponds to only 0.4% (2.3%) of the material supposedly deposited in the Iron Gate I, while the length of this river section (14.5 km) accounts for 12% of the total length of Iron Gate I (117 km). The lower than expected deposition rate can possibly be explained by the fact that the particle mass balances do not take into account the particle bedload, almost all of which will be retained by the dam wall. Also, no significant suspended solids deposition occurs in the main branch of this study, with deposition being limited to larger side bays. Additionally, because such a small amount of deposition occurs during a low flow period and considering that high flows may partially flush the reservoir, it is possible that Iron Gate I is not a significant source of sedimentation. Because the main branch is more subject to flushing than the bays, it is likely that the bays are the only significant long-term sediment sinks.

7. Discussion

Given the sediment removal of 0.4 - 2.3% for the 12% of the total length of the Iron Gate I, a conservative estimate can be made for the entire length. The estimate indicates only 3.3% to 19% of the sediment removal that was postulated by Panin et al. (1999) for the entire Iron Gate I reservoir. While this is an uncertain estimate, as upstream bays and flow conditions are not considered, it is reasonable as a high-end estimate given that flow velocities generally increase with distance upstream from the dam (Teodoru 2002). Reschke (1999) determined that the suspended solids contained an average of 1.9% biogenic silica (Friedl et al. 2003). This translates to 2.5 – 15 kt yr^{-1} of silica retention, or

3.5 – 21% of the 600 kt yr^{-1} postulated by Humborg et al. (1997). While it is clear that some Si is retained by the Iron Gate I, this estimate of Si removal is in good agreement of the 4% Si removal given by Friedl et al. (2003). This estimate is an order of magnitude less then previously expected and in good agreement with the lack of primary productivity and sedimentation found in this study. It is further suspected that any other nutrients that are retained are either particulate or retained by adsorption to settling particles, particularly phosphorus which has a higher affinity for adsorption (Gachter and Muller 2003). However, these quantities should also be much less then previous estimates.

It was generally accepted that the construction of the Iron Gate I Dam resulted in intensive algal growth and increased sedimentation, including diatoms, due to both the increased HRT and improved light transmission (Cociasu et al. 1996, Humborg et al. 2000). This is, however, in direct contradiction to the findings of this study. It was found that the HRTs for both Eselnita Bay and Orsova Bay are very short at 0.4 and 0.5 days, respectively. The HRT has a similarly low value for the lower reach of Iron Gate I. From February to December, the HRT has been found in the range of 10 hours (April, Q_{max} = 9700 m^3/s) to 36 hours (September, Q_{min} = 2400 m^3/s) with an average value of 26 hours (Q_{aver} = 5500 m^3/s).

8. Conclusions

One of the major impacts of damming is the modification of the thermal regime (McCartney et al. 2001). The relatively large mass of quiescent water in reservoirs typically promotes thermal stratification, which supports increased primary productivity. Historical measurements of Si concentrations in the coastal Black Sea before and after Iron Gate I construction reveal that mean concentrations dropped by a factor of 2.4, from 140 μM (Cociasu et al. 1996) to only about 58 μM (Humborg et al. 1997). The decrease of Si was explained by the construction of several dams on the Danube, particularly Iron Gate I, which was thought to result in intensive diatom blooms (Cociasu et al. 1996). A high sedimentation rate of diatoms prevents the return of the Si in their frustules to the water column. Humborg et al. (2000) also agree that reservoirs may act as a silica trap, though the main retention mechanisms are not clearly understood.

This study indicates, however, that in Iron Gate I there is no such development of a thermocline or typical thermal stratification. Iron Gate I can be described as a continuous riverine reservoir exhibiting only weak diurnal stratification. During nighttime the reservoir is usually convectively well mixed. Based on modeling simulations, the thermal stratification and distribution of heat through the water column are mostly inflow/outflow driven. The maximum HRT for the lower reach of Iron Gate I from February to December is only 1.1 day. Based on the findings of this study, the main conclusions can be summarized as follows:

1. The short HRT is likely to severely limit the primary productivity. According to Hynes (1970), if rates of water movement through a reservoir exceed a few millimeters per second, algal development is inhibited. In this study, it was found that the average horizontal water velocity is as high as 16 cm s^{-1}. Additionally, no algal layers were

observed with the ADCP measurements in the main branch. Primary productivity is limited to Orsova Bay, where, given the 15% exchange rate with the Danube, the effects are rather limited for nutrient uptake. Therefore, with the exception of Orsova Bay, the short HRT and high water velocity do not allow the development of a significant quantity of phytoplankton and subsequent nutrient uptake as was previously suggested by Cociasu et al. (1996).

2. Sedimentation is also limited to places where high velocities and turbulence are hindered even during high flow events. In this study, two potentially significant zones of sedimentation have been identified, Orsova Bay and Bahna Island, neither of which existed before the construction of the dam. W2 model simulations support the hypothesis that Bahna Island is a sink for sediments. However, the data indicate that the area near Bahna Island is more subject to resuspension of sediment due to flushing, whereas Orsova Bay may serve as a more permanent sink. It was found that insignificant sedimentation generally occurs within the lower reach of Iron Gate I. It was estimated that between 130 to 770 kt yr^{-1} of suspended solids are trapped annually in the lower reach and adjacent bays of the study area, and that, based on rough estimates for the entire Iron Gate I, as much as 1100 to 6400 kt yr^{-1} are retained. This is only about 3 – 19% of the sediment retention postulated by Panin et al. (1999).

3. Using the measurements of Reschke (1999) for the Si content of the suspended solids, it is estimated that only 4 to 21% of silica is retained by Iron Gate I, which is in good agreement with the 4% determined by Friedl et al. (2003) for 2001 and nearly an order of magnitude less then previous estimates (Humborg et al. 1997).

Based on the results of the present study, it is obvious that Iron Gate I has a short HRT and that construction of the dam did not result in a substantial increase in the HRT of the Danube River. The conversion of the river into a 117 km long reservoir resulted in an increase in HRT of less than 4 days. Furthermore, Iron Gate I is more similar to a river than a reservoir (long and narrow, well-mixed and turbid; exhibiting weak stratification with relatively high average water velocities). Therefore, a sharp increase in primary productivity and nutrient and suspended particle retention is not expected after impoundment and was not observed during this study (Friedl et al. 2003). Moreover, ADCP measurements in the lower part of the reservoir during the October cruise do not reveal any significant zone of primary production.

Future work should focus on further understanding of the sediment dynamics and nutrient cycling in the Iron Gate system, as well as upstream investigations into other possible sinks of sediment and nutrients. Additionally, a more detailed examination of the hydrodynamics of Orsova Bay and other adjacent bays is necessary to determine their roles as sediment and nutrient sinks. An interesting finding is that the stationary ADCP measurements near the dam indicate a large number of gas bubbles, suggesting methane or carbon dioxide release from the degradation of settled organic matter and subsequent loss of carbon from the system (Figure 19). Using the measured velocities, the rise velocity of the measured bubbles was determined to be about 25 cm s^{-1}, correspond to a bubble diameter in the range of 2 – 10 mm (McGinnis and Little 2002). Therefore, the

dynamics of the production, sedimentation and, especially, degradation of organic matter in the lower part of the reservoir should to be investigated further. The methane or carbon dioxide production should be estimated at the observed locations as the loss of methane/carbon dioxide to the atmosphere has important practical implications for the carbon cycle and greenhouse gas emissions. Such information will be vital for understanding and quantifying the environmental impact of the Iron Gate system on the downstream river system and the Black Sea.

9. References

Bale, J. D., and M. D. Giorgino. 1998. Dynamic modeling of water-supply reservoir physical and chemical processes. Proceedings of the First Federal Interagency Hydrologic Modeling Conference, April 19-23, 1998. Las Vegas, NV: Subcommittee on Hydrology of the Interagency Advisory Committee of Water Data: 2-61 to 62-67.

Berkamp, G., M. McCartney, P. Dugan, J. McNeely, and M. Acreman. 2000. Dams, ecosystem functions and environmental restoration. Thematic Review II. 1 prepared as an input to the World Commission of Dams, Cape Town, South Africa.

Cociasu, A., L. Dorogan, C. Humborg, and L. Popa. 1996. Long-term ecological changes in Romanian costal waters of the Black Sea. Marine Pollution Bulletin **32** (1): 32-38.

Cole, T. M., and E. M. Buchak. 1995. CE-QUAL-W2: A two-dimensional, laterally averaged, Hydrodynamic and Water Quality Model, Version 2.0, Instruction Report EL-95-. US Army Engineering Waterways Experiment Station, Vicksburg, MS.

Cole, T. M., and S. A. Wells. 2000. CE-QUAL-W2: A two-dimensional, laterally averaged, Hydrodynamic and Water Quality Model, Version 3.0, Instruction Report EL-2000-. US Army Engineering and Research Development Center, Vicksburg, MS.

Cole, T. M., and S. A. Wells. 2002. CE-QUAL-W2: A two-dimensional, laterally averaged, Hydrodynamic and Water Quality Model, Version 3.1, Instruction Report EL-2002-1. US Army Engineering and Research Development Center, Vicksburg, MS.

DARP. 1997. Nutrient Balances for Danube Countries - Final Report: Danube Applied Research Program, Project EU/AR102A/91. Institute for Water Quality and Waste Management, Vienna University of Technology; Department of Water and Wastewater Engineering, Budapest University of Technology.

Friedl, G., C. Teodoru, and B. Wehrli. 2003. Is the Iron Gate I reservoir on the Danube River a sink for dissolved silica? Biogeochemistry **Accepted**.

Friedl, G., and A. Wüest. 2002. Disrupting biogeochemical cycles - Consequences of damming. Aquatic Science **64**: 55-65.

Gachter, R., and B. Muller. 2003. Why the phosphorus retention of lakes does not necessarily depend on the oxygen supply to their sediment surface. Limnol. Oceanogr. **48** (2): 929-933.

Håkanson, L., and M. Jansson. 1983. Principles of Lake Sedimentology. Springer-Verla, Berlin Heidelberg.

Humborg, C., D. J. Conley, L. Rahm, F. Wulff, A. Cociasu, and V. Ittekkot. 2000. Silicon retention in river basins: far-reaching effects on biogeochemistry and aquatic food webs in coastal marine environments. Ambio **29** (1): 45-50.

Humborg, C., V. Ittekkot, A. Cociasu, and B. V. Bodungen. 1997. Effect of Danube River dam on Black Sea biogeochemistry and ecosystem structure. Nature **386**: 385-388.

Hynes, H. B. N. 1970. The ecology of flowing waters in relation to management. J. Water Pollution Control Federation **42** (3): 418-424.

ICPDR. 2001. International Commission for the Protection of the Danube River. Joint Action Program for the Danube River Basin (January 2001 - December 2005 [Online] http://www.icpdr.org/pls/danubis/DANUBIS.navigator.

Jørgensen, S. E., and G. Bendoricchio. 2001. Fundamentals of Ecological Modelling. *in* Developments in Environmental Modelling. Elsevier, Amsterdam.

Kennedy, R. H. 1999. Basin-wide considerations for water quality management: Importance of phosphorus retention by reservoirs. Internat. Rev. Hydrobiol. **84**: 557-566.

Lorke, A., D. McGinnis, P. Spaak, and A. Wüest. 2003. Acoustic observations of zooplankton in lakes using a Doppler current profiler. Limnol. Oceanogr. Methods (Submitted).

McCartney, M. P., C. Sullivan, and M. Acreman. 2001. Ecosystem impact of large dams. Background Paper Nr. 2. Prepared for IUCN/UNEP/WCD, IUCN and UNEP.

McGinnis, D. F., and J. C. Little. 2002. Predicting diffused-bubble oxygen transfer using the discrete-bubble model. Water Research **36**: 4627-4635.

NR. 1998. National Reviews, 1998, Romania. Technical Report Part B: Water Quality [CD-ROM] Information prepared for GEF - Danube River Basin Pollution Reduction Program. International Commission for the Protection of the Danube River (ICPDR), Vienna, Austria.

Panin, N., D. C. Jipa, M. T. Gomoiu, and D. Secrieru. 1999. Importance of sedimentary processes in environmental changes: lower River Danube - Danube Delta - Western Black Sea System. Pages 23-42 *in* S. T. Besiktepe, Unluata, U. and Bologa, A.S., editors. Environmental Degradation of the Black Sea: Changes and Remedies. Kluwer Academic Publishers, Dordrecht.

Postma, H. 1967. Sediment transport and sedimentation in the estuarine environment. Pages 158-179 *in* G. H. Lauff, editor. Estuaries. Amer. Assoc. Adv. Sci., Washington D.C.

Reschke, S. 1999. Biogeochemische Variabilitäten in der Schwebstofffracht der Donau und deren Einfluss auf das Sedimentationsgeschehen in nordwestlichen Schwarzen Meer. PhD Thesis. University Hamburg, Germany.

Reynolds, C. S. 1997. Vegetative Processes in the Pelagic: A Model for Ecosystem Theory. Ecology Institute, Oldendorf/Luhe, Germany.

Ryding, S.-O., and W. Rast. 1989. The Control of Lakes and Reservoirs, UNESCO edition. UNESCO.

SCOPE. 1999. Scientific Committee on Problems of the Environment of the International Council of Scientific Unions. Background of the global Si cycle [Online]. http://data.ecology.su.se/scopesi/si_dynamics.htm.

Straškraba, M., and V. Straškrabova. 1975. Management problems of Slapy Reservoir, Bohemia, Czechoslovakia. In: Proceedings of a Symposium on the Effects of Storage on Water Quality Reading University, Reading, England: 449-484.

Straškraba, M., J. G. Tundisi, and A. Duncan. 1993. State-of-the-art of reservoir limnology and water quality management. Pages 213-288 *in* Comparative Reservoir Limnology and Water Quality Management. The Netherlands, Dordrecht.

Teodoru, C. R. 2002. Personal communication. EAWAG - Swiss Federal Institute for Science and Technology.

WCD. 2001. World Commission of Dams. First WCD Forum Meeting. Dams and the Danube: Lessons from the Environmental Impact. Presentation by A. Zinke at the WCD Forum in Prague, Czech Republic, 26 March, 1999 [Online] http://dams.org/events/forum_prague_zinke.htm.

Zessner, M., and H. Kroiss. 1998. Retention and losses of nutrients in the hydrosphere. Institute for Water Quality and Waste Management, Vienna University of Technology, Vienna, Austria.

Table 1. Eselnita Bay Morphometry

Area, m^2	0.49×10^6
Volume, m^3	2.5×10^6
Maximum depth, m	10
Mean depth, m	5.1
Length (South to North), m	1000
Maximum width, m	1000
Normal range of annual water fluctuations, m	2.7

Table 2. Stratification in Eselnita Bay

Month (2001)	Stratification (difference between $T_{surface}$ and T_{bottom}), ° C		
	min	max	monthly average
March	- 0.1	1.27	0.1
April	- 0.07	2.59	0.225
May	- 0.01	2.42	0.475
June	- 0.12	2.76	0.382
July	- 0.01	3.11	0.518
August	- 0.08	1.99	0.43
September	- 0.57	1.69	0.03

Table 3. Orsova Bay morphometry

Area, m^2	4.5×10^6
Volume, m^3	46.6×10^6
Maximum depth, m	20.4
Mean depth, m	10.3
Length (South to North), m	3750
Maximum width, m	1750
Annual water level fluctuations, m	2.7

Table 4. Suspended solids concentration with depth.

Orsova Bay		Orsova		Bahna		Dam	
Depth (m)	SS (g m^{-3})	Depth (m)	SS (g m^{-3})	Depth (m)	SS (g m^{-3})	Depth (m)	SS (g m^{-3})
4	5.3	1	6.5	4	5.6	1	5.1
17.5	8.8	34	9.0	27	7.1	23	5.9

Table 5. Sedimentation rates

	kg/s	t/yr
Orsova Bay	4.1	130,000
Bahna Island	8.3	260,000
lower reservoir*	11.9	380,000
Total	24.3	~770,000

*lower part of the reservoir in front of the dam from river km 944.5 to 949

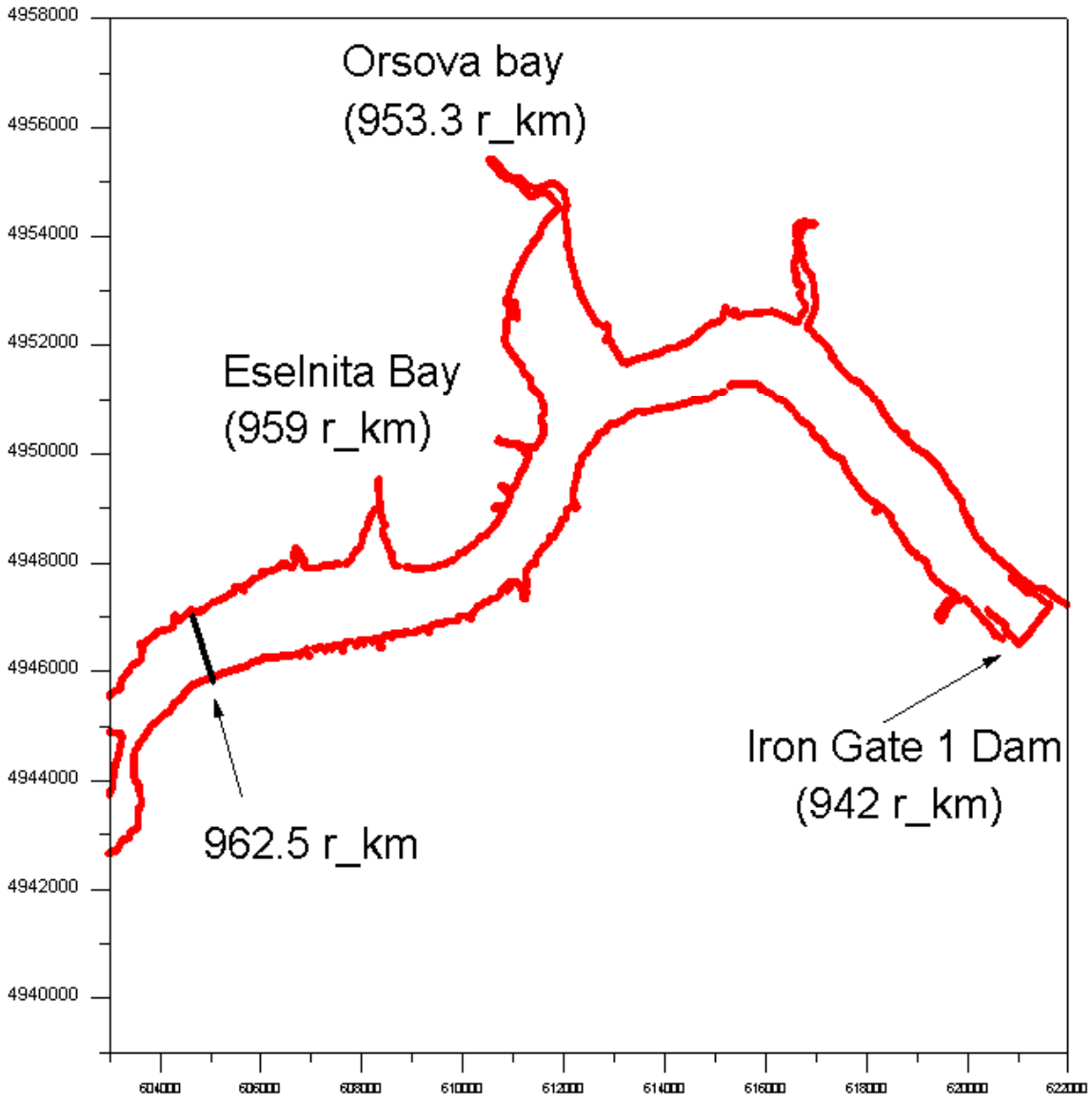

Figure 1. The Danube River and adjacent bays.
(Coordinates are: 44.67° latitude and 22.5° longitude.)

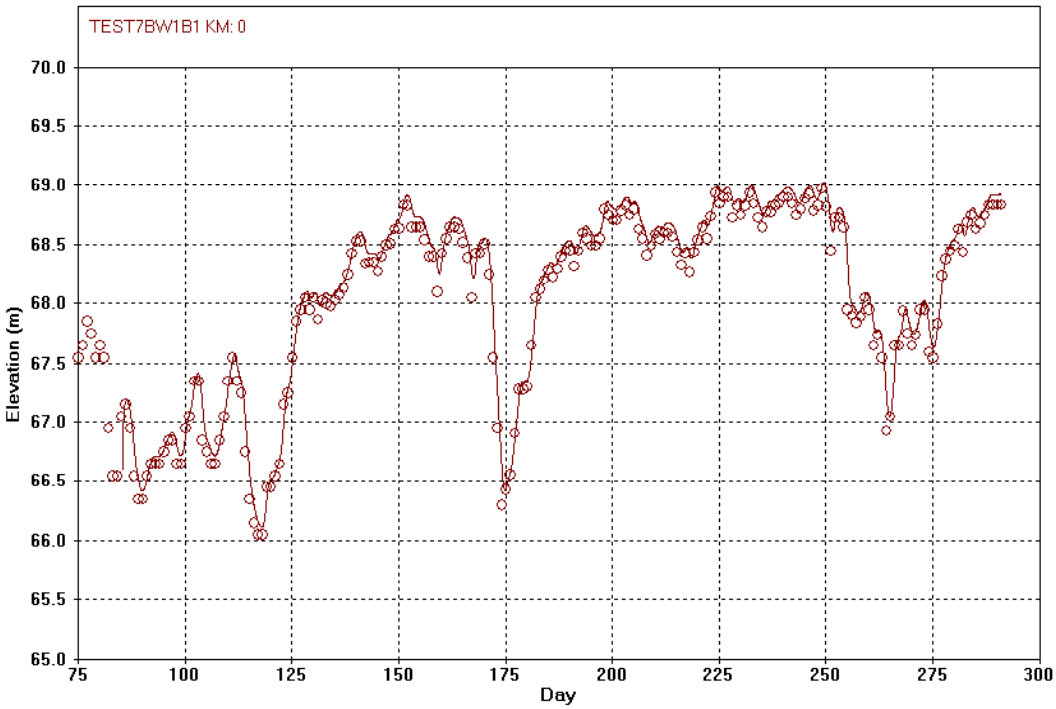

Figure 2. Measured (circles) and W2 predicted (solid line) water levels.

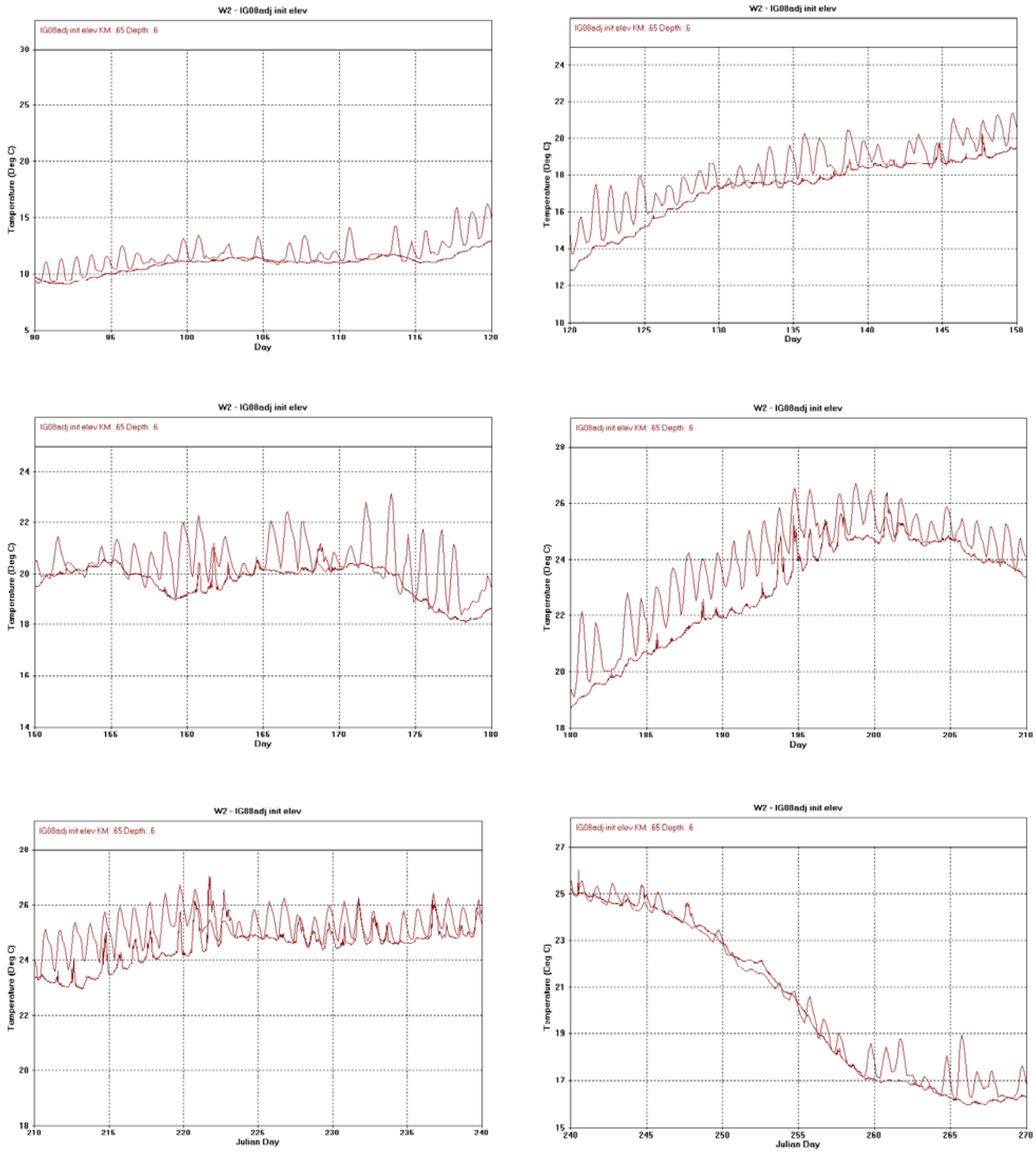

Figure 3. Simulated near-surface (0.6 m below water surface) water temperatures (upper line) and observed temperatures (bottom line) at 0.8 km upstream of the dam.

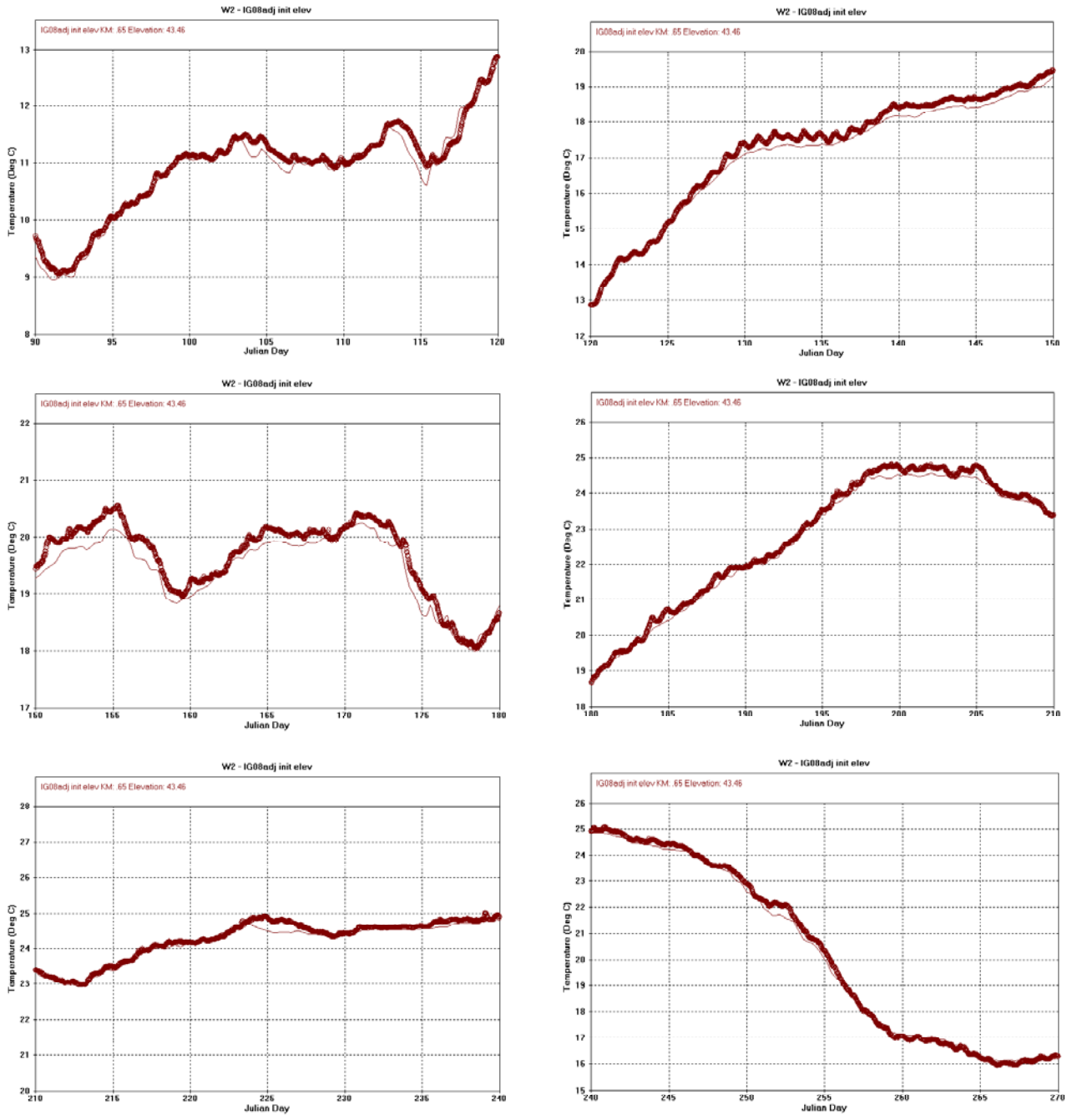

Figure 4. Simulated near-bottom (3.25 m above bottom) water temperatures (thin line) overlaid by observed temperatures (thick line) at 0.8 km upstream of the dam.

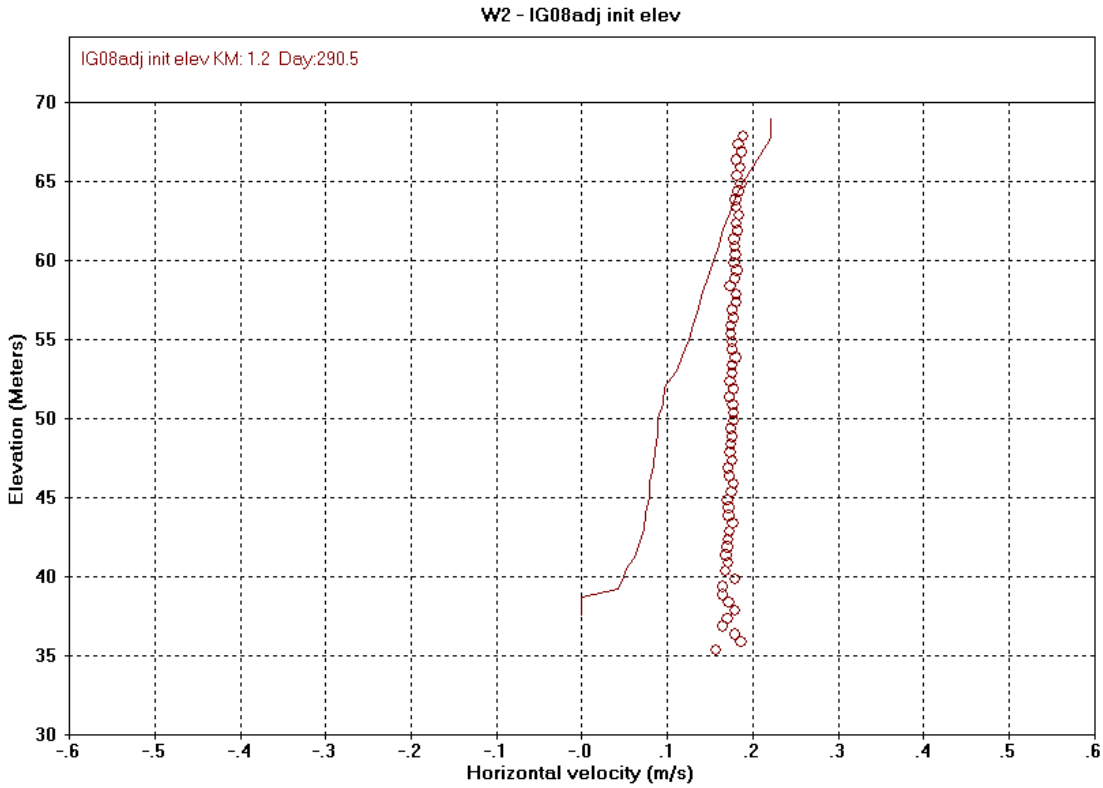

Figure 5a. Computed water velocities (solid line) compared to the measured ones (circles) at 1.2 km upstream of the dam (October 18, 2001).

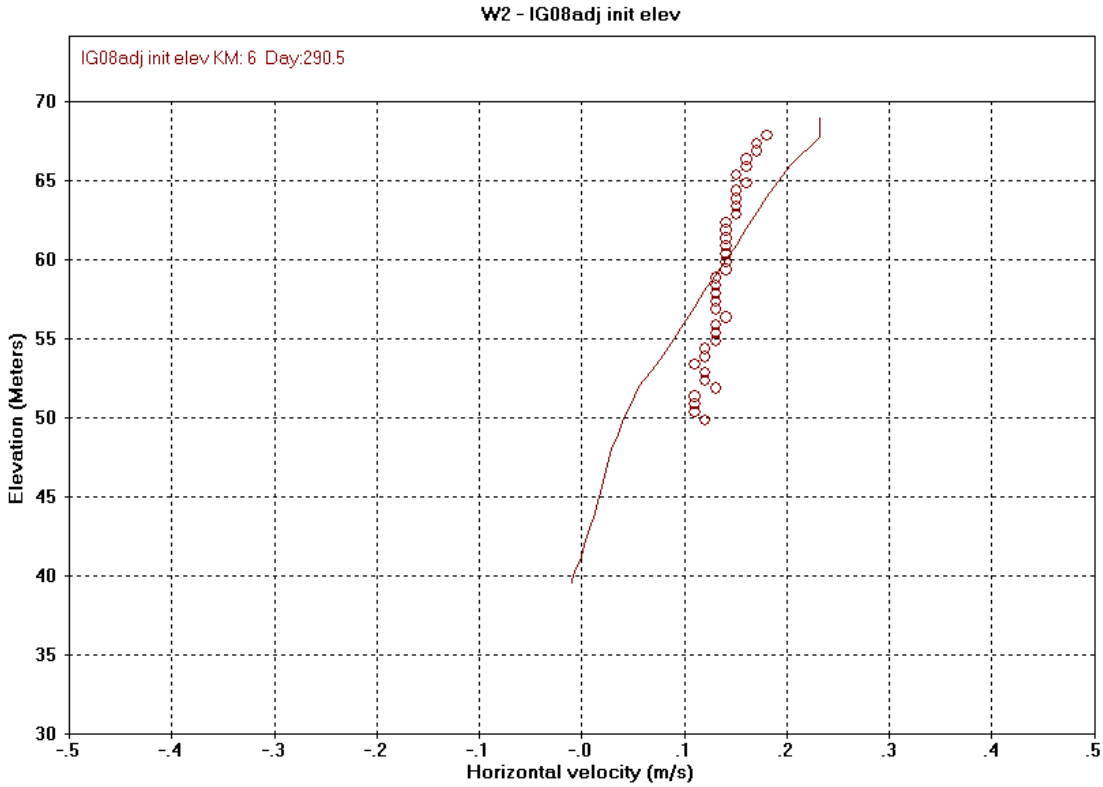

Figure 5b. Computed water velocities (solid line) compared to the measured ones (circles) at 6.0 km upstream of the dam (October 18, 2001).

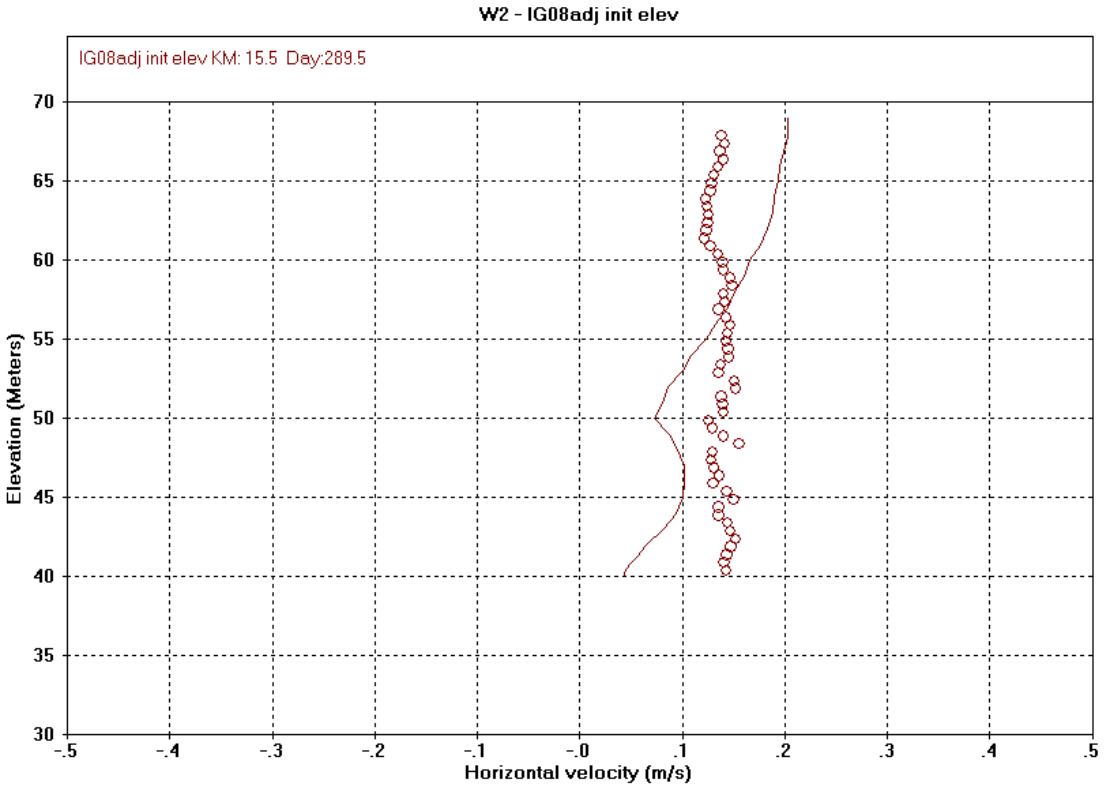

Figure 5c. Computed water velocities (solid line) compared to the measured ones (circles) at 15.5 km upstream of the dam (October 17, 2001).

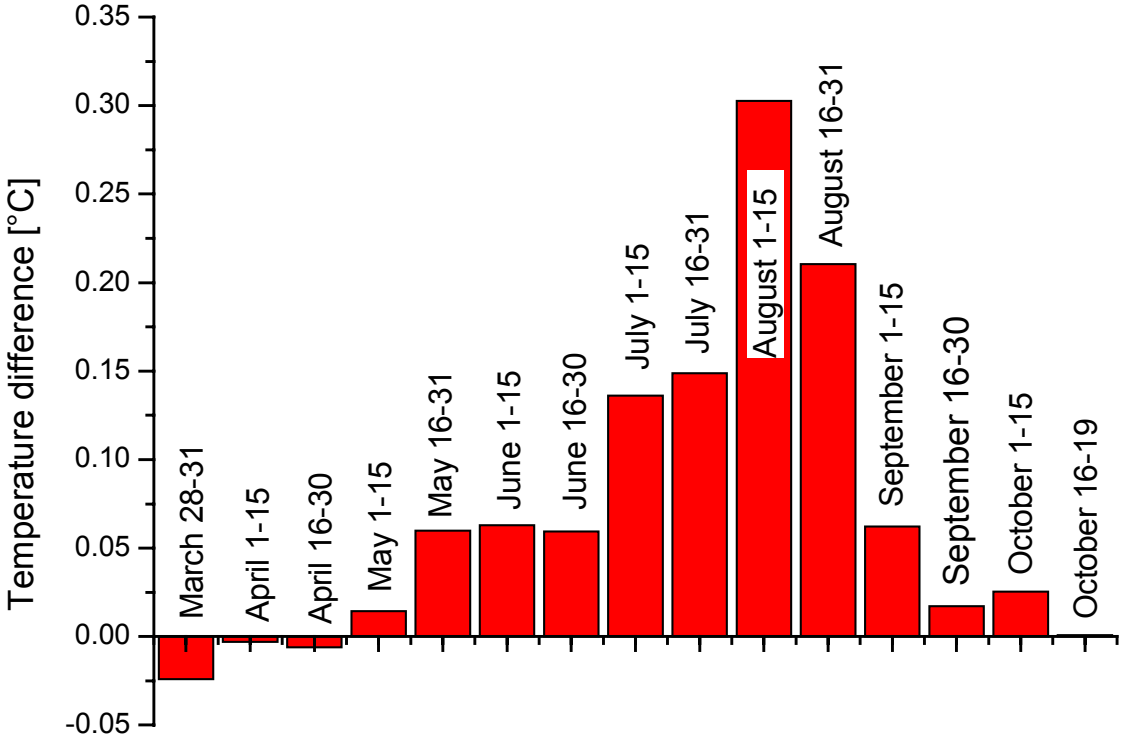

Figure 6. Extent of stratification every 2 weeks in the main branch.

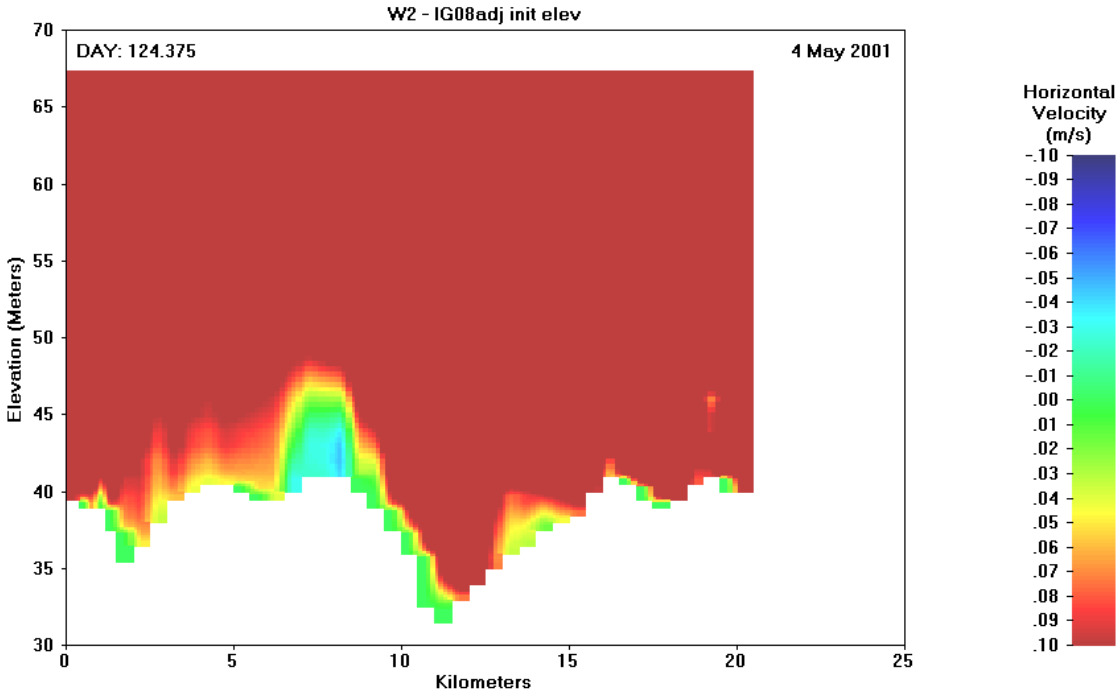

Figure 7. W2 velocity contour showing the formation of a large eddy zone (May 5, 2001), 0-km indicates the dam wall.

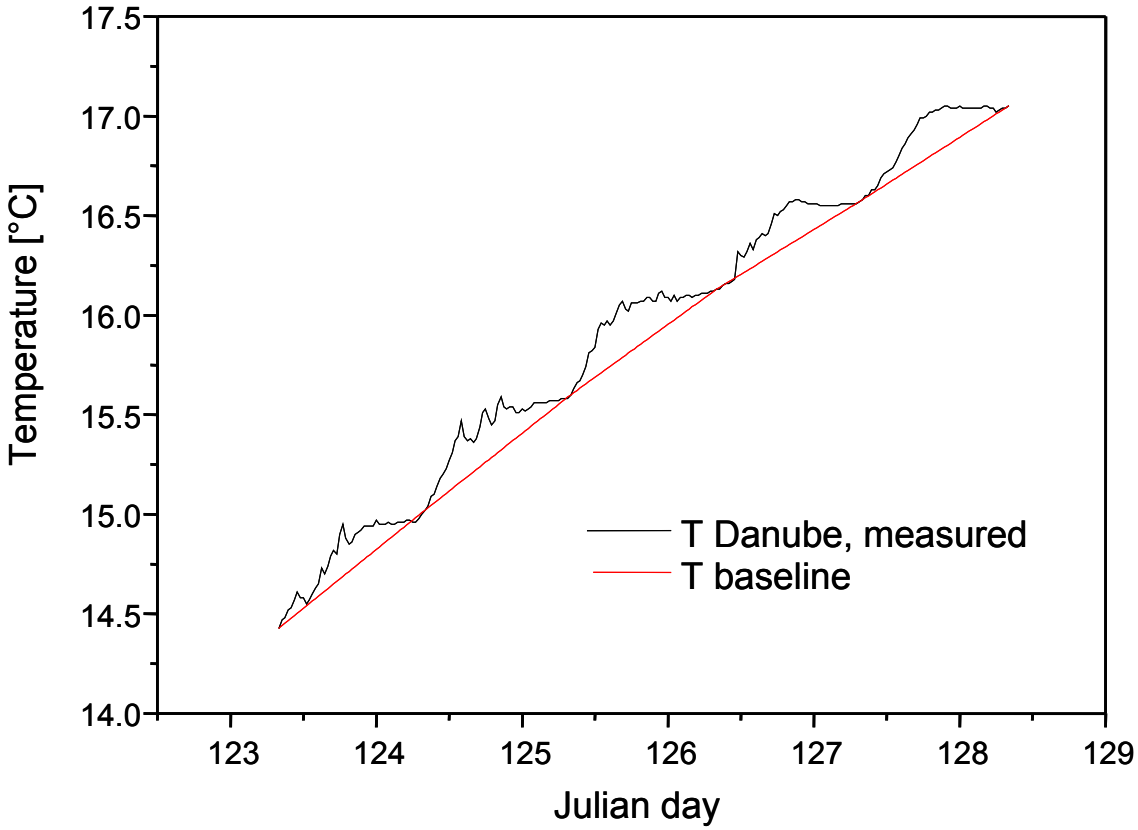

Figure 8. Daily temperature fluctuations in the Danube water (black) and baseline temperature (red).

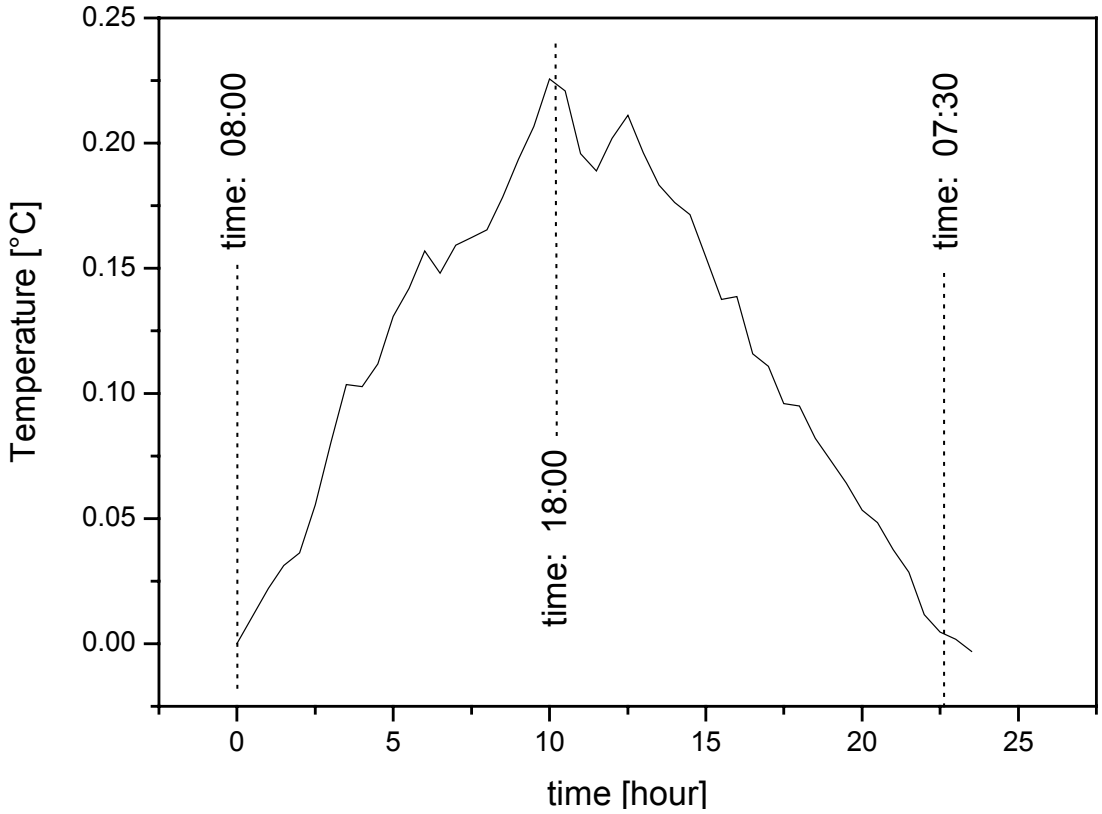

Figure 9. The 5-Day averaged temperature difference between the Danube water temperature and baseline temperature from Figure 8.

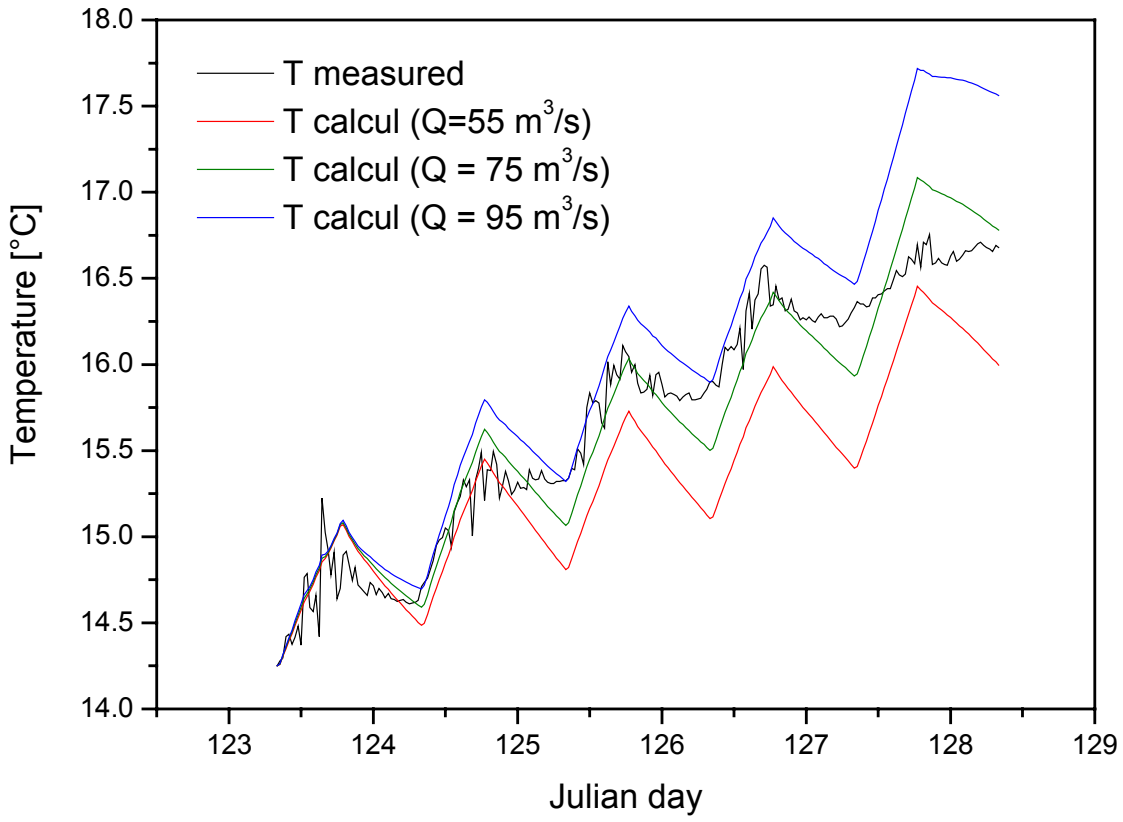

Figure 10. Representation of temperature in Eselnita bay during 5 day calculation (Julian days: 123-127).

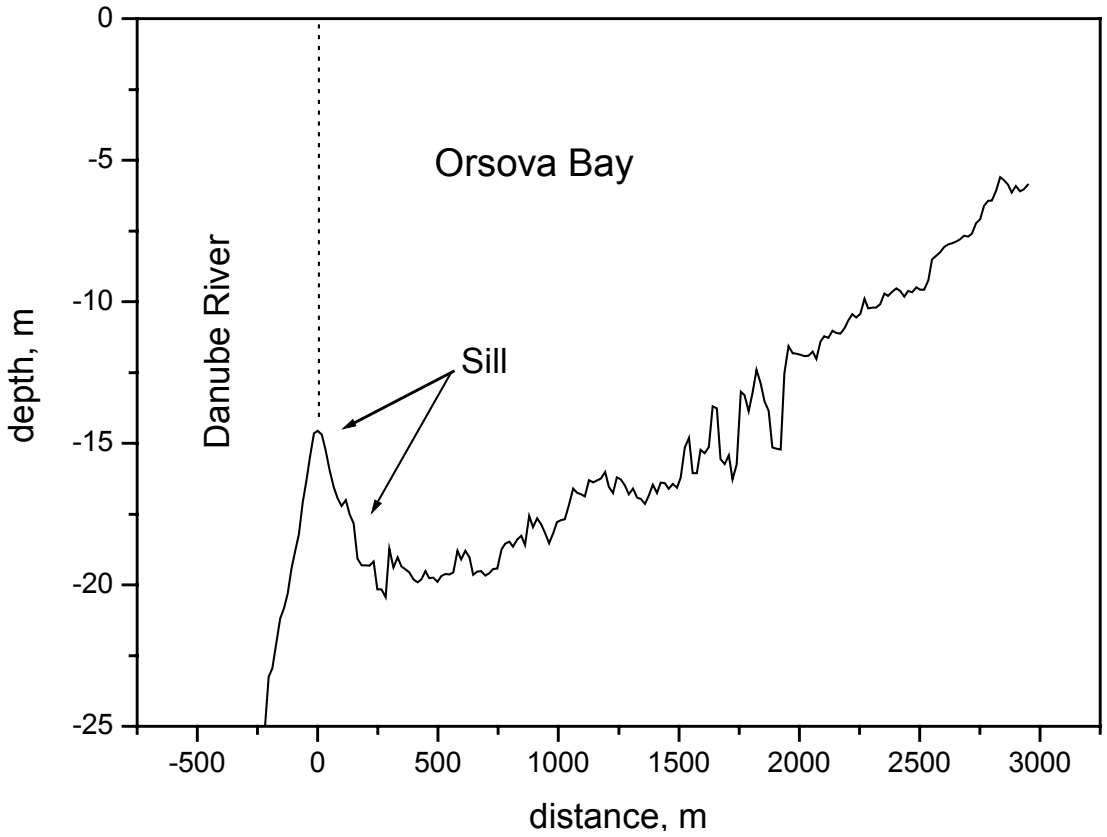

Figure 11. Bottom profile in Orsova bay from ADCP bottom tracking data obtained during the March 2001 Cruise.

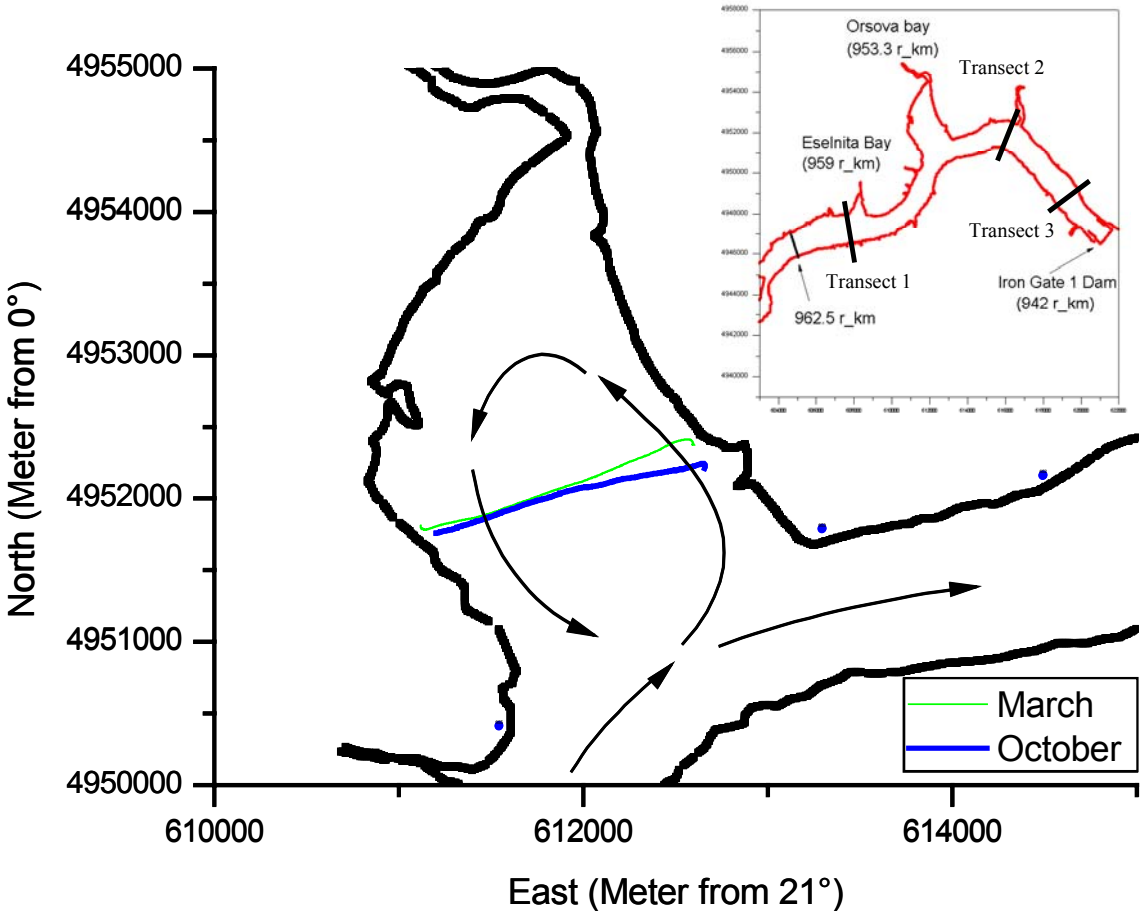

Figure 12. Location of the ADCP transects for March and October, 2001 cruises in Orsova Bay.

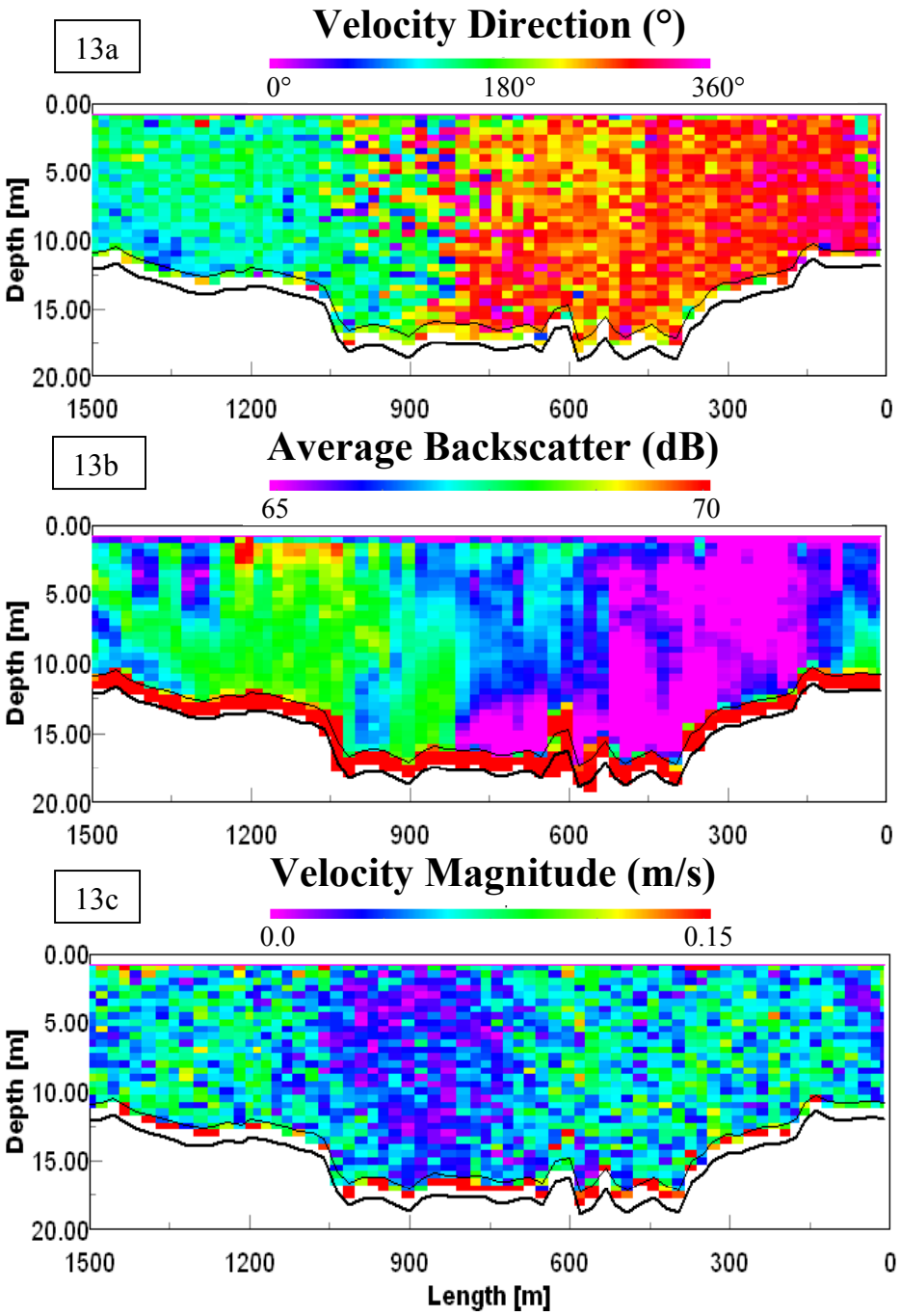

Figure 13. ADCP results from October 2001 transect in Orsova Bay along transect in Figure 12, 0-m corresponds with the east side of the bay. 13a demonstrates a northerly inflow on the east side a southerly outflow on the west side. 13b shows backscatter signal strength showing a greater partial concentration leaving Orsova Bay then entering, while 13c shows the velocity magnitude.

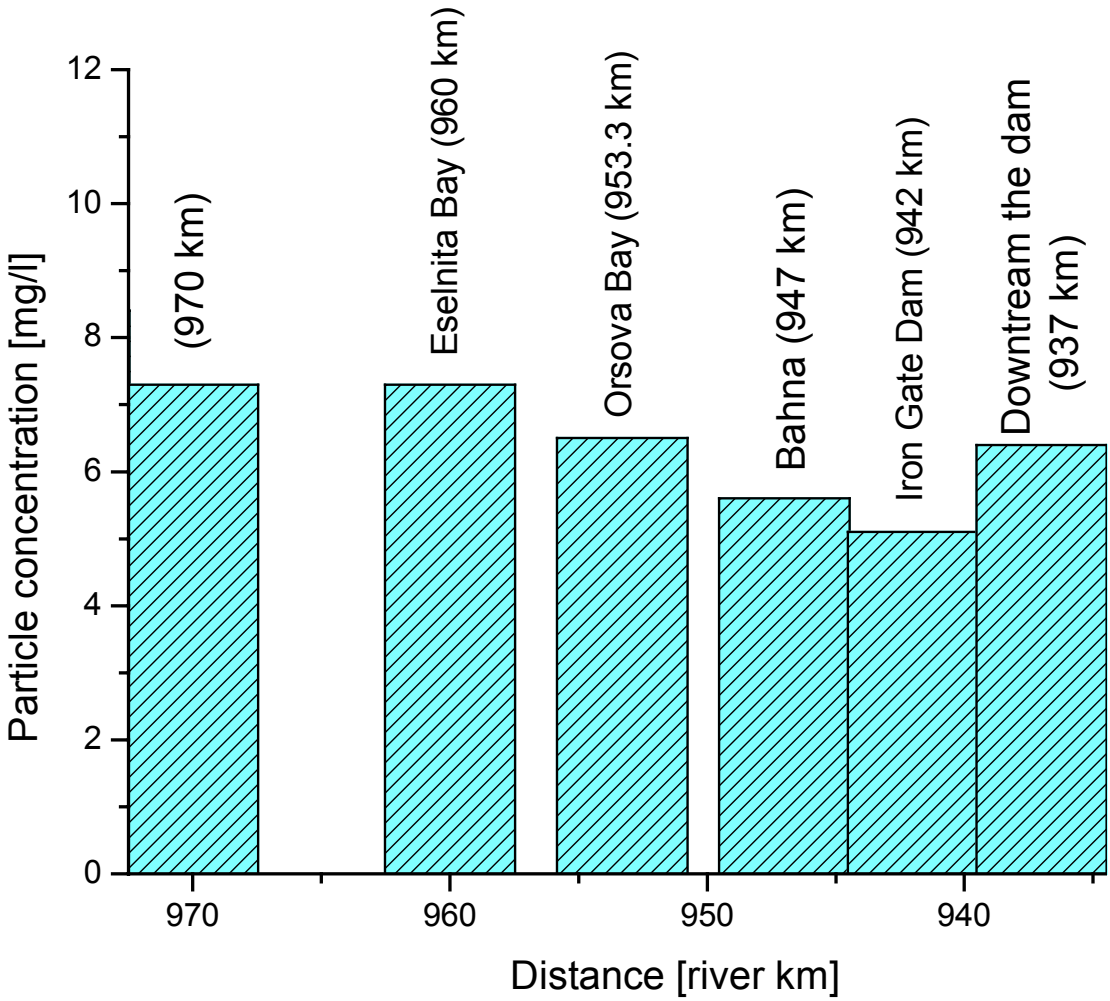

Figure 14. Sediment particle concentrations in the Danube (October 2001).

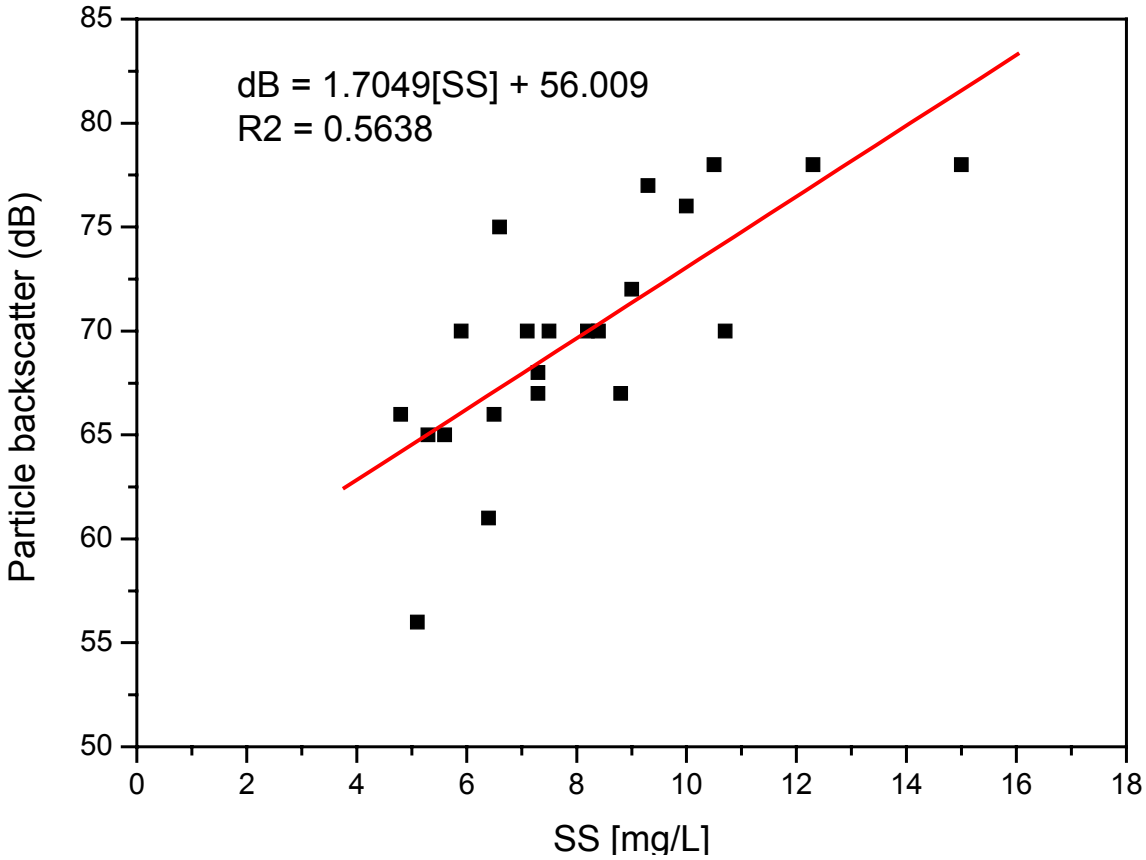

Figure 15. Relationship between ADCP particle backscatter (dB) and concentration of suspended solids (mg/l) based on data obtained during the October 2001 Cruise.

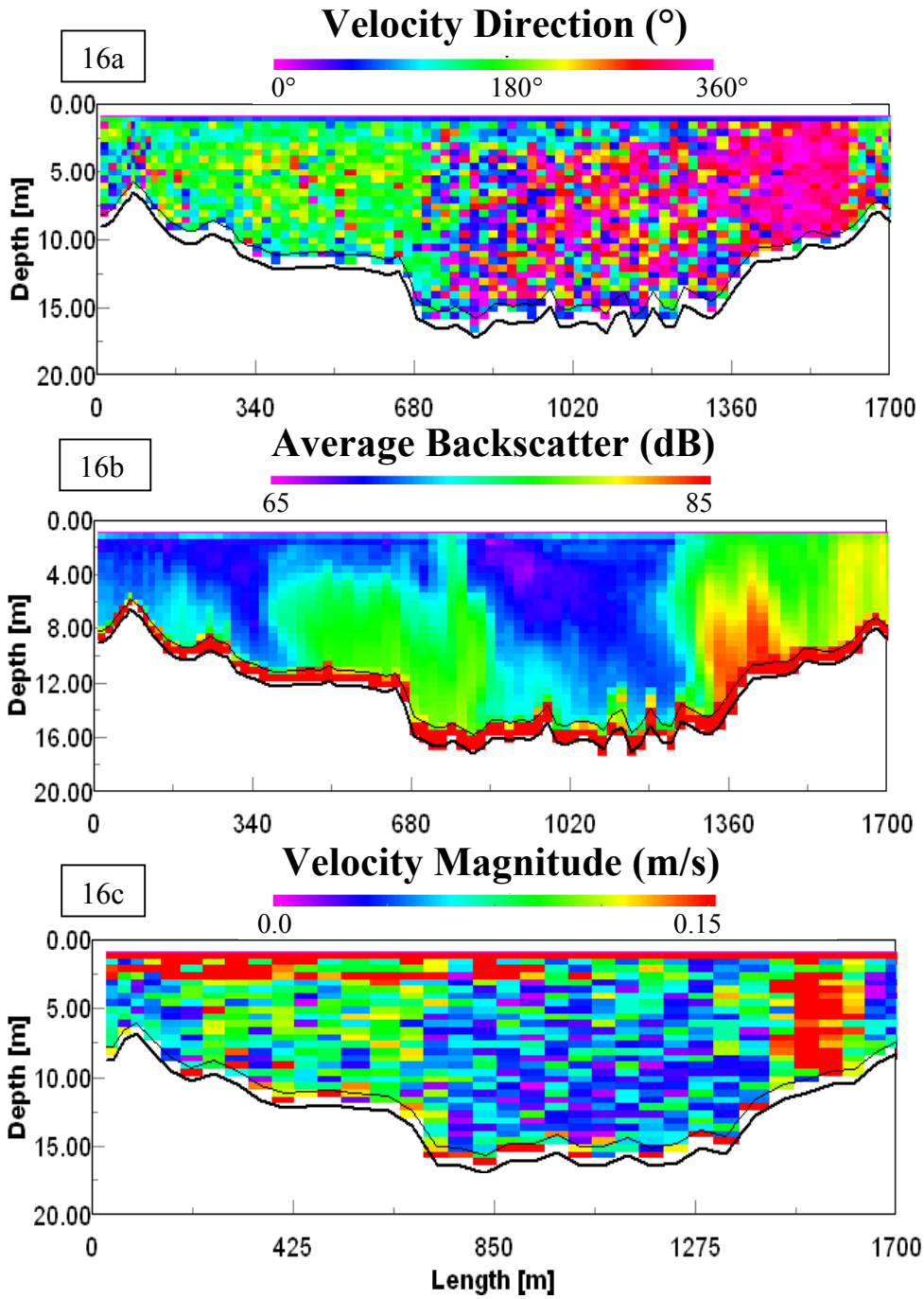

Figure 16. ADCP results from March 2001 transect in Orsova Bay along transect in Figure 12, 0-m corresponds with the south side of the bay. 16a demonstrates a northerly inflow on the east side a southerly outflow on the west side. 16b shows backscatter signal strength showing a greater partial concentration leaving Orsova Bay then entering, while 16c shows the velocity magnitude.

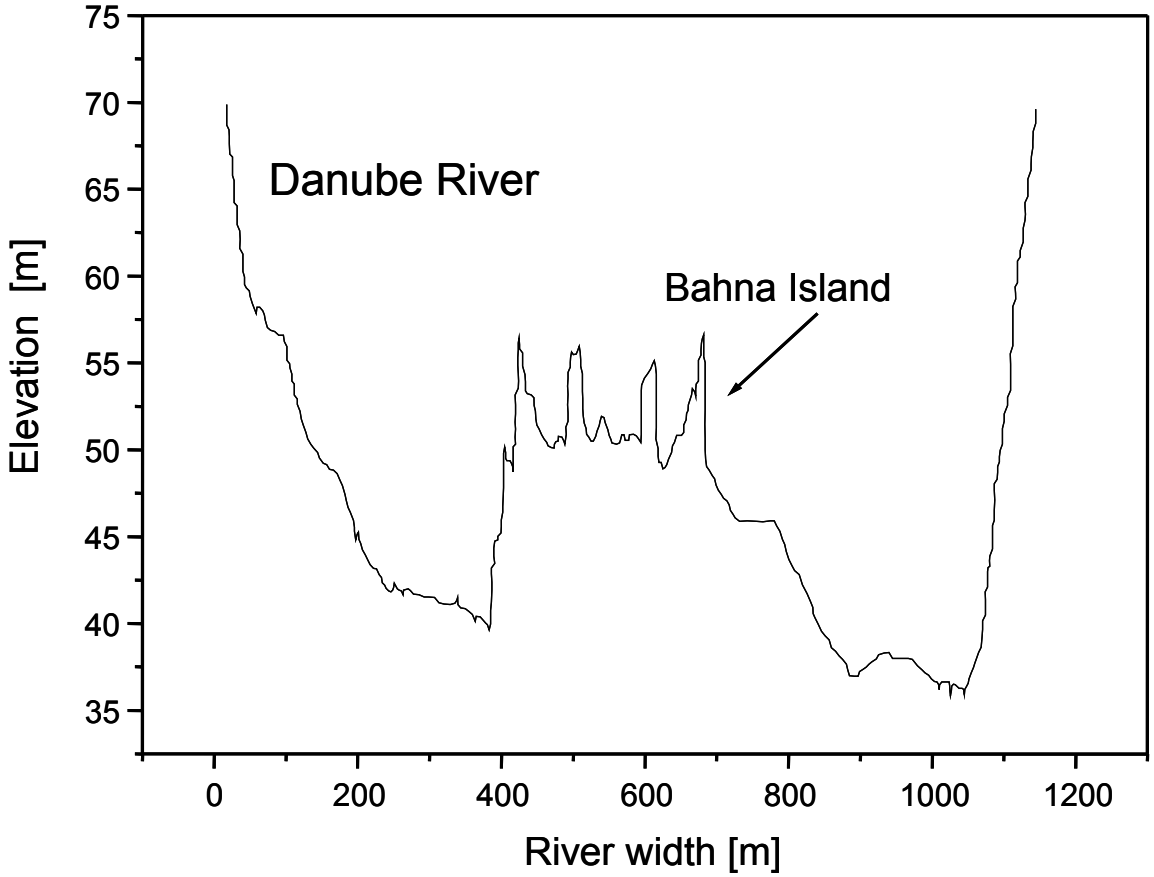

Figure 17. Cross-Section at River km 951 showing Bahna Island.

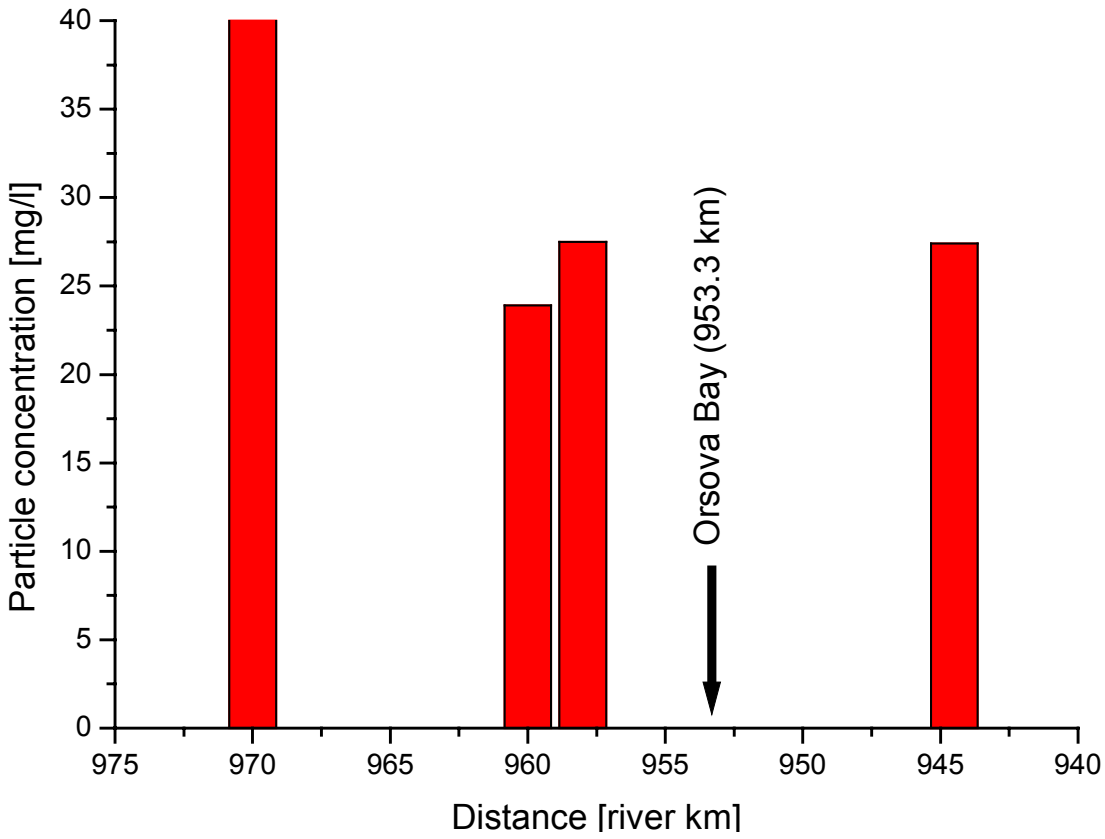

Figure 18. Sediment particle concentrations in the Danube (March 2001).

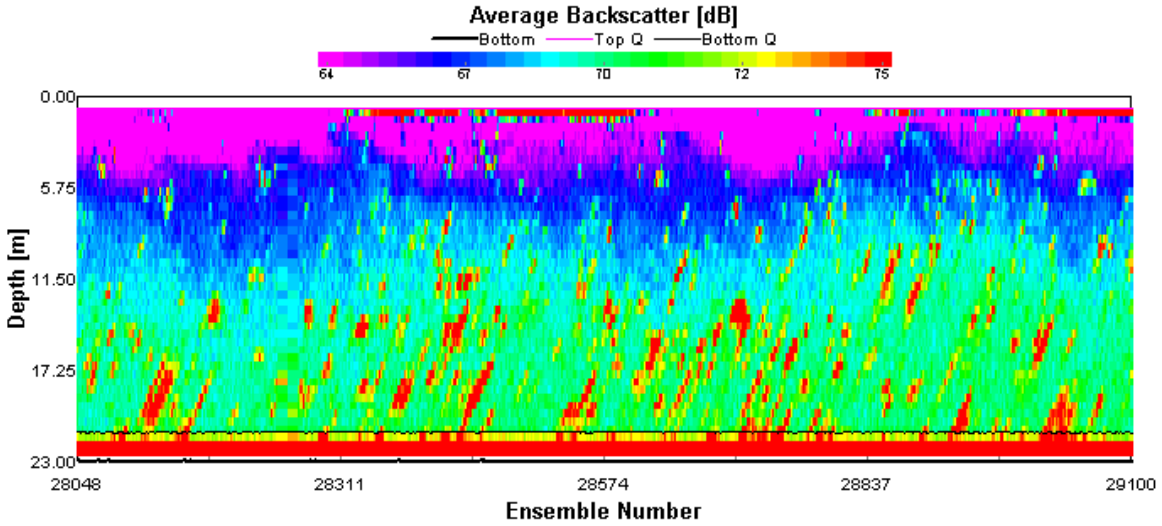

Figure 19. Gas Flux (red) 2.5 km upstream of the Iron Gate Dam.

DANIEL FRANK MCGINNIS

VITA

Daniel Frank McGinnis was born on September 6, 1971 in Portsmouth Naval Hospital, Virginia. His primary and secondary education was provided by the Virginia Beach Public School System, Virginia Beach, Virginia, and the Shawnee Mission School District, Overland Park, Kansas.

Education

- M.S. in Environmental Engineering, Virginia Tech, May 2000
- B.S. in Civil Engineering, Virginia Tech, June 1996
- A.S. in Natural Science, Tidewater Community College, May 1994
- A.S. in Engineering, Tidewater Community College, May 1994

Experience

- 1995 - Present: Graduate Research Assistant, Department of Civil and Environmental Engineering, Virginia Tech, Blacksburg, VA.
- 1999 - Present: Project Engineer, Mobley Engineering Inc., Norris, TN.
- 2000 – 2003: Guest researcher, Swiss Federal Institute for Environmental Science and Technology (EAWAG), Switzerland

Key Publications

Burris, V. L., D. F. McGinnis, and J. C. Little. 2002. Predicting oxygen transfer rate and water flow rate in airlift aerators. Water Research **36**: 4605-4615.

Little, J. C., and D. F. McGinnis. 2001. Hypolimnetic Oxygenation: Predicting Performance using a Discrete-Bubble Model. Water Science & Technology: Water Supply **1**: 185-191.

Lorke, A., D. McGinnis, P. Spaak, and A. Wüest. Submitted. Acoustic observations of zooplankton in lakes using a Doppler current profiler. Limnol. Oceanogr. Methods.

McGinnis, D. F., and J. C. Little. 1998. Bubble dynamics and oxygen transfer in a Speece Cone. Water Science & Technology **37**: 285-292.

McGinnis, D. F., and J. C. Little. 2002. Predicting diffused-bubble oxygen transfer rate using the discrete-bubble model. Water Research **36**: 4627-4635.